High-resolution wave climate analysis in the Helgoland area

Dissertation
zur Erlangung des Doktorgrades
der Naturwissenschaften im Fachbereich
Geowissenschaften
der Universität Hamburg

vorgelegt von

Lidia Gaslikova
aus Moskau

Hamburg
2006

Als Dissertation angenommen vom

Fachbereich Geowissenschaften der Universität Hamburg

auf Grund der Gutachten von Professor Dr. Hans von Storch
und Professor Dr. Jürgen Sündermann

Hamburg, den 8 Februar 2006
Professor Dr. Helmut Schleicher

Abstract

In this work the local near-shore wave climate for the Island of Helgoland is studied. The focus is on the assessment of wave extreme events, which are of major importance for the coastal engineering and management. This problem requires multi-decade wave statistics provided by measured data. The lack of long-term homogeneous observations is often an obstacle to the direct statistical analysis of the local wave climate. On the other hand, regional wave hindcasts are available from simulations for the last decades. In this thesis several so-called downscaling methods are tested, compared and applied to the evaluation of the past local wave climate. These methods make it possible to reconstruct the instantaneous local wave situations from the regional atmosphere/ocean conditions taking the local effects into account. Dynamical downscaling as a shallow water wave model, statistical and statistical-dynamical approaches are considered.

First, the results of the small-scale dynamical wave modeling are validated against the measurements. The dynamically obtained local wave data is compared with the existing regional wave hindcast and is found to better describe the local wave statistics. The statistical downscaling techniques in combination with the dynamical method are proposed as a time-saving procedure for the reconstruction of the instantaneous local wave fields. Linear regression, canonical correlation analysis and the analog method are applied and found to be reasonable in representing the local wave statistics. The linear regression method is chosen for further wave simulation experiments.

The wave climate for the past 40 years is reconstructed and corresponding extreme wave statistics are examined in terms of intra-annual variability, trends and local tendencies. Although the general behaviour of the small-scale wave statistics is similar to that of the regional scale, the local details provide additional information for the development of near-shore constructions. The potential impact of anthropogenic climate change on local wave extreme events is investigated within the scenario study. The changes in magnitude of local wave extremes are evaluated for the global future A2 and B2 IPCC SRES development scenarios based on the regional wind/wave data obtained within the PRUDENCE project.

Zusammenfassung

In dieser Arbeit wird das kustennahe Seegangsklima der Insel Helgoland untersucht. Den Schwerpunkt bildet hierbei die Abschatzung von extremen Seegangsereignissen, welche von ausschlaggebender Bedeutung fur Kustenschutz und Kustenzonenmanagement sind. Diese Anwendungen erfordern Seegangsstatistiken, die auf multi-dekadischen Beobachtungsdaten

basieren. Das Fehlen von moglichst weit in die Vergangenheit zuruckreichenden homogenen Beobachtungen stellt oftmals eine Hurde fur die direkte statistische Analyse des lokalen Seegangsklimas dar. Eine Moglichkeit die eingeschrankte Beobachtungsdatenlage zu verbessern stellen regionale historische Simulationen des Seegangs der letzten Jahrzehnte dar, die in den letzten Jahren vermehrt erstellt wurden. In dieser Arbeit werden verschiedene so genannte Downscaling-Methoden zur Bewertung des vergangenen lokalen Seegangsklimas getestet, verglichen und angewandt. Diese Methoden erlauben es den momentanen lokalen Seegang in Abhangigkeit von den regionalen atmospharischen und ozeanischen Bedingungen sowie ein unter Berucksichtigung von lokalen Effekten zu rekonstruieren. Es werden sowohl ein dynamisches Downscaling-Verfahren in Form eines Flachwasserseegangsmodells als auch statistische und statistisch-dynamische Ansatze betrachtet. Zunachst werden die Ergebnisse der kleinskaligen dynamischen Seegangsmodellierung mit vorliegenden Beobachtungsdaten verglichen. Anschlie?end werden die dynamisch erzeugten lokalen Seegangsdaten mit bereits vorhandenen regionalen historischen Seegangssimulationen verglichen. Dabei stellt sich heraus, dass erstere das lokale Seegangsklima besser beschrieben und auf diese Weise somit ein Mehrwert gegenuber den regionalen Rekonstruktionen geschaffen werden kann. Daran anschlie?end werden verschiedene statistischen Downscaling Methoden in Kombination mit den dynamischen Methoden als eine zeitsparende Ma?nahme zur Rekonstruktion des momentanen lokalen Seegangsfeldes vorgeschlagen und getestet. Es stellt sich heraus, dass sowohl lineare Regression, kanonische Korrelationsanalyse als auch die Analog Methode adaquat fur die Wiedergabe des lokalen Seegangsklimas sind. Im folgenden wird die lineare Regression ausgewahlt, um das Seegangsklima der letzten 40 Jahre zu rekonstruieren. Diese Rekonstruktion wurde anschlie?end hinsichtlich ihrer intra-annuellen Variabilitat, Trends und lokaler Tendenzen von Extremereignissen untersucht. Obwohl das allgemeine Verhalten der kleinskaligen Seegangsstatistik der der regionalen Skala ahnelt, bieten die lokalen Details zusatzliche Informationen fur die Entwicklung von kustennahen Bauten. Der potentielle Einfluss von anthropogen induzierten Klimaanderungen der lokalen Seegangsextreme wurde im Rahmen einer Szenariostudie untersucht. Die Anderungen in der Starke der lokalen Seegangsextreme wurden fur die IPCC-Treibhausgasemmissionsszenarien A2 und B2, basierend auf den regionalen Wind/Seegangsdaten des PRUDENCE-Projekts, abgeschatzt.

Contents

List of Figures

List of Tables

Chapter 1

Introduction

Coastal zones comprise a considerable part of the most developed and populated areas of the world. Providing diverse resources and variety of economical and social opportunities, these areas are at the same time extremely vulnerable and complex natural systems, strongly dependent on the influence of the sea. Therefore, for correct evaluation of the potential dangers for the off-shore and coastal facilities and of the coastal development options, it is important to have adequate, detailed and long-term information about the near-shore sea properties. For such safety and management assessments, many aspects of the sea impact on the shore as well as coastal processes should be considered. These could be, for example, the sea level change, tides, waves and storm surges, erosion, sediment transport, ice coverage and so on, depending on particular application and specific features of the area studied. This study is mainly dedicated to one component of the complex sea-land interaction system, namely to the local waves and wave climate assessment for the coastal zones, having in mind possible applications to the coastal protection and management planning, off-shore construction and vessel design problems, as well as the assessment of long-term changes and potential future developments.

The planning and the life-span of coastal constructions are heavily dependent upon the impact that the facility is supposed to undergo. Consequently, in coastal engineering many applications require the knowledge of wave statistics, especially the magnitude, frequency and duration of wave extreme events, for adequate evaluation of future wave influence. At first approach, the observed data from wave gauges, satellites or radars is considered as the main source for obtaining the wave statistics. Although such data is widely used in applications and give a general insight into the past wave climate, it often suffers from different sorts of inhomogeneity (see e.g. WASA Group [1998]) and/or do not cover long enough periods of time. Another drawback is that the measurement points are not regularly located in space and can be situated rather far from the coastal facilities in question. In this case, the nearest available data can be used together with methods of the wave data transformation to obtain the statistics required. Such methods are usually based on first principals of shallow water processes (see e.g. Coastal Engineering Manual (http://chl.erdc.usace.army.mil)). However, this methodology does not help to overcome original inhomogeneities of the measured wave data. Another approach is provided by wave

modeling and multi-decade wave hindcasts. This method is often used as a complementary tool to the observed data for the reconstruction of the wave climatology with the required accuracy. First, some measurements are needed to validate the hindcast, and then the hindcast itself can be used instead of observations at locations or time periods not covered by the data.

The first attempt to produce a long-term wave hindcast with a dynamical wave model was undertaken within the WASA (Waves and Storms in the North Atlantic) project (Günther et al. [1998], WASA Group [1998]) for the North Atlantic region. The reconstructed period covered four decades (1955-1994) and the wave data was hindcast on a coarse spatial resolution of about 50x50 km. The main aim of this reconstruction was to investigate the storm and wave changes in the past. Several other hindcasts produced during the past decade, for example, global wave reanalysis (Cox and Swail [2001], Simmons and Gibson [2000]) or regional wave reconstructions for the North Atlantic with statistical models (e.g. Kushnir et al. [1997], Wang and Swail [2001]) mainly pursued a similar purpose to describe the wave climate and tendencies of the past in general. However, for coastal zones and shallow water areas with complicated bathymetry the reconstructions obtained are rather coarse and hardly applicable. The next qualitatively new step towards a better description of the local near-shore wave climatology was made within the HIPOCAS (Hindcast of Dynamic Processes of the Ocean and Coastal Areas of Europe) project (Soares et al. [2002]). Unlike the major part of previous studies, this project was aimed at providing wind, wave and storm surge hindcasts for the European coastal seas appropriate for the coastal applications, which require producing more homogeneous wind fields, increasing the spatial resolution and considering shallow water and coastal processes. This task has been successfully completed and a medium-scale wave hindcast for the last four decades with approximately 5x5 km spatial resolution was obtained. The data has been used for different studies and applications such as wave risk assessments, hazard modeling or simulation of ship movements as well as boundary conditions for high-resolution wave models. At the same time, this hindcast still remains weak in its ability to represent the local wave statistics for basins with complicated coastline and bathymetry.

This thesis. The general aim of this work is to investigate the local wave climate in the coastal zones of the North Sea with respect to past and future changes. This task requires development and implementation of methods to obtain proper long-term high-resolution (tens to hundreds of meters) wave statistics. The central part of the study is dedicated to the development and investigation of a methodology allowing the use of the medium-scale wave data for coastal applications, i.e. the determination of the best ways to obtain the local wave statistics from the existing medium-scale hindcast. For this task the objective is twofold and comprises (1) evaluation of the relevancy of existing multi-decade wave hindcast for coastal protection and management applications and its ability to represent the small-scale near-shore features and (2) introduction and evaluation of the dynamical and statistical methods for obtaining adequate long-term high-resolution wave statistics from the medium-scale wave hindcast. A further part of this work is aimed at analyzing local wave statistics for the past four decades obtained with the selected methodology, focusing

on the wave extreme events as the most important characteristic for coastal protection and management needs. The objectives include investigation of the relation between the regional wind/wave climatology and the local wave climatology, and determination of past tendencies for local wave extreme events. Along with the understanding of the past wave climatology, the prospective wave climate is studied. In this work two approaches to the evaluation of the future wave extremes are considered. The first one is based on the extreme value analysis of the past local wave extremes and extrapolation of these obtained statistics into the future. The second approach is aimed at illustrating the response of the local system to global anthropogenic climate change. Here the two global IPCC scenarios, that have previously been applied at the regional scale, are used for the local wave assessments.

Methods and tools. Until now most of the high-resolution dynamical wave modeling experiments have been made for episodical wave simulations of selected storms or case studies and the modeled time period of such simulations varied from several hours to several years. Here the ability of the dynamical models to produce multi-decade wave simulations and provide adequate wave statistics is investigated and discussed. The statistical downscaling models applied to the medium-scale wave data could provide an alternative to dynamical wave modeling. The statistical downscaling experiments for the ocean waves were earlier limited by the applications to the downscaling of extreme wave statistics on the coarse (tens of kilometers) spatial scale (e.g. Kushnir et al. [1997], WASA Group [1998], Wang and Swail [2001]). In this study the models appropriate for the high-resolution coastal wave applications are selected and implemented. The data provided by the HIPOCAS project was chosen as the medium-scale wave dataset forming the basis for the study. To our knowledge, it represents the longest homogeneous wave hindcast for the North Sea, providing the data with the finest resolution among available long-term hindcasts for the North Atlantic and taking shallow water processes into account.

The surroundings of Helgoland Island located in the German Bight were chosen as an example area for testing the methodology. Local wave effects are expected in the region because of the presence of two islands of rather small size (about 1 km^2) and complicated bathymetry in the surrounding area. This allows the testing of the quality of the medium-scale hindcast in an environment for which it was not explicitly intended. The deficiencies of the existing wave climate reconstruction are shown and the methodology for localization of the wave statistics for non-trivial surroundings is tested.

Objectives and procedure. A more specific description of the goals of this work and procedure for their achievement are:

- Application of the dynamical spectral wave model to the localization of the medium-scale wave data.
- Validation of the obtained local wave data against measurements, and evaluation of the dynamical model's abilities and limitations in representation of the near-shore wave statistics.
- Skill assessment for the existing wave hindcast in representation of the coastal wave

statistics by the evaluation of the additional information which can be provided by small-scale wave modeling based on this data.

- Introduction, application and comparison of the statistical models to the downscaling of the medium-scale wave parameters and evaluation of their ability to adequate represent small-scale wave statistics.

- Application of the appropriate downscaling method to the long-term small-scale wave simulations for the last four decades, description of the obtained wave climate, revealing local changes and trends and relation of them to the regional atmosphere/ocean situation. Estimation of the magnitude and frequency of expected extreme wave events based on the obtained statistics.

- Application of the downscaling method to the climate change scenarios with the aim to compare the influence of different global scenarios on the local wave climate.

This thesis is grouped into three main parts and concluding comments. In Chapter 2 the basic concept of dynamical wave modeling and a brief description of the spectral wave model developed at the GKSS Research Center and used in this work are presented. The specification of the HIPOCAS hindcast data and the details of the high-resolution wave modeling experiment are given. The second part of this chapter is dedicated to the comparison of the HIPOCAS medium-scale and modeled small-scale wave parameters with observations from different sources, and to the evaluation of the quality and uncertainties of these two datasets in representation of the instantaneous wave parameters as well as wave statistics. In the last part of the chapter the simulated high-resolution wave data are compared to the data from the medium-scale hindcast with the goal of evaluating the added value obtained by the small-scale modeling focusing on wave extreme statistics. In the third chapter the statistical-dynamical approach to the downscaling of medium-scale wave data is investigated. Three statistical methods are proposed as possible candidates for the high-resolution wave downscaling models. The results of their application to the localization of medium-scale wave parameters are compared with the outcome of the dynamical model. Different aspects of the statistical approach such as application to the multiple downscaling of several wave parameters, potential restrictions and computational costs are considered and discussed. In Chapter 4 the results of the long-term high-resolution wave hindcast provided by the statistical model are described and the obtained extreme wave statistics are used for evaluation of the changes in past wave climate and for the estimation of the future wave extreme events. The connection between regional changes in wind and wave climate with the local extreme wave statistics is investigated and discussed. The high-resolution wave field projections obtained for the end of the 21 century based on the IPCC scenarios are assessed and the climate change issue is discussed in connection with the small-scale wave climate. General discussion and some concluding remarks close the thesis in Chapter 5.

Chapter 2

Dynamical wave modeling

2.1 Methods, data and tools

In this section the main principles and features of the spectral wave modeling are described. In particular the K-model is discussed as the main tool for the wave simulations. Subsequently, the HIPOCAS project, the main source of the external forcing data for the K-model experiments, is described. Finally, the model domain in the German Bight is specified and the details of the experiment setup are presented.

2.1.1 K-model. Description and features.

Wave models usually describe the evolution of a sea state depending on initial and boundary conditions as well as external fields like wind, currents and bathymetry. The sea state is defined as a number of wave trains with different wave lengths and periods generated at or coming to a specific location at certain time. Within this concept two classes of wave models can be distinguished (for recent overview see Ris [1997] or Cardone and Resio [1998]). So-called "phase-resolving models", characterized by explicitly determined superposition of wave trains considering their phases, belong to the first group. Such models are advantageous in the problems where the changes in the environment occur on the scale of wave lengths and periods or where diffraction is important. These models are often used for specific small areas such as harbors or for short-time applications. The second class contains "phase-averaging" or spectral models. In these models the wave trains which form the sea state are considered independently of their phases. With this approach the sea surface can not be described in detail and the spatial and time resolutions of these models are supposed to be larger than the typical wave length and wave period. These models are used for the most of medium and large scale applications due to the computational reasons as advantageous with respect to the phase-resolving models. They also allow the easier and more accurate consideration of the random-phase source functions such as wind energy input and wave dissipation. Further in this study the phase-averaging wave models are considered. The theoretical background for this kind of models can be found in Komen

et al. [1994]. Here only the main equation and related terms relevant for this work are introduced.

The linear wave theory was developed for the idealized conditions of homogeneous and stationary wave fields, then it was generalized for slowly varying fields (i.e. with the depth and currents slowly varying in space and time with respect to the wave length and wave period). The mathematical description of the sea state is given by the wave spectrum. Here the spectrum F(**k**) is defined as the density function of the energy distribution over the wave components with different wavenumber vectors **k**. The frequency-directional ($F(f,\theta)$) or wavenumber-directional ($F(k,\theta)$) spectra are also considered in applications. Frequency f and wavenumber k are connected by the Doppler shift equation and the dispersion relation:

$$2\pi f = \sigma(k,h) + \mathbf{k}\vec{U}, \qquad \sigma^2 = gk\tanh(kh)$$

where σ is the intrinsic frequency, h - the water depth, g - the gravitational acceleration and $\vec{U}$ - the current field. Since it is impossible to specify the instantaneous sea state in all details, the statistical theory of linear random waves describes the sea surface by the probability to find particular sea state. The sea state is defined as a superposition of waves with different surface displacements (η_i). The knowledge of the joint probability function of the surface displacements $P(\eta_1, \eta_2, \ldots, \eta_n)$ is generally required to find the probability of a certain sea state occurrence. The wave spectrum is then defined as the Fourier transform of this joint probability function. The evolution of the wave spectrum in time is described by the action balance equation:

$$\partial_t N + \nabla \cdot (\dot{\mathbf{x}} N) + \partial_k(\dot{k} N) + \partial_\theta(\dot{\theta} N) = S(N)$$

where $N(k,\theta;\mathbf{x},y,t)$ is the action density dependent on the wavenumber (k) and direction (θ) for each location ($\mathbf{x} = \{x_1, x_2\}$) and moment of time ($t$). Action density is connected to wave spectrum by

$$N(k,\theta,\mathbf{x},t) = F(k,\theta,\mathbf{x},t)/\sigma$$

The first term on the left-hand side of the balance equation represents the local rate of change of the action density in time, the second term represents the propagation of the action in geographical space. The third term represents the shift of wavenumber due to variations of depth and currents and the last term represents the refraction caused by depth and/or currents. The source function in the right-hand side of the equation represents the energy sources and sinks in the system. It varies within different formulations and generations of the spectral wave models and in general has the form

$$S(N) = S_{in} + S_{nl} + S_{dis}$$

where S_{in} represents the energy input by wind, S_{nl} represents the nonlinear wave interactions and S_{dis} represents the energy dissipation by several processes such as wave breaking, bottom interactions, etc. The specific form of the source function for the actual model is given in the next subsection.

For the wave simulation in this study the K-model is used, which is a third generation spectral wave model adapted to small-scale shallow water applications. Third generation models are characterized by the transition to full two-dimensional discretization of the wave spectrum instead of artificial separation of the wind and swell parts of spectrum. The development of third generation models started in mid 1980s by WAMDI Group [1988]. This approach has been successfully used for the major part of spectral wave models constructed for both open ocean applications (e.g. WAM-cycle4 (Günther et al. [1992])) and small-scale and shallow water applications (e.g. high-resolution version of WAM (Monbaliu et al. [2000]) or SWAN (Ris et al. [1999])). The K-model was developed on the basis of the WAM-cycle4 model with some changes aiming mainly at the adaptation of the model to small-scale coastal zone applications. With the increasing spatial and time resolutions and consideration of areas with shallow water and complex topography, the model faces the problems of inhomogeneity and non-stationarity of external fields. The main part of the wave theory was developed for idealized conditions which can be accepted for the most of medium-scale deep-water applications but need a strong revision and adaptation to the near-shore small-scale environment. The changes between WAM and K-model include transitions from the frequency-direction (f, θ) to the wavenumber-direction (k, θ) domain. This allows avoiding additional multipliers with partial time derivatives in the balance equation, which is crucial in non-stationary cases (Schneggenburger [1998]). Another difference is related to the form of the source function. Non-linear wave-wave interactions have been neglected following the reasoning of Schneggenburger [1998], who argued that in shallow water the assumptions of homogeneity for the application of this theory are violated. Instead, a non-linear dissipation source function (Günther and Rosenthal [1997] or Schneggenburger et al. [1997]), accounting for the dissipation by wave turbulence, is used. In the K-model energy input by wind is parameterized by a modified Philips linear function (Cavaleri and Rizzoli [1981]) and a modified Snyder exponential function (WAMDI Group [1988]) similar to the WAM model. Bottom dissipation is taken into account according to Hasselmann et al. [1973].

The modeled and measured wave fields were originally given in the form of a wave spectrum but for practical reasons different representations of spectrum or integrated parameters are used. This provides the opportunity to relate model results to observed data in a sense that integrated parameters can be easily statistically interpreted as characteristics of the sea state. The most usable integrated parameters are the moments m_n:

$$m_n = \int F(f, \theta) f^n df d\theta, \qquad n = -1, 0, 1, 2$$

and quantities related to them. The zeroth order moment m_0 is the total variance of the spectrum which proportional to the total energy and defines another frequently used integrated parameter the significant wave height (SWH):

$$H_s = 4\sqrt{m_0}$$

which corresponds to the mean of the highest third of the observed waves (Longuett-Higgins et al. [1963]). Different integrated periods can also be useful. The peak period T_p is defined

through 1-D spectrum $E(f)$:

$$E(f) = \int F(f,\theta)d\theta$$

$$T_p = f_{max}^{-1}, \qquad E(f_{max}) = \max_f(E(f))$$

Other integrated periods are defined as

$$T_{m_1} = \frac{m_0}{m_1}, \qquad T_{m_2} = \sqrt{\frac{m_0}{m_2}}, \qquad T_{mean} = T_{m_{-1}} = \frac{m_{-1}}{m_0}$$

and T_{m_2} period corresponds to the observed zero-upcrossing period. The mean wave direction corresponds to the next integrated parameter:

$$\bar{\theta} = \arctan \frac{\int F(f,\theta)\sin\theta df d\theta}{\int F(f,\theta)\cos\theta df d\theta}$$

Further, these quantities are used for comparison of model results with observations. Model output include integrated parameters for the total sea state, wind sea and swell as well as the full frequency-direction wave spectra for selected locations. The swell part is defined as the energy components which travel faster than parallel to them wind components.

The numerical schemes for the K-model implementation differ for the propagation-refraction part and for the integration of the source function. The explicit first-order upwind scheme was used for both propagation and refraction, similar to WAM cy. 4. The scheme is conditionally stable and the stability CFL criterion was applied in form

$$|\dot{x_1}\frac{\Delta t}{\Delta x_1}| + |\dot{x_2}\frac{\Delta t}{\Delta x_2}| + |\dot{k}\frac{\Delta t}{\Delta k}| + |\dot{\theta}\frac{\Delta t}{\Delta \theta}| \leq 1$$

For applications with prerequisite small spatial resolution or large external field gradients, such as highly variable bathymetry, the stability criterion can cause significant increase of model computational time since the integration time-step is decreased. This problem can be partially solved by applying the criterion to each part (propagation and refraction) separately and obtaining different suitable time-steps for propagation and refraction processes. Centered implicit scheme similar to WAM cy. 4 was taken for the source-term integration. This adaptation makes the K-model more appropriate to high spatial resolution applications. A more detailed description of the K-model can be found in Schneggenburger [1998].

Although those improvements have been made for reduction of the computational time of the K-model for the small-scale applications, the feasibility of multi-annual wave simulations was still in question. The code has been parallelized and run on a 7 CPU's node of DKRZ (German Climate Computing Center) super-computer. The improved model code was tested and performance was about 6 times faster than the original version.

2.1.2 HIPOCAS. Short project description.

As has been mentioned in Chapter 1, the part of this study is, in some sense, a logical extension of the HIPOCAS project towards a more detailed near-shore wave climate description. Keeping this in mind, the main part of the external data used for modeling in this study stems from the HIPOCAS results and it seems to be expedient to give a short overview of the project goals, implementation and results in this thesis. Here the motives and technical details of the project are briefly presented together with the description of datasets used in the K-model simulation. The main results of the HIPOCAS validation and data analysis will be described together with the similar tasks of the present study in following sections. This European project was carried out during 2000-2003 and was aimed at providing homogeneous and high resolution hindcasts of wind, wave and storm surge climatology for European Coastal Areas for the period 1958-2002. Detailed description of areas studied within the project can be found in Soares et al. [2002], further description here is restricted to the Southern North Sea region.

The quality of numerical wave and surge hindcasts is strongly dependent on the accuracy of the upper boundary conditions, i.e. driving wind fields. As has been shown in recent studies, the uncertainty in wind fields (Holthuijsen et al. [1996]) or a too coarse time resolution (Brauer and Weisse [2000]) have a considerable impact on the predicted wave fields. Therefore, obtaining more homogeneous and detailed wind fields was the first goal of HIPOCAS. This wind hindcast was based on NCEP (National Center for Environmental Prediction) reanalysis (Kalnay et al. [1996], R. Kistler and Fioriono [2001]) and subsequent dynamical downscaling. The regional atmosphere model REMO (REgional MOdel) was set up for the European coastal areas as well as for the areas relevant to the generation of swell which may propagate into selected coastal seas. It was driven on lateral boundaries by the NCEP reanalyzed atmospheric fields with 200 km resolution. The results were stored every hour on a spherical grid with a resolution of about 50 km (for details see Feser et al. [2001]). This dataset is referred to later as the REMO wind.

The hindcast of the sea level evolution and current components was performed by the Coastal Division of the Federal Engineering and Research Institute (BAW) with the finite element hydrodynamical model TELEMAC2D. The model was driven by the REMO wind and the influence of Atlantic external surges has been taken into account by assimilating water elevation measurements at Aberdeen. Results, available on an irregular grid from few kilometers in the Northern North Sea to hundred meters in German Bight, were saved hourly. For the wave hindcast the WAM-cycle4 wave model was set-up with a one-way nesting technique. The coarse grid with spatial resolution of 0.75° lon. x 0.5° lat covered the entire North Sea and part of Northeast Atlantic. For this simulation the WAM deep-water version was governed by the REMO wind. The model output was stored every 3 hours and later referred as the HC (Hipocas Coarse) run. The nested fine grid covers the Southern North Sea between 51°N and 56°N, and between −3°W and 10.5°E with a resolution of about 5 x 5 km. It was driven by hourly REMO wind fields and HC wave spectra on the boundaries. In addition, for this run, the shallow water effects have been taken into account by using the shallow-water version of the WAM model. Model results

including wave spectra were stored hourly and referred to later as the HF (Hipocas Fine) dataset.

2.1.3 Experiment setup. Model domain, boundary conditions and forcing fields.

As an example coastal area for high-resolution shallow water wave modeling experiments, the Helgoland Islands and surroundings have been chosen. Two islands (Helgoland and Düne) are situated in the south-eastern part of the German Bight about 70 km off the mainland. The islands have a size of about 1 and 0.6 sq.km. The main-island harbor is protected by a breakwater ring. In addition, numerous breakwater walls provide protection of the coasts from the wave influence. Most of these constructions are up to 90 years old and some of them were partially damaged during the war and later not completely reconstructed. In recent times there were attempts to reassess local wave climate and extreme wave statistics using state of the art wave models and to evaluate safety ability of existing protection constructions (Vierfuss [2002]). Further steps towards the local wave climate

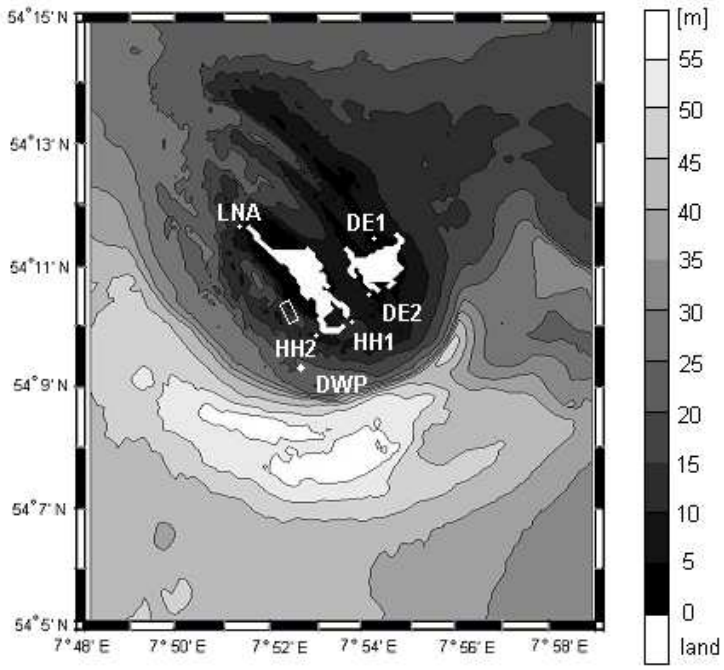

Figure 2.1: K-model domain and bathymetry in meters. The location of a deep water buoy used for validation is indicated by DWP. The rectangle indicates the area for which radar measurements taken from a telecommunication tower at the main island are representative. LNA, HH1, HH2, DE1 and DE2 represent model points near coastal facilities and are used for assessing model performance.

assessments are made in this work. The bathymetry of the area around Helgoland is characterized by a large water depth gradient to the west and south from the islands (Fig. 2.1). It is believed that because of the complicated topography, the shallow water near-shore area and the small size of the islands themselves, the wave parameters at the coastal zone are not adequately represented by the medium-scale North Sea wave hindcasts like HIPOCAS and additional refinement of the wave data with consideration of shallow water processes is required to obtain the reasonable near-shore wave statistics. This makes the Helgoland area a good example for testing the quality of the medium-scale wave hindcast. At the same time, the local wave hindcast obtained during the work is useful for the local coastal protection. For these purposes the dynamical wave model is applied to the high-resolution wave simulations in the Helgoland coastal zones.

To create adequately developed and remote enough from the lateral boundaries wave spectra at the near-shore zone, and having in mind the spatial resolution of the boundary spectra, the model domain is set up as a 10 x 15 km area around Helgoland islands (Fig. 2.1). Spatial resolution is chosen based on a balance between the accuracy of the wave representation adequate for for the engineering purposes and the computing resources required. Computational costs increase significantly with the refinement of the spatial resolution, partially because of the increased number of the active model points, and partially because of shorter model integration time steps required by the stability conditions of the numerical scheme. Finally, 100 m equidistant spatial resolution and 4 second propagation time step were adopted. During model integration, wave spectrum has 28 wavenumber and 12 wave direction bins.

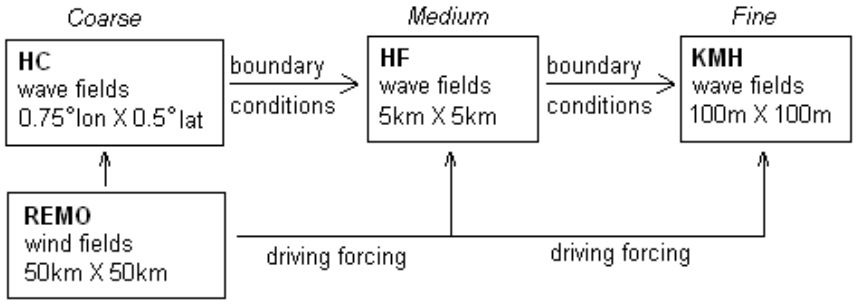

Figure 2.2: The main experiments discussed in this chapter.

The bathymetry of the model area was obtained from the BAW (Norbert Winkel, pers. comm.) in an unstructured grid about 50 m and interpolated to the K-model resolution. 3-hourly wave spectra from HF dataset were used as boundary conditions for the high-resolution K-model simulation. Forcing sources comprise hourly 10 m height wind fields from the REMO dataset, time-variable water depth and currents. For obtaining the latter, two datasets of hourly water level and current fields from HIPOCAS were interpolated in space to the K-model grid. In previous long-term wave simulations (e.g. WASA, HIPOCAS) the changeable water depth and currents were not considered. In this study the influence

of these fields on the simulated wave parameters was found to be appreciable and will be discussed in the next chapter. Finally, integrated parameters at each grid point of the K-model domain were stored hourly as well as the wave spectra for certain locations near the protection facilities. This high-resolution wave simulation has been performed for the 12-year period from January 1990 until November 2001 and referred later as KMH (K-Model Hindcast).

2.2 Model validation

Comparison of the modeled data with observations is one of the necessary conditions for further confident utilization of model results. For the K-model in the described formulation, several validation experiments have been provided for different areas, time and spatial scales and variable internal model parameters. The ability of the model to reproduce integrated wave parameters on medium scales for the shelf seas and comparison with the results from another wave models such as WAM or HYPAS (Günther and Rosenthal [1985]) was shown by Schneggenburger [1998] with the example of Noth Sea storm. In the same work, the applicability of the K-model to small tidal basins with variable currents was studied with the example of the Sylt-Rømøbasin (eastern North Sea). Until now most of the validation experiments for the K-model considered instantaneous integrated parameters obtained for periods of several days to several months or selected storms. In this section the results of the K-model validation for Helgoland are presented. Most of the experiments are aimed at elaborating the quality of K-model long-term results in a statistical sense and at checking the existence of systematic errors coming either from K-model itself or from the external forcing fields. Although the main part of the validation experiments for the HIPOCAS wind and wave fields was carried out within the project (Weisse et al. [2002]), here some additional comparisons for German Bight are made between the HF wave heights and satellite data with the aim to assess the rate of the error provided by boundary conditions into the KMH simulation. It is shown later to what extent observed wave conditions are reproduced by KMH. The main sources and characteristics of uncertainties which should be considered during further data analysis are pointed out.

2.2.1 Comparison of the HIPOCAS wave statistics with the satellite data

Satellite altimeter data is a commonly used source for the model validation and data assimilation procedures. Altimeter wave data from ERS2 and TOPEX satellites is available for the German Bight for several years in late 90s. The tracks of both satellites do not pass through the K-model domain and therefore cannot be used directly for comparison with KMH results. However, satellite data provides the opportunity to assess the quality of the HF wave hindcast for the Helgoland surroundings and, therefore, to make an additional evaluation of the boundary conditions for the K-model hindcast. Earlier, ERS2 altimeter

data was compared with HF wave simulation for the southern North Sea and slight overestimation of high waves by the model has been revealed (Matthias Zahn pers. com.). In the present study a similar comparison has been made for the surroundings of Helgoland using three sources of altimeter data. The TOPEX wave data was obtained from the GFZ-Potsdam dataset (Schöne et al. [2000]). Two differently processed datasets for the same period were available from the ERS2 satellite, namely, the Meteomer dataset (Bonicel et al. [1997]), later referred to as ERS_Met and the GFZ-Potsdam dataset (ERS_Pot). All the data for significant wave height (SWH) was selected for the period 1998-2000 and the area from 6°E to 8.4°E and from 53.6°N to 55.8°N. Each observation record was representative for mean over an area of about 6x6 km. Hourly SWH fields from the HF simulation were used for comparison. Only the altimeter data, for which times differ from the HF model times by less than 10 minutes, were used so as to avoid the time interpolation.

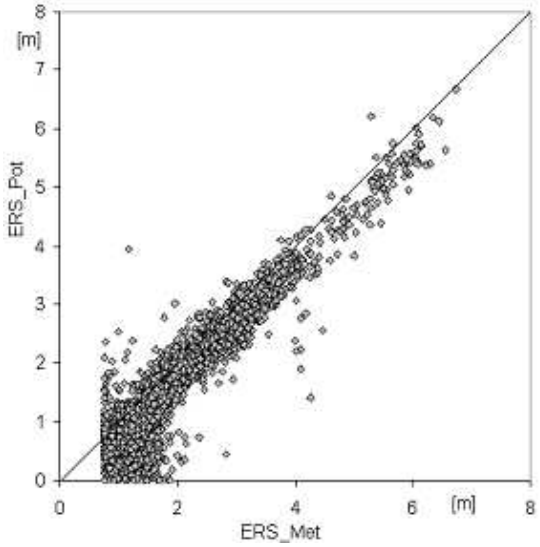

Figure 2.3: Significant wave heights from the ERS satellite altimeter datasets postprocessed by Meteomer (x-axis) and GFZ-Potsdam (y-axis) for the period 1998-2000.

Figure 2.3 shows the results of comparison between ERS_Pot and ERS_Met datasets. From the scatter-plot it is revealed that the two datasets differ significantly. Firstly, it concerns the processing of small waves where for ERS_Met the cutoff at 0.77 m was accepted. For the waves higher than 2 meters the wave heights from ERS_Pot dataset are, in general, lower than the data from ERS_Met with the bias of about 0.37 m. Thus, together with high correlation (0.94) the differences between two processing procedures are mainly expressed by SWH bias. It is beyond the scope of this study to develop any correction techniques or to investigate which altimeter data is more reliable, but the differences described above should be taken into account during the analysis of the model data. There is no opportunity to compare ERS_Pot and TOPEX wave heights for the area and period of interest because most of the time their tracks do not cross each other.

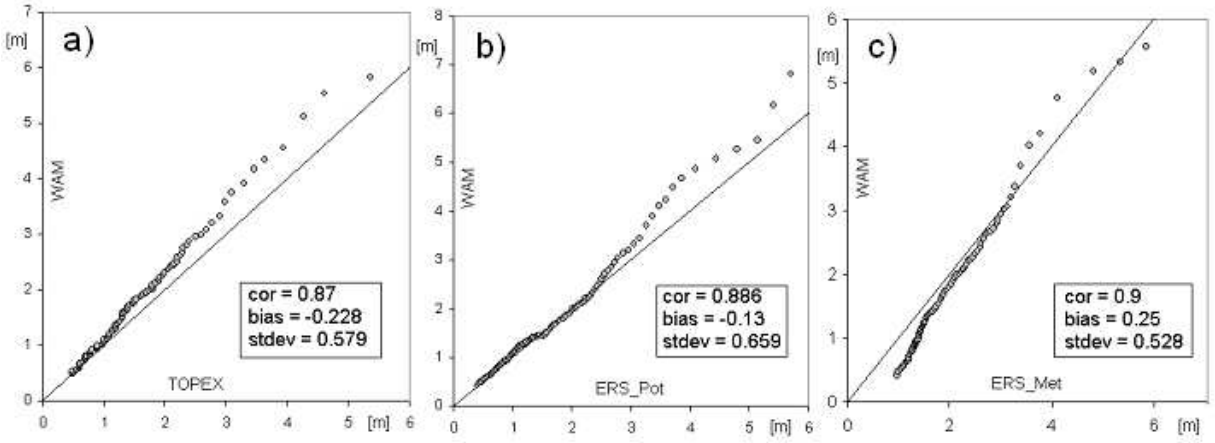

Figure 2.4: Quantile-quantile plots of SWH between satellites (x-axis) and WAM model results (y-axis) for common dates during the period 1998-2000. Quantiles from 0.01 to 0.99 are shown with 0.01 interval.

To evaluate the correspondence of the HF modeled wave heights with different altimeter datasets, the quantile-quantile plots were used and correlation, bias and standard deviation were calculated for each pair of datasets (Fig. 2.4). Modeled SWH data shows similar behaviour with respect to ERS_Pot and TOPEX datasets characterized by overestimation of waves higher than about 2-3 meters. For TOPEX this overestimation is more pronounced and appears for the wave heights starting from 2 meters which amounts to 20% of the highest waves. In case of the ERS_Pot dataset the modeled SWH values are too large for upper 15% of the waves. The bias is larger with respect to TOPEX for the modeled data (0.23 m for TOPEX vs. 0.12 m for ERS_Pot). With respect to ERS_Pot, model results appear to be slightly more scattered with standard deviation 0.66 for ERS_Pot and 0.58 for TOPEX. These moderate deviations together with rather high correlation coefficients suggest a generally good agreement between modeled and observed SWH up to 85 percentiles. Coming to ERS_Met data, it can be seen that the shape of quantile-quantile dependency is similar to that of ERS_Pot with obvious bias detected from the comparison of these two satellite altimeter sources. Nevertheless, the correlation between ERS_Met and HF wave heights is slightly higher than for other satellites. Summarizing, modeled HIPOCAS fine grid wave heights are overestimated for upper 10-15% of the waves for the German Bight, which corresponds to earlier validation experiments carried out within HIPOCAS project for the southern North Sea.

2.2.2 Comparison of the K-model results with in situ measurements

For the period of interest there were no long-term measurements close to coastal facilities but within the model area two wave observed datasets are available. The first one is

provided by the BSH (Bundesamt für Seeschiffahrt und Hydrographie) waverider buoy located approximately one kilometer south-west from the island. The water depth there is about 20 m. The measured quantities comprise 9 parameters from which significant wave height, peak period and mean direction for the period from March 1998 to October 2001 are used for the comparison with the K-model results. Another data source is the WaMoS II (Wave and Surface Current Monitoring System) radar (Hessner et al. [2001]) permanently mounted on a telecommunication tower on the main island since March 1998 and providing wave parameters averaged over the rectangular surface area in a distance of about 500 m south-west from the islands (Fig. 2.1).

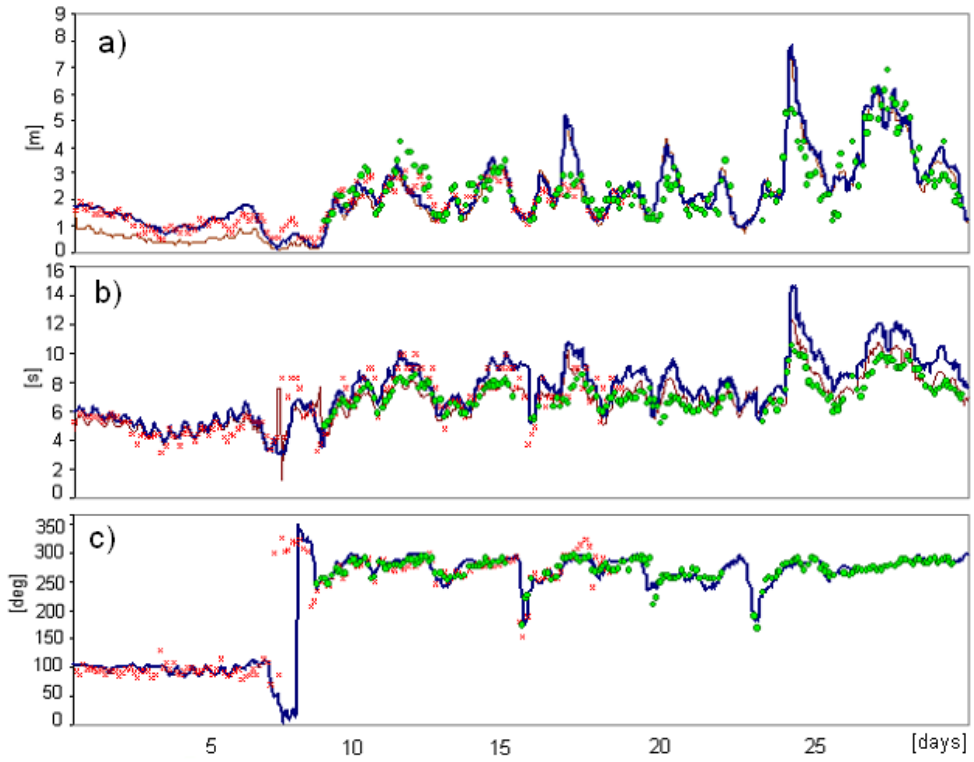

Figure 2.5: Hindcast (KMH) and observed wave parameters at DWP and the central point from the area covered by radar measurements for October 1998. From top to bottom: significant wave height in meters, peak period in seconds and mean direction (coming from) in degrees. Buoy measurements are shown as crosses, radar measurements are shown as circles. The K-model hindcast at the buoy (DWP) location is given by a blue line; hindcast at the central point of radar rectangular is given by a thin brown line.

At first, to assess the quality of modeled instantaneous values with respect to observations, significant wave heights, peak periods and mean directions from all three data sources (K-model, buoy and radar) were compared for October 1998 (Fig. 2.5) and in general a good agreement between all datasets can be inferred. A closer look at differences provides a reasonable explanation for the major part of them. At the first decade of examined month the

modeled SWH values are lower at the radar area than at the buoy position. At the same time easterly wind dominates the territory which causes the island shadow effect in the area located west from the islands making the waves smaller. This effect is diminished at the DWP position located farther to the south, which is in agreement with the buoy observations (Fig. 2.5a). The radar data for this case is not available. For the second part of the period considered, the buoy and the radar observations are close to each other as well as to the model results at the two locations. The discrepancy between observed and modeled data occurs for some high wave situations where SWH appears to be overestimated by the model. A similar tendency was observed for the HF SWH with respect to the satellite data (2.2.1). The impact of the boundary conditions (HF) on the K-model results is discussed later. For peak periods, more pronounced differences between buoy and radar locations for the measured as well as for modeled data can be detected. Slight overestimation of peak periods by the model, especially for some high wave situations, can be observed. The measured wave directions are similar for both locations and the hindcast produced by the K-model appears to be quite reasonable and close to the observations.

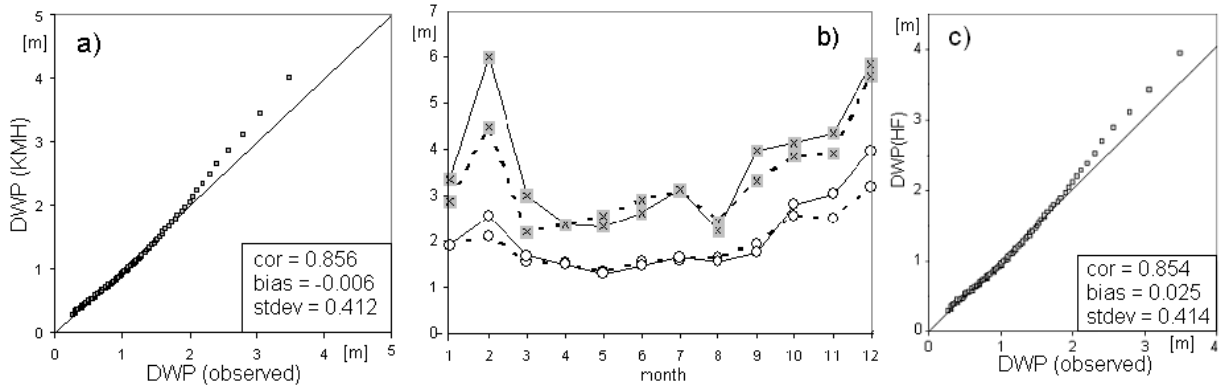

Figure 2.6: a) Quantile-quantile plot of observed by buoy (x-axis) and hindcast by K-model (y-axis) significant wave heights at DWP for 1998-2001. Quantiles from 0.05 to 0.99 are shown with 0.01 interval. b) Observed (dashed) and hindcast (solid) monthly 90%-tiles (circles) and 99%-tiles (crosses) of significant wave height at DWP. In all cases quantiles have been compared only for dates for which observational data have been available. c) Quantile-quantile plot of observed by buoy (x-axis) and hindcast by HIPOCAS (y-axis) significant wave heights at DWP for 1998-2001. Quantiles from 0.05 to 0.99 are shown.

Figure 2.6a shows a comparison of modeled and observed significant wave height distribution for the period 1998-2001. For the lower 90% of the distribution a rather good agreement between model and buoy observations can be seen. In the range between about 1.0 to 1.5 meters the K-model slightly underestimates the buoy data. For the highest 10% of the waves an overestimation by the K-model of up to 80 cm can be inferred, indicating that the highest waves occur too often or are too severe in the KMH simulation. Figure 2.6b shows a more detailed comparison of observed and hindcast averaged monthly 90 and 99-

percentiles. For the 90-percentile a reasonable agreement can be inferred. An exception is found in the months November, December and February for which the model tends to show higher extremes. A similar condition holds for the 99-percentile that represents the most extreme events. For the 99-percentile KMH values are somewhat higher also for March, September and October.

To check whether the overestimation of the high waves is caused mainly by the driving boundary conditions or by the K-model physics, percentiles of the HF hindcast and the buoy SWH data were compared (Fig. 2.6c). The overestimation of observed high waves was found to be of the same order of magnitude for the HF run as for the K-model. This bias in upper percentiles of boundary conditions (HF) is consistent with the results of the HF comparison with satellite data for the German Bight shown in 2.2.1. This behaviour can be explained by deficiencies of the model spatial resolution or by the uncertainties in driving forcing and model physics of the HF run. In case the bias is caused by a too coarse spatial resolution of the HF run, the K-model is supposed to improve the wave data representation with respect to HF by taking into account processes on finer scales. However, this can be not the case for the buoy position because of the relatively deep water at the location (20 m), which diminishes the importance of such wave processes as refraction and bottom dissipation. The errors in the HF data caused by uncertain external forcing or internal physics can hardly be corrected by the K-model because a higher (in case of overestimation) energy is expected to be transferred by the K-model to the interior locations from the boundaries. Consequently, it can be concluded that the overestimation of the most severe wave events is at least partially a result of the too high waves provided at the K-model boundaries. In addition to the biased boundary conditions, the possible reasons of the K-model and buoy data discrepancies are the uncertainties in bathymetry and wind data used by the K-model as well as measurement errors.

2.3 Added value for the small-scale wave simulation in terms of extremes

The previous section demonstrated the similarity of the local wave parameters modeled by the K-model and measured wave data. The differences between the model results and observations at DWP can mainly be attributed to the driving HF hindcast. Based on this, it is assumed that the small scale features simulated by the K-model share some resemblance with reality and, therefore, the KMH experiment is considered in the following as a substitute for reality. This allows the testing of to what extent improvements in the representation of near shore extreme wave statistics can be achieved by the application of dynamical wave modeling (here K-model) to the medium-scale wave data (here HF). The improvement will be assessed relative to the HF hindcast, as these data is readily available and thus can be considered as a first guess of the prevailing near-shore wave conditions.

First the extent to which the HF hindcast may be used to reasonably assess long-term wave statistics in the coastal zone is investigated. Here the evaluation is mainly focused

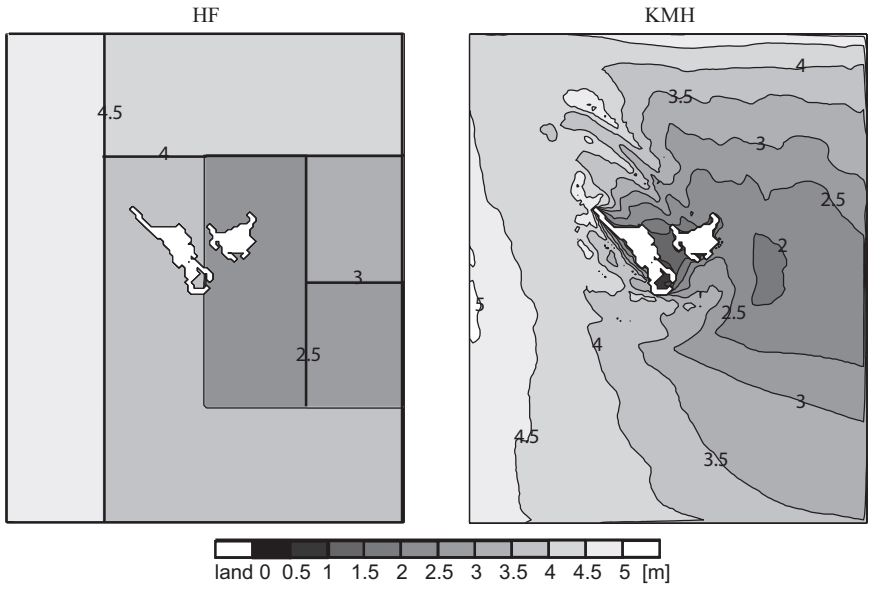

Figure 2.7: 99%-tiles of significant wave height in meters derived from 3-hourly data for the period 1990-2001 from the HF hindcast (left) and KMH experiment (right).

on the statistics of extreme events for the significant wave heights as they are essential for coastal protection. Additional information about the quality of instantaneous HF wave heights and other wave parameters is given in the next chapter in the context of the quality assessments for different downscaling models. For the current experiment three datasets are analyzed, namely significant wave height from the HIPOCAS coarse grid hindcast with about 50 km resolution (HC), the HIPOCAS fine grid hindcast with about 5 km resolution (HF) driven by the HC simulation, and the KMH hindcast with 100 m resolution driven by the HF run (see also Fig. 2.2).

Figure 2.7 shows a comparison between the 99-percentiles of significant wave height for the period 1990-2001 obtained from the HF and the K-model hindcast. It can be seen that for both simulations a similar large-scale pattern of extreme wave statistics is reproduced. The pattern is characterized by highest waves occurring in the western part of the K-model domain that continuously decrease eastwards. East of Helgoland a distinct area with relatively low wave extremes can be found which is mainly caused by the shadowing effect of the islands against the prevailing wind and wave directions. The large-scale similarity between both simulations is primarily a consequence of both simulations having identical wave conditions at the K-model boundaries or, in other words, that the K-model uses boundary conditions from the HF hindcast. In addition, the same wind fields have been used in both simulations.

Despite a large-scale similarity between the HF and the KMH hindcasts, small scale differences in extreme wave statistics are obvious (Fig. 2.7). In particular, the island shadow effects are more pronounced and extend further eastward in the K-model simulation. South-

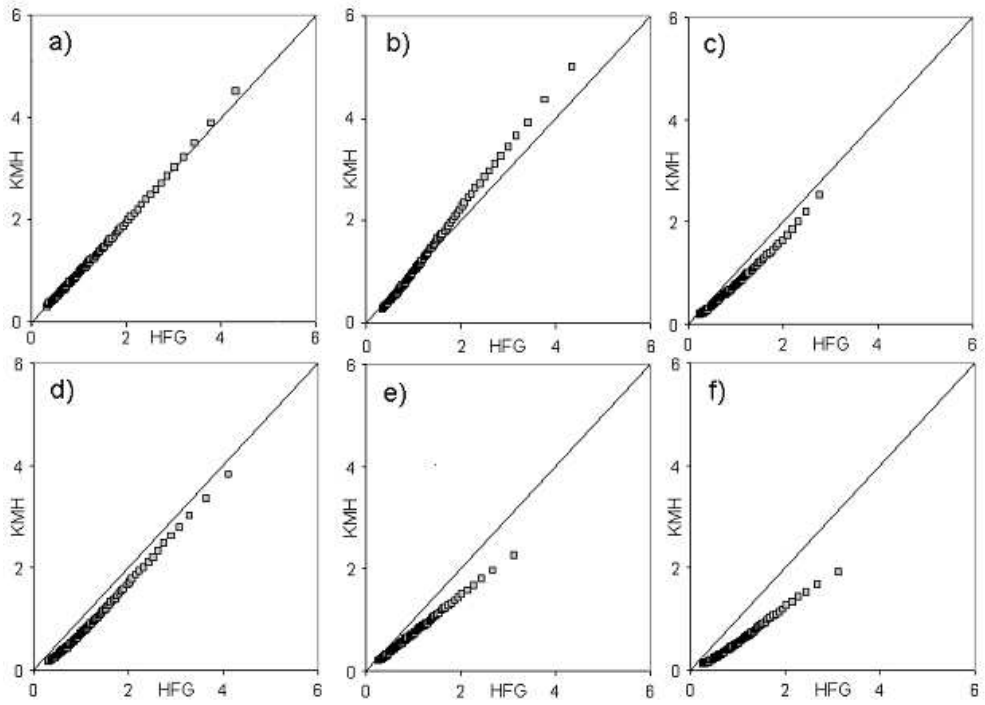

Figure 2.8: Quantile-quantile plots of HF and KMH simulated significant wave height in meters for the period 1990-2001 at points a) DWP b) LNA c) HH1 d) HH2 e) DE1 f) DE2.

eastwards of Helgoland the 99-percentile of significant wave height is about one meter higher compared to the HF simulation. Furthermore, for the K-model run, small scale features of the bathymetry are visible in the distribution of the wave extremes. While large-scale features of extreme wave statistics are quite similar in both simulations, the small scale differences may be significant for coastal protection. Figure 2.8 shows a comparison of the frequency distribution for significant wave heights near different coastal facilities obtained from the HF and the KMH hindcasts. The positions of the analyzed points can be inferred from Figure 2.1. Although the K-model is driven with boundary conditions from the HF run and both simulations utilize the same wind forcing, differences in the frequency distributions, in particular for near coastal locations, do emerge. The details of these differences depend on the location. At DWP both hindcasts are rather similar. Here water depth is about 20 meters and the shadowing effect of the island plays a minor role as the prevailing wind and wave directions are from the southwest to the northwest. At LNA the situation is different. LNA is also located at the western side of the island, but here bathymetry effects become important. While the lower 75% of the simulated wave height distributions are still rather similar in the HF and the KMH, the uppermost 20% are remarkably higher in the K-model simulation (Fig. 2.8b), demonstrating the results of shoaling[1] for the KMH waves.

[1]Shoaling occurs when the waves enter shallow water. The wave speed and wave length decrease,

Near the Helgoland harbor (HH1, HH2) shallow water effects and the strong gradients in the bathymetry play a significant role. Here small water depths cause the reduction of the wave heights and, independently of their heights, waves are generally lower in KMH. To the east of the main island, waves are also generally smaller in the K-model hindcast. This can be inferred from the comparison of the wave height frequency distributions at DE1 and DE2, two locations near the coastal protection structures at the north and south shores of the smaller Düne Island (Fig. 2.8e,f). Generally, the effect is larger for higher waves and mainly results from a combination of lee and shallow water effects. Although the differences between HF and KMH wave statistics are significant and strongly location dependent, it appears that for all locations the relationship between KMH and HF wave statistics is almost linear which is also the case for the instantaneous SWH values (not shown here).

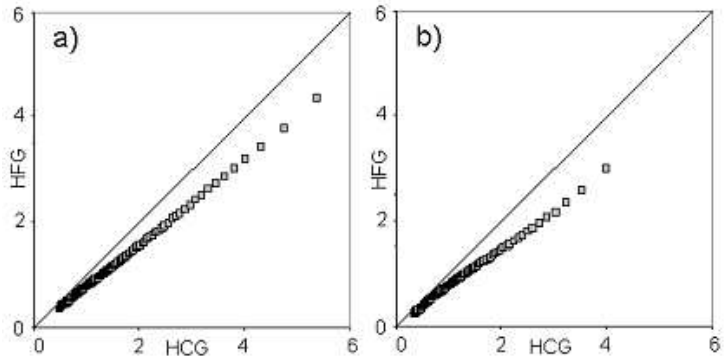

Figure 2.9: Quantile-quantile plots of HC and HF simulated significant wave height in meters for the period 1990-2001 at points a) LNA and b) DE1. Quantiles from 0.05 to 0.99 are shown with 0.01 interval.

For completeness, an analogous comparison has been made between the HC and the HF hindcast. Results for LNA and DE1 are shown in Figure 2.9. The situation is similar to the comparison of the HF and the K-model hindcasts. Both simulations (HF and HC) utilize the same wind forcing and the coarse grid simulation provides the wave boundary conditions for the medium-scale hindcast. Comparing the HC and the HF simulations, the general overestimation of the SWH by coarse grid run is observed. Partially, this is caused by the differences in the WAM model setup, namely in the water depth treatment for these two simulation runs. Namely, in the case of HC, the deep-water version of the model was used, which does not include refraction. At the same time large fraction of the differences in the simulated wave height distribution may be attributed to the presence of the islands. While they are present in the HF simulation, the islands have not been considered in the HC hindcast as they are too small to be resolved in the spatial resolution used. As a result waves are generally higher in the HC hindcast. Summarizing, the spatial resolution is an important issue for the modeled wave statistics representation as well as for the consideration of the variable limited water depth and shallow water processes.

consequently, the energy per unit area increases, following by the increasing of the wave heights.

2.4 Summary

In this chapter an overview of the dynamical approach to the high-resolution wave modeling for coastal zones was given and the wave simulation experiment with the spectral wave model was defined. The K-model was applied to produce 12-year hindcast of the high-resolution wave fields for the Helgoland coastal area using the wave and wind fields from the HIPOCAS project as boundary conditions. During the quality test of the boundary conditions the results of the comparison of the HF wave fields with the satellite data for the German Bight appeared to be consistent with the validation experiments made earlier for HF datasets and showed a good agreement with the observations, with the tendency to overestimate the highest 10% of the waves.

During the comparison of the KMH instantaneous wave parameters (significant wave heights, peak periods, mean directions) with the data from the waverider buoy and from the WaMoS radar situated in the area, the modeled wave representation was found to be realistic. Analyzing the wave statistics, the simulated data showed a good agreement with measurements in terms of distributions, although the upper percentiles of the modeled SWH appear to be overestimated. The latter is partially caused by the boundary conditions which provide too high waves in the case of severe storms. Finally it was concluded that the KMH shares some resemblance with reality and in the following part of the study will therefore be considered as a "substitute reality".

The comparative analysis of the wave height frequency distribution and extreme wave statistics from the HC, HF and KMH experiments representing the wave simulations on different scales has revealed that spatial resolution and shallow water effects may have a significant influence on the wave statistics. The impact of the dynamical refinement procedure is not uniform among the different locations around the island. In this way, for some location these effects can be crucial for the assessment of near-coastal wave climate.

The possibility of the spectral wave model application to the very high resolution multi-decade wave hindcast is limited by the fulfilment of several conditions. One is the presence of adequate medium-scale boundary conditions and relatively good resolved forcing fields such as water depth variations and currents. Another condition is the ability of the model to produce long-term simulations within feasible time. For the spectral wave models, including K-model, the consideration of high spatial resolution is followed by an enormous increase of the model integration time. In this case some additional methodology is needed to transfer the information from a long-term, but poorly resolved hindcasts (such as the HF simulation), to local wave conditions similar to that obtained with the dynamical model.

Chapter 3

Statistical-dynamical approach to the wave simulation

It has been shown in the previous chapter that for an adequate assessment of the nearshore wave statistics the large-scale wave data needs additional processing or downscaling. The spectral wave model provides successful dynamical downscaling. However, faster methods are sometimes required, especially in case of long-term hindcasts or scenario studies and of limited computational resources. The strong dependency of the local (KMH) wave parameters on the boundary conditions (HF) provides the opportunity to apply less time-consuming empirical downscaling models transforming medium-scale HF wave conditions directly to the detailed high-resolution wave fields. The basis for the construction of the statistical inter-scale relationships is provided by the medium-scale HF wave dataset and by the corresponding local wave data obtained with the K-model. In case of reliable and sufficiently homogeneous long-term measurements being available at the site of the construction, they may be used instead of the K-model data. However, when such data is not available, or information for some area surrounding the observation location is also required, a very high-resolution wave model simulation (such as KMH), validated with at least some existing data, is the best possible option. Thus, the combination of the statistical methods and high-resolution wave data obtained with the dynamical method form the statistical-dynamical approach investigated further.

In this chapter the general concept of downscaling is described together with a review of the methods and recent applications. Several statistical techniques are applied to the wave parameter downscaling with the main goal to obtain reliable small-scale extreme wave statistics. The results of the method's application to the Helgoland area are compared between each other and with the independent dynamically obtained wave data. Comments about the performance of the models, improvement options and potential limitations conclude the chapter.

3.1 Downscaling introduction

The concept of downscaling is the translation of the climatological fields across the spatial scales. It is based on the idea that regional or local climate is conditioned by larger-scale climate and, therefore, the information about the global (or regional) climate together with some of the regional (or local) details, such as topography or coastlines, define to some extent the local climate. Historically, the idea of downscaling can be traced back to works from the mid of the twentieth century in synoptic climatology and weather typing (e.g. Grosswetterlagen (Baur et al. [1944]), Barry and Perry [1973]) where the types of synoptic situations were related to distinctive local weather patterns. The term "downscaling" was introduced relatively recently, initially in connection with the General Circulation Models (GCMs). The GCMs are the commonly used tool for impact, change and scenario studies on global or continental scales. They are able to model the system response to large-scale external or internal perturbations. At the same time GCMs have a of parameterizations for small-scale physical processes and rather coarse resolution (the best one at the moment is about 100 km), which is an obstacles to an adequate description of local climate. One of the main objectives of the climatological studies is the application of atmospheric or ocean data to reveal the economically or socially related impact of physical environment on human system. This requires the impact and changes to be on a local-scale basis and that is hardly reliable even with state of the art GCMs. Thus, a need for a more detailed climate description was recognized and the downscaling concept seemed to be the logically straightforward approach to the problem. The discussions of the GCM's abilities of regional climate assessments along with the proposed and applied downscaling methods can be found in numerous studies (e.g. von Storch et al. [1993], Hewitson and Crane [1996] and references therein). The downscaling procedure was later transferred to regional and local-scale applications.

The downscaling techniques can be divided into two general categories. One is the process related methodology based on a regionally/locally scaled dynamical model driven by the larger-scale (for example GCM output) information. This approach is focused on nested models and is implemented, for example, in the Regional Climate Models (RCM) (e.g. Denis et al. [2002]). The direct description of the small-scale physical processes in the model makes the relations between large and small scale fields flexible within the determined physical laws. The response of the system to external perturbations has theoretical basis which helps to understand and explain the system behaviour. It is difficult to consider all processes influencing the system. For a part of local processes the precise form of the dependency is often not clear, so they are skipped or replaced by more simple parameterizations. This adds some uncertainty in representation of the modeled system. On the other hand, the increase of the number of processes considered in the model processes makes the model more complicated. Such models are often computationally demanding and their applicability for long-term simulations and impact studies is limited.

The second category includes empirical downscaling techniques. In these methods the relationship between the fields on different scales is derived empirically and usually from

observed data. The small-scale fields consistent with the modeled large-scale situation can be found directly, applying the derived relationship to the large-scale modeled data. The obvious benefit of the empirical methods is the computational efficiency with respect to the dynamical approach. The derived inter-scale connections often help to explain or better understand the relations between the fields for which the physical picture is not completely clear. Thus, the method serves both the assessment of the small-scale variables unreachable with the dynamical models and the investigation of the inter-scale relation principles. The general limitations of the empirical methods comprise the necessity of availability of sufficiently long observed data for the empirical model construction and fulfillment of several assumptions on the properties of the data and relations. For the application of the empirical downscaling the validity of three conditions is assumed: (a) the large-scale predictors are realistically modeled by the global/regional model, (b) the relation between large and small scale fields remains unchanged under the changing climate conditions, (c) the predictor fully represents the climate change signal.

The relative simplicity of empirical downscaling methodology, as well as the time-saving procedure and the broad applicability, made them an appropriate tool for re-scaling applications on various scales and for a wide range of fields. Despite numerous studies and widespread applications of the empirical downscaling, there is no unified gradation of downscaling techniques according to their abilities. Therefore, for different predictors and predicted fields, scales (from global to regional, from regional to local) and desired statistical parameters (e.g. daily or monthly means, seasonal anomalies or yearly extremes, etc.) the downscaling models are normally constructed and tested on a case-by-case basis. A review of downscaling methods, their prospects and limitations in the connection to GCM output downscaling can be found, for example, in Wilby and Wigley [1997] or Murphy [1999]. A review of empirical downscaling techniques and a set of references on recent works concerning downscaling applications for various fields and scales can be found in von Storch et al. [2000] or in IPCC TAR WG1 Section 10.6 (Giorgi et al. [2001]).

Here the classification of empirical downscaling methods similar to that in IPCC TAR 2001 is briefly presented focusing on the methods used further in the study. The variety of the empirical downscaling methods can be grouped into three types. For the regression-like techniques, the statistical relation in form of *transfer functions* between the single point or field of large-scale predictor and the small-scale predictand is derived. This category comprises linear and non-linear methods. Typical and frequently used linear techniques are the linear regression and the Canonical Correlation Analysis (CCA). They are applied, for example, in ocean-related studies where the relation between sea-level pressure and monthly sea-level variations (Cui and Zorita [1998]) or yearly salinity variability (Heyen and Dippner [1998]) is explored. Other studies were dedicated to the modeling of extreme events in form of upper monthly or seasonal percentiles of wave heights (WASA Group [1998]) or storm surges (e.g. Langenberg et al. [1999]). The non-linear approach includes models based on artificial neural networks. They are applied when the inter-scale relations are not completely clear or have considerable non-linearities. A neural network is often more powerful but less interpretable than a linear method. Examples of applications can

be found in Crane and Hewitson [1998] or Weichert and Bürger [1998]

The next empirical downscaling type is formed by the *weather typing* approach evolved from the traditional synoptic climatology. Here the weather classes or circulation patterns are defined according to certain classification scheme. This can be objective methodology like the Principal Components Analysis or a subjective classification (e.g. Grosswetterlagen). Then each weather type is related to a certain local situation or variable. The observed data is often used for relation detection. For each weather type the corresponding local situation is sometimes simulated with a dynamical model. The method is then referred to as statistical-dynamical downscaling. One of the variety of the classification downscaling techniques is the analog method. Here each large-scale record is considered as a single class. The method was described and applied for example in Zorita and von Storch [1999]. The third type of empirical downscaling methods includes *weather generators*. These stochastic models replicate not the observed sequence of events, as in the case of the other two types of the downscaling models but the statistical properties of small-scale fields such as means or variance. Most of the applications are related to the representation of daily precipitations and some secondary variables like temperature or wet-day amount (e.g. Wilks and Wilby [1999])

3.2 Wave modeling with empirical downscaling techniques

Turning to the problem investigated in this study, the downscaling methods are considered as a tool for the small-scale near-shore wave modeling. The abilities of the dynamical approach have been tested in previous chapter on the example of the shallow water wave model. To test the extent to which empirical downscaling in combination with high-resolution dynamical wave modeling can be used to assess the near-shore wave climate, several statistical methods are applied to the problem. The basis for the construction of the statistical inter-scale relationships is provided by medium-scale wave fields obtained from the HF hindcast and the local wave data from the K-model simulation.

Downscaling techniques such as Canonical Correlation Analysis or analogs are often applied to monthly, seasonal or annual statistics (e.g. Zorita and von Storch [1999] or WASA Group [1998]). However, some applications, such as the simulation of ship movements, would require high-resolution instantaneous data. Therefore, the extended downscaling concept is proposed and its ability to estimate 3-hourly wave data is tested. Instead of directly linking large and small scale wave statistics, all statistical models related 3-hourly wave data from the HF and the K-model hindcast. Small-scale wave statistics is derived subsequently from the instantaneous data. The most required wave parameter is the significant wave height (SWH), so, for simplicity of the models comparison and as a first step, all experiments in this section are limited to SWH downscaling. Having in mind an almost linear relation between the HF and KMH significant wave heights (see section 2.3) two regression-like statistical models have been chosen for the downscaling purposes, namely,

linear regression and CCA (von Storch and Zwiers [1999]). In addition, the analogs classification method (Zorita et al. [1995]) is also applied. The weather generator methodology seems not to be adequate for the problem as it does not provide tools for instantaneous hindcasts. The chosen methods are commonly used, therefore, only the specific features of the application are pointed out and detailed descriptions of the methods can be found in given references.

3.2.1 Linear regression

In order to fit and test the statistical models the K-model hindcast period was split into a five year training period (1990-1994) and a seven year validation period (1995-2001). For linear regression (LR) 3-hourly SWH and wind directions from a single grid point in the HF simulation located near the southwestern boundary of the K-model domain have been chosen as predictors. High correlation between instantaneous SWH for different HF locations around Helgoland (about 0.996) allows the use of a single HF point to represent the external wave situation for the entire K-model domain. The regression model is conditioned upon the wind directions in such way, that in fact eight regression models were built separately for each of eight wind direction sectors starting from [-22.5, 22.5]. For each grid point i in the K-model domain and each of the eight wind direction sectors j a regression model

$$y_{i,t} = a_{i,j}x_t + b_{i,j}$$

was built, where $y_{i,t}$ represents downscaled wave height, and x_t represents the predictor (HF wave height). The coefficients $a_{i,j}$ and $b_{i,j}$ were fit using a least square method.

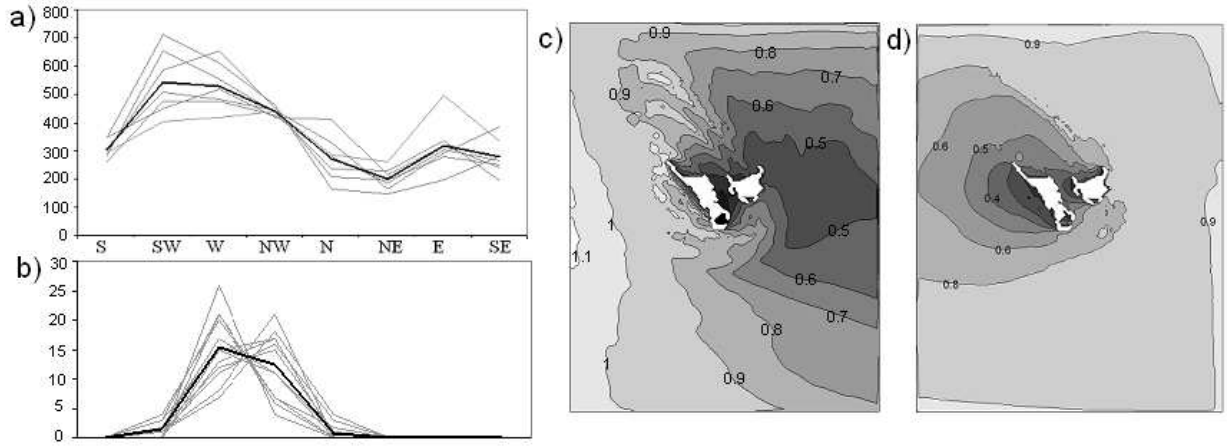

Figure 3.1: a) Annual wind direction distribution (grey lines) for 1990-2001 and the mean over this period (black), y-axis represents the number of cases occurred for each wind direction sector b) Similar distribution for the winds associated with the waves higher than 99%-tile value c) Regression coefficients for significant wave heights from LR model for westerly and d) easterly winds

In Figure 3.1c,d the obtained regression coefficients of the LR models associated with westerly and easterly wind situations are shown as an example. The coefficients demonstrate the averaged relation between medium-scale and small-scale wave heights for the Helgoland area. At the same time, the spatial patterns of coefficients display the generalized spatial distributions of local SWH for westerly and easterly wind cases independently on the SWH magnitude. The SWH pattern related to westerly winds is characterized by the local wave heights similar to the magnitude of the medium-scale HF SWH in the western part of the model area and steadily decreasing waves farther to the east with the minimum between and just to the east from the islands. For the easterly winds the pattern differs. Here the coefficients are less than 1 everywhere, this means the local waves under easterly wind conditions are lower than the waves for the western boundary in the medium-scale representation. The coefficients are quite similar for the eastern, southern and northern parts of the model domain, then they decrease gradually and almost concentrically towards the area of the lowest local waves, which is situated to the west from the islands. The spatial patterns of the regression coefficients generally follow the bathymetry features for the windward part of the domain. For the leeward part of the area the coefficients mostly display the shadow effect of the islands. Such behaviour was revealed for the coefficients of all direction sector models considered. This demonstrates how the linear regression model can consider and capture the local effects originally simulated by the dynamical model.

Before coming to the description of other models and comparisons of the statistical methods, some comments about the wind and wave climate around Helgoland for the considered in downscaling twelve-year period (1990-2001) should be given. This makes the later discussion of the properties and the skills of the models easier, and the explanation of behaviour of different models becomes more clear. In order to detect the prevailing wind directions for each year and yearly distribution eight wind direction sectors have been chosen in the same way as for the linear regression models. The number of cases for which the wind directions are found in each sector is calculated for each year. These yearly distributions and the mean over the twelve-year period are shown in Figure 3.1a. As it can be seen, the winds from the west, south-west and north-west directions, i.e. the winds coming from the open North Sea, occur almost twice more often than northerly and easterly winds. To obtain the wind statistics corresponding to the wave extreme events, the same procedure was performed for the winds associated with the waves higher than 99-percentiles. It appears that high wave events occurred under the westerly or north-westerly wind conditions (Fig. 3.1b). Looking at the LR coefficient for the westerly winds (Fig. 3.1c), it appears that it's spatial pattern is similar to the spatial pattern of the 99-percentiles of KMH SWH shown in Fig. 2.7. This confirms the prevalence of the westerly wind situations responsible for the wave extreme events.

3.2.2 Canonical Correlation Analysis and Analog method

Canonical Correlation Analysis is a method for analysis of the joint variability of two multidimensional variables. In this method such pairs of patterns are found that for each pair the correlation between the corresponding pattern coefficients is maximized. At the

same time, the corresponding correlations are found. Usually, the major part of the joint variability is explained by first few patterns. As soon as these patterns are constructed, one variable can be reconstructed from another one with a certain error level. The magnitude of the error depends, in particular, on how much variability of each field is explained by the used patterns. The higher the explained variance and the correlation between the corresponding coefficients, the lower the rate of the error. For more details see Appendix A.2. In the Analog method one variable is reconstructed from another using a pool of typical situations.

For both CCA and Analog methods the medium-scale HF 3-hourly significant wave heights at the locations around the islands were used as predictors. The local KMH 3-hourly significant wave heights were used as predictand. Again, the available data was split into training (1990-1994) and validation (1995-2001) periods. For the CCA the number of degrees of freedom was reduced by applying the empirical orthogonal functions (EOF) (e.g. von Storch and Zwiers [1999]) (for the basic concept see Appendix A.1), which have been computed for the HF and the KMH SWH anomaly fields. For the HF dataset the leading two EOFs explain about 99.1% of the total SWH anomaly variance, for the K-model dataset the explained variance is about 98.3%. Canonical correlation patterns were subsequently computed based on the leading two EOFs. In Figure 3.2 the first two CCA patterns for KMH and HF are shown. The first set of patterns explains 97.4% of the total variance for the KMH dataset and 98% of the variance for HF, the correlation between the amplitude time-series of these patters is 0.997. So, it appears that the first CCA patterns explain most of the variance and corresponding time-series are highly correlated, showing the strong dependency between regional and local SWH patterns. For both KMH and HF the coefficients of the first pattern are of the same sign, larger values appear in the western part of the area and smaller values appear to the east from the islands. Physically this means, that the changes in SWH occur simultaneously and are more intensive in the western part of the model domain, which is consistent with the wave height spatial distribution for westerly winds (Fig. 3.1c). The second set of CCA patterns is bipolar and, probably, has this structure because of the request of orthogonality for the patterns prescribed by the CCA procedure. The correlation of the time-series is 0.65, it explains 0.6% of the KMH fields variance and 1.1% of HF SWH variance. For the CCA reconstruction both patterns were used, which totally explain about 99% of variability for both datasets. Finally, the 3-hourly SWH fields for the validation period have been derived on the basis of these patterns.

For the analog method a pool of analogs was constructed from the 3-hourly SWH fields 1990-1994 of the KMH hindcast and the corresponding principal components of the leading two EOFs of the 3-hourly HF SWH anomaly field. Subsequently an analog for each date of the validation period was determined. For this, the HF SWH data of the validation period was projected onto the first two EOFs for the fitting period and for each pair of principal components obtained the nearest pair (analog) from the training period was determined. The KMH wave height field belonging to this pair was then selected as the analog wave height field for the corresponding date in the validation period.

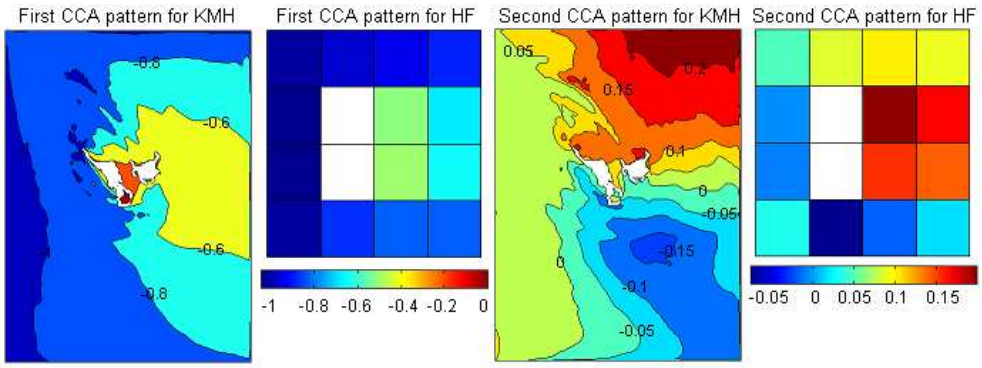

Figure 3.2: First two canonical correlation patterns of the significant wave height anomalies for KMH and HF.

3.2.3 Validation experiments for instantaneous significant wave heights

To test the skill of different downscaling methods in representing near-shore wave climate and, in particular, the instantaneous significant wave heights, results obtained using different techniques have been compared with those from the KMH simulation. Table 3.1 shows the bias and the standard deviation of the SWH difference at the various locations specified in Figure 2.1 for the different downscaling models. It can be seen that the bias is largest when coarse grid data from the HF simulation are used directly to estimate the wave conditions at the near-shore locations. The largest standard deviations of SWH differences occur for the HF and analog data depending on the location. So, it appears that the SWH data produced with the analog method differs from KMH with the variance rate similar to HF but with much less bias than the medium-scale data. For linear regression and CCA the results are comparable. LR provides slightly smaller error with standard deviation up to 0.17 m and bias less that 0.02 m depending on the location.

The degree of difference between KMH and statistically obtained instantaneous SWH fields for the entire model area is assessed by the root mean square error (rms). The spatial patterns of the differences between KMH and each of three models are shown in Figure 3.3. The rms values vary between 0.05 and 0.2 meters for linear methods (LR and CCA) and reach up to 0.4 meters for the analogs. Although the spatial patterns and magnitudes differ, there are several regularities valid for all methods. So, for the western and south-western parts of the modeled area the minimum errors over the entire domain can be seen, which means that the skill of the constructed models in representation of the wave heights at these locations is the best. The shape of this better represented area is similar to the contour-lines of the bathymetry and corresponds to the relatively deep water area. Further to the east the depth becomes less than 20-25 meters and the increasing error values can be observed. For all methods the maximum differences with respect to the dynamically obtained wave heights occur along the north-western Helgoland coast. Here

STDEV [m]	DWP	LNA	HH1	HH2	DE1	DE2
HF - KMH	0.159	0.302	0.191	0.286	0.272	0.289
LR - KMH	**0.097**	**0.163**	**0.104**	**0.159**	**0.128**	**0.085**
CCA - KMH	0.108	0.255	0.179	0.19	0.163	0.1
Analog - KMH	0.224	0.364	0.234	0.385	0.218	0.184
MR (dir) - KMH	0.089	0.183	0.181	0.154	0.131	0.114
MR (tp) - KMH	0.095	0.133	0.099	0.153	0.119	0.082
BIAS [m]						
HF - KMH	0.04	-0.045	0.17	0.257	0.228	0.39
LR - KMH	**0.004**	**0.011**	**-0.0002**	**0.0008**	**0.019**	**-0.0006**
CCA - KMH	0.005	0.023	-0.015	0.004	0.025	-0.009
Analog - KMH	0.012	0.022	-0.007	0.012	0.2	-0.004
MR (dir) - KMH	-0.006	-0.012	-0.046	-0.003	0.01	-0.008
MR (tp) - KMH	0.003	0.007	0.001	-0.002	0.017	-0.0007

Table 3.1: Bias and standard deviation of differences in meters between significant wave heights obtained from different downscaling techniques and KMH for the points near coastal facilities for the 1995-2001. In bold face the minimum values within first four methods are marked. The last two lines concern SWH comparison for the multiple regression experiments.

the steep depth gradient causes intensive bottom dissipation and shoaling. These processes are sensitive to the variable water depth and the SWHs here are only partially dependent on the boundary conditions and approaching external waves. Therefore, the statistical models are not able to provide equally accurate wave reconstruction as for the deep water areas. Similar considerations apply to the area to the north from the island where the oblong shoal activates the shallow water processes, which makes the accurate SWH representation not completely feasible for the statistical methods.

The next experiment addresses the problem which often arises for the regression-like downscaling methods, namely, the underestimation of the temporal variability of the reconstructed fields. This property was revealed and discussed in a number of studies dedicated to the downscaling methods and procedures (e.g. Katz and Parlange [1996], Zorita and von Storch [1999]). To test how the SWH fields reconstructed by LR, CCA and analog methods are subject to the underestimated variability, the variances of the SWH from statistical models and KMH at each grid point are compared. The corresponding relations are shown in Figure 3.4. For the fields obtained with linear regression the variances are slightly overestimated for the south-western part and underestimated to the east from the island, here the ratio goes down to 0.9. For the CCA the underestimated variability is more pronounced but too much variability in the western part of the model domain can still be observed. For the analogs the area of too low variability is shifted to the north with respect to LR but remains approximately the same by magnitude, whereas the overestimation of the variance on the west becomes stronger and the ratio of the variances reaches 1.05. A plausible explanation of the low-variance behaviour is that the local wave heights variability only

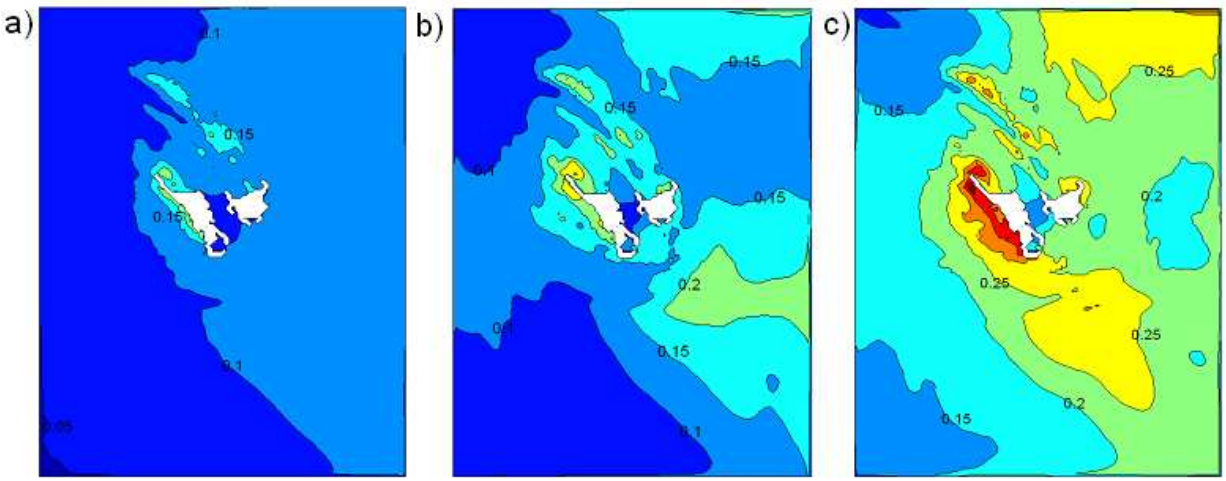

Figure 3.3: Root mean square errors between instantaneous SHW obtained from statistical methods a) LR, b) CCA, c) analog and KMH in meters.

partially depends on the larger-scale variations. Thus, the inter-scale relations reflected in the downscaling models do not capture all processes which influence the small-scale environment. This appears to be the case for the area located easterly from the island where all three models show underestimated variability. The slightly overestimated variability of the LR data detected for south-western area can be explained by very high correlation between HF and KMH SHW at these locations (about 0.996). For the training period the variability of constructed LR data is only slightly lower than the KMH variability, which is determined by the definition of the LR model. For the validation period and for the areas of high HF/KMH correlation the variability of LR becomes as high as variability of KMH. No theoretical limitations of the LR variability are supposed for this period, therefore, it varies around the KMH variability, deviating to both higher and lower values.

In reference to the properties and limitations of the methods revealed for the representation of instantaneous detailed SWH fields, possible reasons for the modeled SWH behaviour are discussed. Figure 3.5 illustrates the SWH instantaneous features. Here the 3-hourly SWH at LNA location obtained from the statistical models as well as the driving HF wave heights and KMH wave heights are shown for October 1998. This period is characterized by the presence of two classical wind situations (see Fig. 2.2). Easterly winds at first eight days and westerly winds for the rest of the month form two different wave field patterns (Fig. 3.1c,d) and influence the performance of statistical models. While the SWH obtained with linear regression follow the wave heights from the dynamical model for the first part of the month, the CCA and analog results are closer to the HF wave heights. For the westerly wind period (from 9 October) all statistical models are closer to the KMH. This is consistent with the larger errors (Fig. 3.3) and smaller variability (Fig. 3.4) shown by CCA with respect to LR and can be partly attributed to the EOF patterns used for the CCA model construction and the CCA patterns used for the field reconstruction. The first EOF

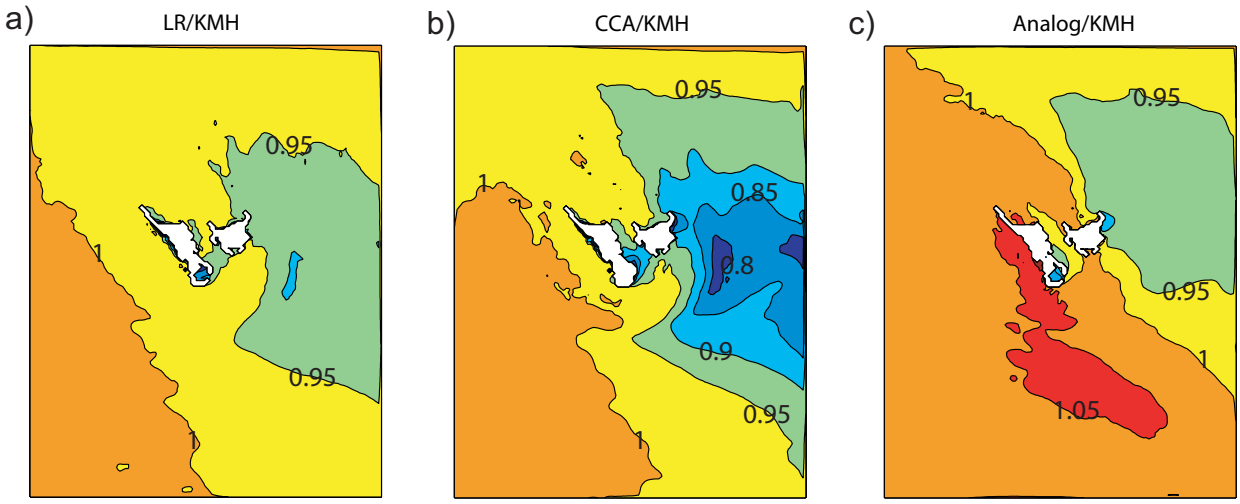

Figure 3.4: Explained variance of a) LR, b) CCA, c) Analog with respect to KMH.

pattern is very similar to the first CCA pattern (Fig. 3.2) and explains 97% of total KMH wave height variance. This EOF pattern can be associated with the most frequent for the area westerly wind conditions, the same concerns the first EOF of the HF SWH dataset. The first EOF pattern has a major impact on subsequent CCA model construction and the SWH fields reconstruction. This is followed by the limited ability of the CCA to downscale adequately the wave heights for other than westerly wind situations.

Similar behaviour of the SWH from the analog method is accompanied by the additional variability as illustrated by Figure 3.5. This is consistent with the overestimated variability for the western part of the model domain (Fig. 3.4c). As it can be seen from Table 3.1 and Figure 3.3, the analog method shows the worst performance among the tested methods not only for variability but also in terms of errors (bias or rms). Besides the use of EOF patterns which do not explain all wave situations adequately (similar to CCA), the uncertainty and especially overestimated variability of the analog results can be attributed to the incompleteness of the analog pool. For this method that means a fitting period longer than 5 years is required to accumulate the sufficient set of significant wave height patterns. This problem could be a strong limitation in the case of applications to scenario studies, as wave situations which did not occur during the fitting period or which were not included in the analog pool can not be detected and reproduced by this method.

The linear regression shows stable performance independently on the external forces and wind directions. The dominant westerly wave pattern and less frequent easterly wave situations are represented adequately because they were initially separated and equally treated during the model training procedure. This gives the LR a superior quality relative to CCA and analog. The uncertainties observed in LR SWH representation are related to the incapability of the model to capture the small-scale time-variable fields like water depth variations, currents and correspondent shallow water processes in full. In general, the SWH

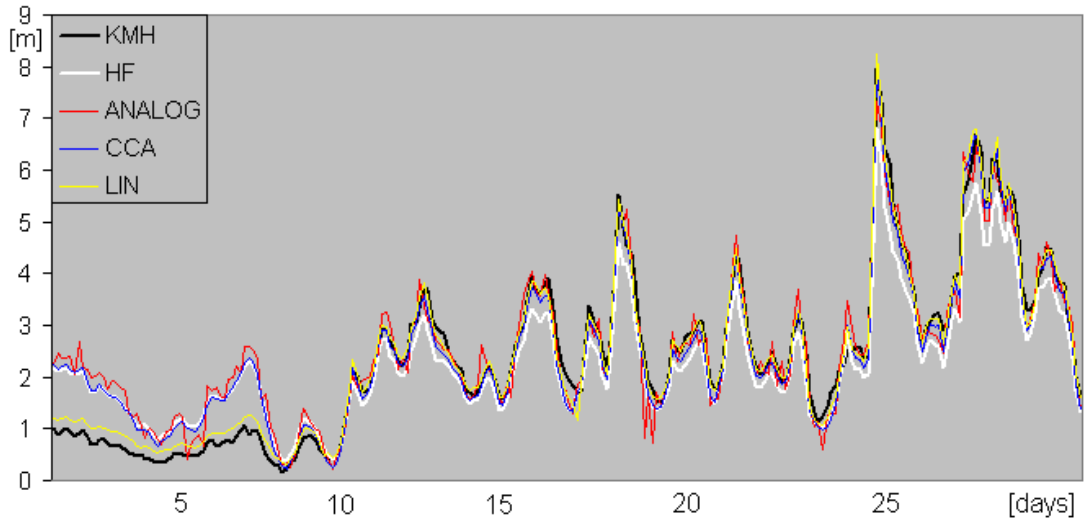

Figure 3.5: Significant wave heights in meters obtained from two dynamical (KMH, HF) and three statistical (LR, CCA, Analog) models at LNA point for the October 1998.

representation given by all three methods is closer to KMH than the medium-scale HF wave heights and the instantaneous wave height fields are reasonably reproduced in most of the cases.

3.2.4 Validation experiments and assessment of the added value for wave statistics

Next, the extent to which the properties of the described statistical models for the instantaneous SWH influence the representation of wave statistics is explored. Figure 3.6 shows a comparison of wave frequency distributions obtained from the different statistical models and dynamical HF with KMH simulation. It can be seen that, despite the differences in representing instantaneous values, the capability of the statistical models in reproducing the wave statistics of KMH run appears reasonable. The degree of agreement slightly differs depending on location. For the comparison the quantile-quantile plot of the KMH with the HF reference run is also shown. For the deep water points the agreement between statistically downscaled, dynamically downscaled (KMH) and derived from HF frequency distributions is comparable. For the areas where the influence of topography (LNA) and other external forces such as island sheltering (e.g. DE1) is larger, the distributions obtained from downscaled data are closer to that derived from the K-model for all the methods, while that derived from HF provides stronger systematic deviations.

In order to assess the ability of different downscaling techniques in representation of extreme wave statistics for the entire model domain, the annual 99-percentiles of SWH at each grid point for the validation period 1995-2001 are compared. The skill of the methods

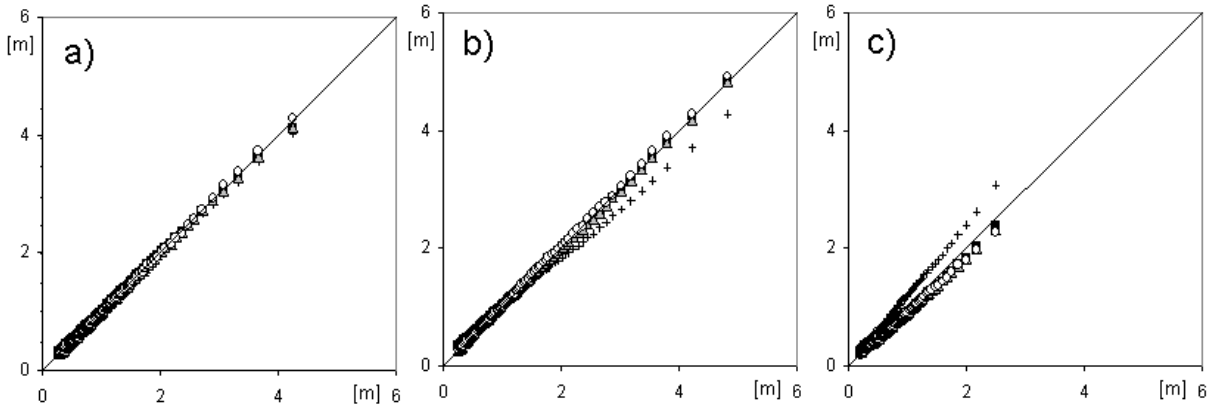

Figure 3.6: Quantile-quantile plots of simulated significant wave height with different techniques in meters for the period 1995-2001 at points a) DWP b) LNA c) DE1. HF (crosses), LR (black squares), CCA (triangles) and Analog (circles) at y-axis against KMH (x-axis). Quantiles from 0.05 to 0.99 are shown with interval 0.01.

to improve the coarse-grid SWH representation was measured using the Brier skill score (B) (von Storch and Zwiers [1999]).

$$B = 1 - \frac{S^2_{for}}{S^2_{ref}}$$

Here S^2_{for} and S^2_{ref} represent the mean squared errors of the "forecast" (in this case provided by different downscaled data sets LR, CCA and Analog) and "reference forecast" (here HF hindcast) with respect to observed data. In face of missing observations the K-model simulation represents the substitute reality. Any positive value of B indicates that the downscaling method achieves an improvement relative to the HF data. The best performance corresponds with B=1, which means that the downscaled data is as good as the "observations". A negative value of B indicates that the method performs worse than the HF reference. The result is shown in Figure 3.7. As it can be seen, all statistical methods introduce enormous additional skill in representation of the spatial distribution of the SWH yearly 99-percentile relative to using data from the HF hindcast directly. Depending on the method the skill varies from 0.9 to 0.99 except for the analog method in the year 2001, where the skill score fell down to the 0.81. The linear regression shows the best and the least variable skill score values higher than 0.95 independently of a year. The analogs shows the worst performance in wave extremes representation which is consistent with the results for the instantaneous values comparisons. Nevertheless, the improvement obtained with all techniques is significant.

In addition to testing the statistical method's ability to improve the coarse grid SWH field representation, the errors for the upper percentiles of the statistically downscaled SWH fields were calculated with respect to KMH upper percentiles. In previous section the errors

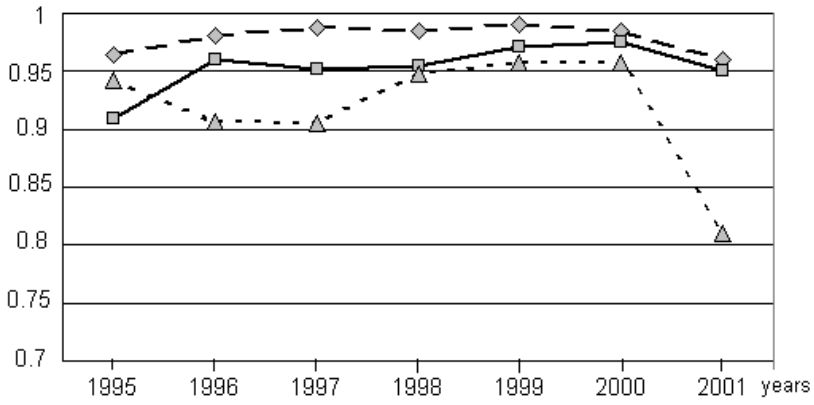

Figure 3.7: Brier scores for the 99%-tile of yearly SWH from 3 statistical methods: LR (dashed line), CCA (solid line) and Analogs (dotted line).

of instantaneous SWH values from statistically and dynamically obtained datasets were considered. However, this analysis does not reveal in which part of the SWH distribution the major differences occur. Thus, it can appear that major part of uncertainty falls at the high wave part of the distribution, or vice versa, the wave extremes are reproduced most accurate. To answer this question, the differences between means over annual 99-percentiles from statistical methods and KMH were calculated and shown in Figure 3.8. As in the case of instantaneous values, some differences in models extreme wave representation are found. For three models the spatial patterns of slightly positive and negative deviations of extremes differ. The area of less accurate SWH representation around the islands looks similar for LR and CCA with underestimated extremes to the west and overestimated extremes to the north from the islands. The maximum rms errors of instantaneous values were also detected for these areas (Fig. 3.3a,b). The proximity of the coastline and shallow water in these zones presume the increased importance of the local time-variable and non-linear processes (current influence, shoaling, bottom dissipation). The processes are not considered by the statistical models and this is reflected by the higher uncertainty of the reconstructed data. For the analog the errors of the reconstructed SWH upper percentiles (Fig. 3.8c) are also spatially correlated with the differences in temporal variability for instantaneous SWH (Fig. 3.4c). The overestimation of wave extremes occurs for the areas showing too much temporal variability and too small extremes correspond to the area of underestimated variability. In these cases the wave extreme events are artificially over- or under- estimated due to model uncertainty. Summarizing, for all statistical methods and for the major part of the model domain the wave extremes are represented with rather good accuracy and differences with the KMH lie within 0.1 meters, the exceptions being the distinctive shallow water area north of the island which was poorly resolved by each method, and the area of increased variability for the analog in south-western part of the domain.

Until now the statistical models were constructed and tested for the Helgoland area.

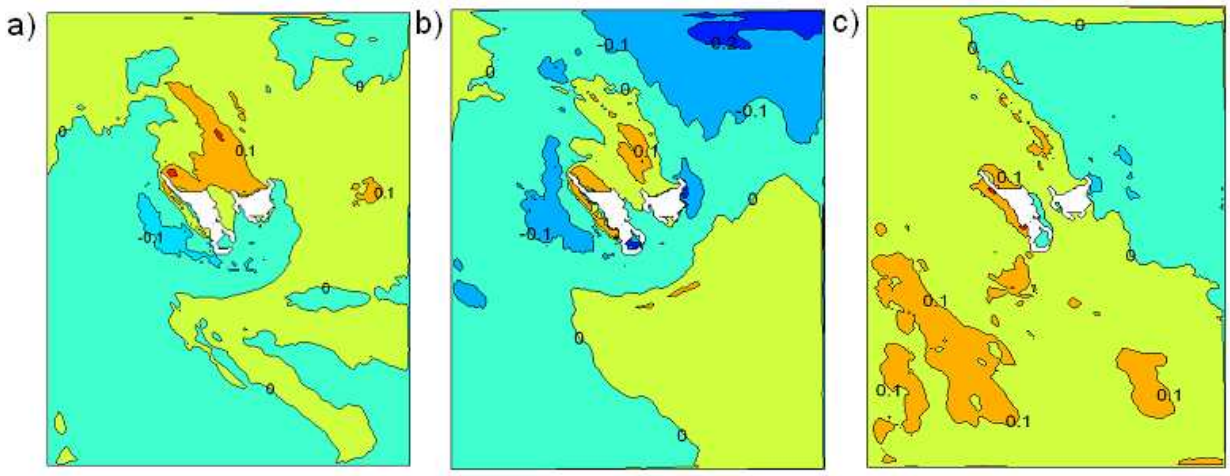

Figure 3.8: Difference in meters between the means of yearly 99%-tiles of SWH obtained from a) LR, b)CCA, c)analog and KMH for the period 1995-2001

The potential applicability of the statistical-dynamical approach to other coastal areas and the level of generality of the conclusions made in this section are interesting. First, the basis of the described approach is the dynamical wave model. The abilities and limitations of the K-model in implementation to different coastal areas are partially discussed in Schneggenburger [1998] and a principal universality of the model, using the tunable parameters, was supposed. Concerning the applicability of the statistical model to the arbitrary area, first of all rather strong dependency of the local waves from the boundary (medium-scale) wave fields is required. For example, weak connection with the open sea (such as in case of harbors), strong dependency on the local, not connected with the sea-waves processes (e.g. area with the depth of several meters, mouth of the river) makes the use of the statistical downscaling in proposed form hardly applicable. The presence of the mainland as one of the boundaries for the model domain could also be an obstacle to the statistical models. In such environments the local wave fields induced by the winds from the dry-land are not dependent on the regional wave conditions but only on the local wave processes and the wind. On the other hand, the wave extreme events for such areas are coming from the open sea and are normally connected with the landward winds. So, the wave extreme events could still be adequately represented by the proposed statistical-dynamical approach.

3.3 Multiple regression

So far, the methods have been applied to SWH only and most of the study is founded on SWH statistics. Although the significant wave height represents one of the most frequently analyzed and most crucial wave parameter, other parameters are also important for particular applications. For instance, the wave steepness can be inferred from wave periods

and wave heights, which is an important issue for the design of vessels. Another example of the quantity dependent on the wave period is the wave induced bottom stress which is important for the sediment transport and coastal erosion evaluations. Other parameters, such as the wave direction, are crucial, especially for extreme wave analysis within the coastal protection problem where it is important to know which direction the severe waves are coming from. Considering the high demand for other than SWH wave parameters, this section is dedicated to the downscaling experiments for the wave direction and peak period fields simulation together with the significant wave heights.

The multiple regression (MR) technique accommodates the construction of the relations between several predictor variables and several dependent predictands simultaneously. As it has already been mentioned, the choice of the predictor's set is crucial but subjective and depends on application and reconstructed field. For an adequate reconstruction of the small-scale variable it is important to consider the main processes or fields which it is influenced by. The consideration of several medium-scale processes or fields in the small-scale field construction adds a more realistic variability to the predicted field in case it is dependent on this added predictor. Along with the improvement of small-scale field representation this gives the insight into the sensitivity of the small-scale variable to the medium-scale fields included in the downscaling and a better understanding of inter-scale dependencies. The reconstruction of several predictands simultaneously gives a more comprehensive picture of the small-scale system. In case of wave fields, this approach is a compromise between the single wave parameter (SWH, wave direction, etc) and the full wave spectrum reconstruction.

The general form of the multiple regression model, which is the modification of linear regression model, can be written as:

$$Y_t^k = A_0 + \sum_{i=1}^{l} A_i^k X_t^i$$

where Y_t^k represent the k-th predicted variable at time t, X_t^i represent the i-th predictor variable at time t and regression coefficients A_0^k, A_i^k are fit by least square method.

3.3.1 Significant wave heights and mean wave directions

The first multi-downscaling experiment was performed for the mean wave direction and SWH fields. The datasets were split into training (1990-1994) and validation (1995-2001) periods as in the case of simple linear regression. The HF SWH and wave direction at single HF grid point were taken as the predictors. For the computational convenience these time-series were transformed to the meridional (u) and zonal (v) components represented in the model by X_t^1 and X_t^2 variables. The u- and v- components of the KMH SWH and wave direction at each KMH grid point were used as the predicted variables Y_t^1 and Y_t^2. The regression models (sets of regression coefficients) were built for each KMH grid point and eight wind direction sectors (same as for simple linear regression).

STDEV(error) [deg]	DWP	LNA	HH1	HH2	DE1	DE2
HF - KMH	16.829	42.017	66.844	48.44	68.764	73.711
MR(dir) - KMH	16.313	22.904	36.593	19.111	11.538	26.285
BIAS [deg]						
HF - KMH	2.558	7.529	14.032	22.267	44.61	44.61
MR (dir) - KMH	1.064	1.072	2.783	1.416	-0.069	1.135

Table 3.2: Bias and standard deviation of differences in degrees between wave directions obtained from HF, multiple regression and KMH for the points near coastal facilities for the 1995-2001.

The comparison of the downscaled instantaneous SWH values with the KMH results at the points near coastal facilities is shown in Table 3.1. The results of multiple downscaling for the SWH are close to the results from the simple linear regression. This suggests weak or no dependency between the small-scale wave heights and medium-scale wave direction variations within the framework of each constructed model. More precisely, the SWH/wave direction dependency is partially taken into account by using separate regression models for different wind direction sectors. For the medium-scale wave data near Helgoland the wave directions are strongly correlated with the local wind directions. Thus, the large-scale wave directions are considered in the small-scale SWH spatial patterns defined by each of eight models (see 3.2.2). The variations of the medium-scale wave direction within 45-degree sectors seem to be of small importance for the local wave heights.

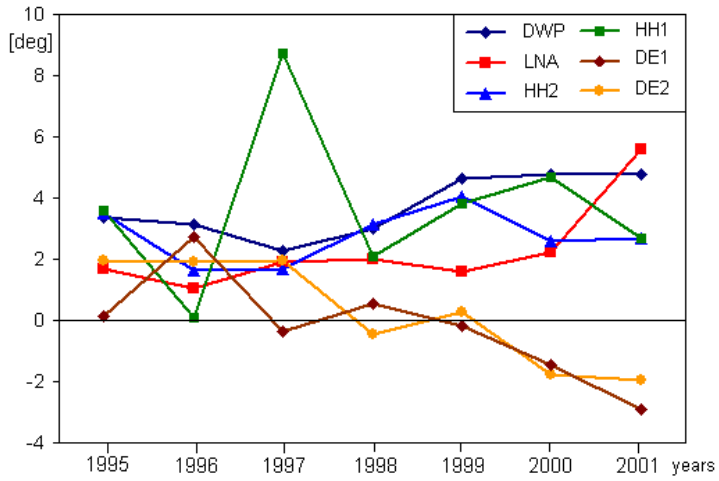

Figure 3.9: Differences in degrees between the mean wave directions correspondent to the upper yearly 1% of highest waves obtained with MR and KMH at selected locations.

The ability of the constructed downscaling model to reproduce the small-scale wave directions at single points of the investigated area is assessed for instantaneous values and

annual statistics. The comparison of reconstructed 3-hourly wave direction values with the KMH results together with the comparison of KMH and HF results for wave directions is shown in Table 3.2 in the form of standard deviation of the difference and bias for selected points. The biases of downscaled wave directions are small and do not exceed 3 degrees for all tested locations. The accuracy described by standard deviation is everywhere less than 37 degrees in all cases, with the worst cases at the HH1 point near the harbor entrance and DE2 point located south to Düne island. For the most common synoptic situation, with westerly wind and waves coming from the open North Sea, these locations are blocked from the direct wave propagation by the Helgoland island. Thus, refraction plays the major role in the wave transformation. Together with the small depth at the locations (about 10 meters) this increases the importance of the water depth variations and current fields participating the refraction process. Consequently, these local processes influence the small-scale wave directions rather than the boundary conditions. As soon as the local time-variable fields are not considered in the downscaling model, the results for these locations are less predictable with the model used.

Looking at the results of the HF/KMH comparison (Table 3.2) it can be seen that the coarse-grid (HF) representation of wave directions suffer from a strong bias and higher variability of the error with respect to the downscaled (MR) results. Only in the case of DWP the HF wave direction representation is close to the small-scale data. A considerable bias in wave directions for all other points is expected and can be explained by the poor resolution of shallow-water areas in HF simulation and by the absence of an adequate topography for the modeling of correct refraction process. It appears that the wave direction field is more sensitive to the adequate topography as well as to the shallow water processes than the significant wave height field and that the downscaling procedure brings significant and qualitative improvement to the instantaneous near-shore wave direction representation.

Besides the instantaneous wave direction values, for the evaluation of wave statistics the directions of the highest waves should be known. The next test was made to assess the quality of the wave directions for the highest waves reconstructed by MR model. For each year of the validation period (1995-2001) and each grid point from the KMH and MR SWH datasets the records with the wave heights larger than annual 99-percentile were extracted. The 3-hourly data was used, consequently, about 30 SWH values per year are higher than 99-percentile and fall into the selected set. The wave directions for the same dates were chosen and formed the yearly sets of "high wave" directions. Then the mean wave directions were computed from the each year set and the difference between MR and KMH means was taken. The results for selected points are shown in Figure 3.9. The errors of the mean wave directions for all years lie within a 9-degree band. Even for those locations (HH1, DE2) where the instantaneous MR wave directions deviated strongly from the KMH results, the agreement of the mean wave directions of highest waves is good.

To get an impression of the high wave directions distribution, the KMH and MR "high wave" directions from the yearly sets were grouped in 10 degree sectors starting from [-5,5] for each location. The number of records fallen into each sector was associated with the sector and in Figure 3.10 the results for the period 1995-2001 are shown. In addition,

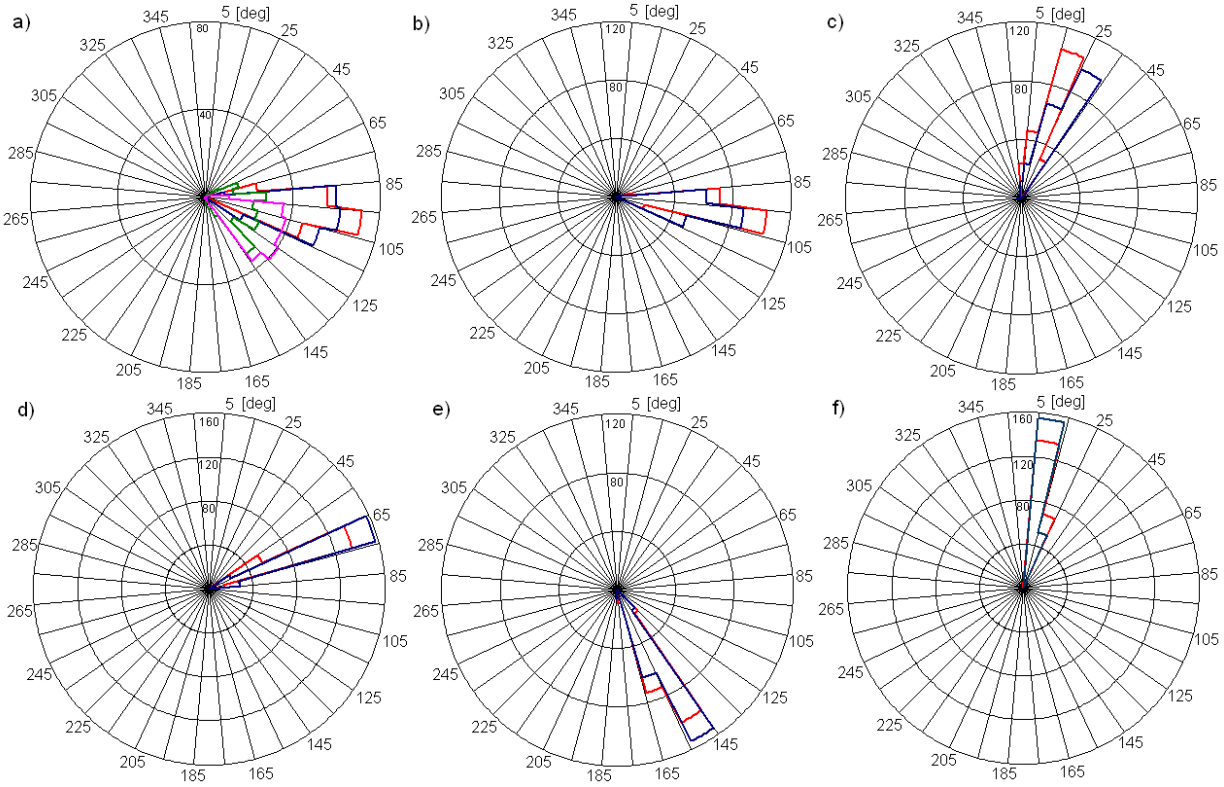

Figure 3.10: Distribution of wave directions (going to) correspondent with the 1% of highest waves obtained from KMH (red) and MR (blue) for the years 1995-2001 at the locations a) DWP b) LNA c) HH1 d) HH2 e) DE1 f) DE2. In addition, a) distribution of wave directions for the 1% of highest waves obtained from HF (pink) and corresponding wind directions (green). The length shows the number of the records.

the directions for highest 1% of the waves for the HF used as predictor for the regression model and corresponding wind directions are shown in Figure 3.10a. All small-scale wave directions corresponding to high wave events are grouped within a 20-30 degree wide sector depending on the location. The wind directions are concentrated in eastern sectors which corresponds to the westerly and north-westerly winds and is consistent with the extreme wind direction distribution (Fig. 3.1b). This means the high wave events within the K-model domain happened under similar external wind/wave conditions belonging to the north-westerly storm situation. For the locations situated to the west from the island (DWP, LNA, HH2) the wave directions remained considerably unchanged with respect to boundary conditions with slight turn to the north due to refraction caused by the bottom slope in the relatively shallow water area. For the southern locations behind the islands (with respect to westerly waves) (HH1, DE2) the northward wave directions prevail, which is mainly explained by the presence of the main island and consequent wave refraction. The almost southward wave directions at DE1 have the same reasons. The spread of the

HF wave directions as well as wind directions on the boundary is larger than the spread of the wave directions obtained with both KMH and MR at the locations inside small-scale model domain. This can be explained by the influence of the internal small-scale processes and the seabed profile defining the wave directions side by side with the external wind/wave forcing. The results for the MR wave directions data demonstrates the ability of the model to keep this influence and to consider the small-scale features although they are not resolved explicitly in the model. The slight shift in the MR obtained directions at HH1 with respect to KMH can be attributed to the part of the refraction caused by local time variable fields (water depth, currents) which are not represented in the MR model. In general, the downscaled wave direction fields capture dynamically obtained high wave directions and reflect the main features and configuration of the extreme wave situations.

3.3.2 Significant wave heights and peak periods

The second multiple-regression experiment deals with the construction of SWH and peak period fields. The SWH and peak period for the single point from HF simulation were taken as the predictors X_t^1 and X_t^2. The small-scale SWH and peak period fields from KMH were chosen as the model predictands Y_t^1 and Y_t^2. The rest of the procedure is similar to the first multiple regression experiment (3.3.1).

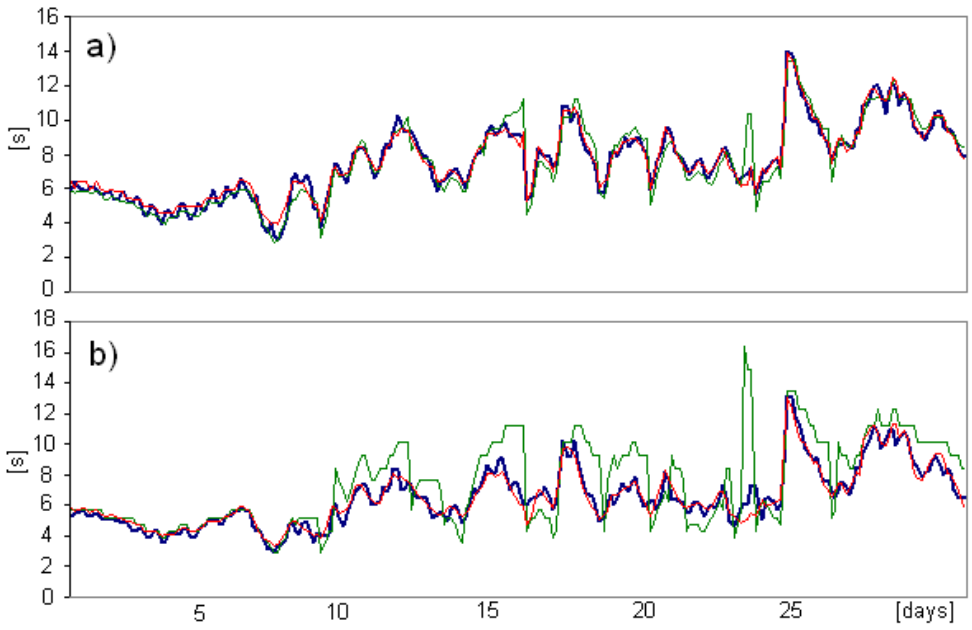

Figure 3.11: Peak periods in seconds for October 1998 obtained from KMH (blue), HF (green) and MR-tp (red) at points a)DWP, b)DE1

The comparison of the results for instantaneous SWH showed (Table 3.1) that the consideration of the peak period as the second predictor makes a slight improvement in

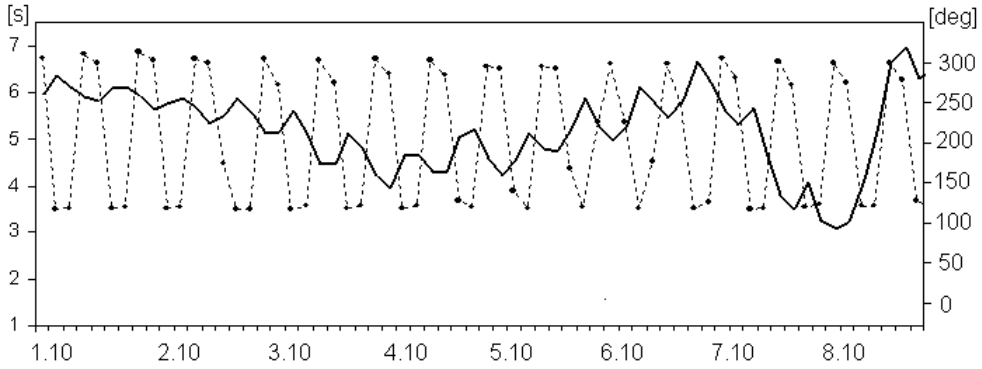

Figure 3.12: Current directions (dashed) in degrees used as an input for the K-model and peak periods (solid) in seconds simulated by the K-model for the 1.10-8.10.1998

STDEV(error) [s]	DWP	LNA	HH1	HH2	DE1	DE2
HF - KMH	1.08	1.27	1.63	1.26	2.17	1.97
MR(tp) - KMH	0.976	0.876	1.002	0.86	0.647	0.902
BIAS [s]						
HF - KMH	-0.13	0.06	-0.17	0.278	1.064	0.419
MR(tp) -KMH	0.018	0.04	0.038	0.037	0.067	0.065

Table 3.3: Bias and standard deviation of differences in seconds between peak periods obtained from HF, MR and KMH for the points near coastal facilities for 1995-2001.

the representation of downscaled wave heights with respect to simple linear regression. The standard deviations of the differences between MR and KMH wave heights are lower than for the LR data, biases are comparable and sometimes lower, depending on the location. This suggest the favoring of the idea that the medium-scale peak period data brings additional information into the local wave system with respect to the medium-scale SWH. This is also supported by the appearance of the regression coefficient matrix which has a non-diagonal form with all elements nonzero.

To investigate the relations between HF and downscaled with KMH and MR peak periods the instantaneous values from three datasets at the selected locations are compared and the results are shown in Table 3.3. In addition, the peak periods at the locations DWP and DE1 are plotted for October 1998 (Fig. 3.11). The first peculiarity visible on the plots is the pronounced cyclic structure of the KMH time-series for both points especially noticeable for the first 10 days of the period. The strong correlation between the tidal cycle and the local maximum and minimum of peak period can be detected (Fig. 3.12). Here the peak period and current directions were compared at the DWP location for eight days in October 1998. During that period the waves were steadily directed to 290° and current directions switched between 115° during flood and 305° during ebb tides. Thus, the

currents were almost following and opposing to the wave direction. The difference between the neighboring peaks up to 1 second can be detected. This corresponds to the results of Moghimi et al. [2005] who showed that for the shallow water environment the wave periods are sensitive to the tidal currents and water depth variations and that for significant wave heights this effect is less pronounced. Both HF and MR datasets underestimate the peak period variability connected to the tides.

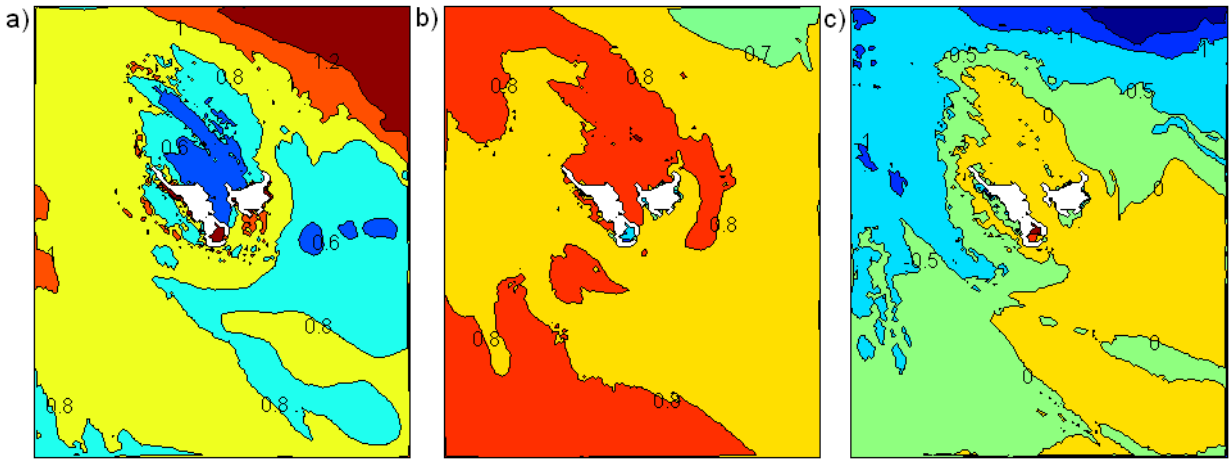

Figure 3.13: a) Rms error in seconds between instantaneous peak periods obtained with MR and KMH b) Explained variance by the peak periods obtained with MR with respect to KMH peak periods c) Difference in seconds between the means of annual 99%-tiles of peak periods obtained from MR and KMH

For the second part of the period considered the situation changes. Under the westerly wind and storm conditions the HF peak periods differ significantly from the downscaled data, especially for the DE1 point. As in the case of significant wave heights, the representation of the peak periods given by the medium-scale model for the area just behind the island with respect to westerly wind is rather poor (see Table 3.3) with strongly overestimated peak periods. For the DWP the discrepancy between HF and KMH is not so large but the MR model still improves the coarse grid peak periods.

As for the quality of the MR modeled peak period data with respect to KMH and for the entire model domain, the rms errors of instantaneous values vary from 0.4 to 1.2 seconds (Fig. 3.13a) with the minimum rms in the shoal part north to the island, the same area has the best explained variance larger than 0.8 (Fig. 3.13b). In general, the MR data underestimate the variance of dynamically obtained peak periods and the explained variance of the MR data with respect to KMH does not exceed 0.9. In comparison with the SWH, where statistically obtained fields represent more than 90% of the KMH SWH variability for the major part of the modeled area (not shown), the multiple regression shows less skill in representation of the peak period variability. The extreme peak periods modeled by MR differ from the KMH 99-percentiles within 0.5 seconds for the major part of the area. Only in the northern part of the model domain the underestimation up to

1.5 seconds is detected. The worst representation of instantaneous as well as extreme peak periods by the MR model occur in the north-eastern part of the model area. These locations are mostly remote from the south-western corner of the model area where the HF point used as the basis for the regression is situated. When the statistical model was constructed for the SWH fields using only one point from the HF simulation, it was assumed that the SWH time-series at all HF grid points associated with the KMH model domain were highly correlated (with the correlation about 0.996). Therefore, the use of all these time-series for the regression would not bring additional information with respect to the use of one of them. For the peak period the correlation between the time-series from south-western and north-eastern HF points is lower (about 0.86). In this situation the use of one time-series for the downscaling procedure limits the skill of regression model in representation of peak periods in the locations remote from the south-western part of the model domain. Nevertheless, the multiple regression model adequately reproduces peak periods and improves the HF data. This is especially important for the locations in close proximity to the island where the HF data suffers from major deviations with respect to KMH and the MR has a good skills.

3.4 Summary

The empirical downscaling was proposed as a complementary tool to the time-consuming dynamical wave modeling to obtain detailed near-shore wave statistics. Three statistical methods, namely, linear regression, Canonical Correlation Analysis and analog were applied to the downscaling of the HF SWH and trained on the dynamically obtained KMH high-resolution SWH fields.

Compared to the KMH wave data, the statistically obtained SWH fields showed a different range of uncertainty. In general, the methods successfully reproduce the temporal and spatial variability of SWH and details corresponding to the high-resolution topographic features. Some discrepancies occur because of unconsidered time-variable small-scale fields such as currents and water level change, which influence the wave parameters in the shallow water environment. The temporal variability is adequately captured by linear regression with slight underestimation for a part of the area, the underestimation appears to be larger for the CCA and the analog showed overestimated variability for most of the modeled area. The statistically obtained wave extreme events showed a good agreement with KMH extremes.

It was found that all three methods considerably improve the representation of the instantaneous wave parameters and estimation of extreme wave statistics compared to the driving medium-scale hindcast. It is therefore suggested that in the face of limited computer resources and compared to the direct use of less well resolved data, high-resolution wave model simulations in combination with coarse grid boundaries and statistical downscaling approaches can yield an improved representation of extreme wave statistics for near-coastal areas.

The linear regression model shows the best results in comparison with the dynamically downscaled data and gives the opportunity for the construction of more than one integrated

wave parameter. The skill of the multiple regression model in simulation of two wave parameters simultaneously was examined for the pairs SWH/wave direction and SWH/peak period. The representation of SWH fields for MR was found to be similar to the results obtained with LR. The instantaneous wave directions as well as the wave direction distribution for high waves are represented reasonably well with respect to KMH and capture the main specific details for the area. The representation of MR peak periods is significantly improved with respect to HF data but suffer from underestimated variability. The uncertainties in the peak period representation around the island are partially attributed to high sensitivity of peak periods to small-scale variable fields such as tidal currents and water depth variations.

Based on a balance between the quality of simulated data and required computational resources, LR (or MR in case of several parameters) statistical method in combination with the dynamical K-model appeared to be the most acceptable tool for downscaling long-term wave data and obtaining small scale wave statistics. It solves both the problem of insufficient time and space resolution presented in medium-scale multi-decade wave hindcasts and extremely high computational costs for long-term high resolution dynamical wave hindcasts.

Chapter 4

Wave climate assessments for past and future

This chapter is dedicated to the evaluation and description of the wind/wave climate for German Bight and Helgoland. The data used for the analysis of the wave climatology of the last four decades is obtained from HIPOCAS and the linear regression model described in the previous chapter. These wave statistics are used for the revealing of the past changes in wave extremes as well as for the extreme value analysis and consequent assessment of the expected frequency and magnitude of the wave extremes. In the second part of the chapter the earlier experiments concerning scenario studies for the future wind, wave and surge climate of the North Sea region are surveyed. As an example, two scenarios for Helgoland are constructed based on the results of two IPCC scenarios elaborated on regional scale by PRUDENCE project and the issue of local scenario studies are discussed.

4.1 Hindcast

During the last two decades there were numerous attempts to reconstruct the past wave climate on global and regional scales. The recent efforts (i.e. Kushnir et al. [1997], Günther et al. [1998], Cox and Swail [2001] or Soares et al. [2002]) provide wave datasets of different qualities for the last 40-50 years. The main objectives of such studies were to bring together and investigate consistency different historical data, to provide homogeneous long-term wave hindcast and to analyze the rate and reasons of changes happening in wave climate during past decades based on obtained datasets.

In the mid nineties the regional study of the North Atlantic wave climatology was carried out within the WASA project (WASA Group [1998]) with the main goal to prove or reject the hypothesis of the worsening of wave and storm climate in the North Atlantic. The main motive for this work was the substantial worsening of the North Atlantic wave climate during past four decades evidenced by different analysis of observed data (i.e. Bacon and Carter [1991], Hogben [1994], etc.), but due to various kinds of inhomogeneities most of the analysis gave only bounded and rough impression about wave climate changes. For the

WASA project the pressure observational records for about the last 100 years for different parts of North Atlantic and in particular southern and eastern North Sea were analyzed. The increase of geostrophic wind speeds (and consequently storm index) for the past decades was confirmed but the absolute values for the end of the 20th century appeared to be comparable with that from the beginning of the century. The past increase of geostrophic wind speeds seemed to be explained in a major part by inter-decadal internal variability (Alexandersson et al. [1998]). It was also pointed out that the consideration of the data only from 1960 onward may lead to artificial dramatizing of the increasing trends.

To avoid the inhomogeneities in observed wave data, the reconstruction of past wave climate within the WASA project has been made with a dynamical wave model driven by operational wind analysis for the period 1955-1994 (Günther et al. [1998]). The analysis of the model output showed a slightly increasing trend for high wind speeds and large wave heights (3-4 cm yr^{-1} for annual 99-th SWH percentiles) for the North Sea and the Norwegian Sea. The average SWH showed for the 40-year period increase with the rate of approximately 0.2% per annum and thus, the model results did not support the observed and reported earlier 1-2% upward trend. On the other hand, it has been found that the atmospheric forcing for the wave model still suffered from the lack of homogeneity, which makes more difficult to determine the distinction between the trends and climate variability.

Because of the development and significant improvement of wave models used for wave reanalysis and hindcasts during past decade, the quality of simulated medium scale wave fields is considerably dependent on the homogeneity and time resolution of the driving wind data and partially on the wave model resolution (i.e. Brauer and Weisse [2000], Sterl et al. [1998]). The skills of state of the art wave models in representation of ocean wave fields and high dependency of the simulated wave accuracy on driving forcing allow for the use of modeled wave data as a quality control of the driving wind fields (i.e. Sterl et al. [1998] or Swail and Cox [2000]). As the consequence, the availability of homogeneous and long-term wind data becomes crucial for adequate wave hindcasts and most of the wave and storm related studies focus at first on wind data reanalysis and quality evaluation. Among recent studies two global 40-year wave reanalysis have been made, first one by Cox and Swail [2001] was based on NCEP/NCAR Reanalysis (National Center for Environmental Prediction and National Center for Atmospheric Research) surface wind (Kalnay et al. [1996]), and the other one used ERA40 ECMWF (European Center for Medium-range weather Forecasts) Reanalysis wind fields (Simmons and Gibson [2000]). The results of both reanalysis for wind and waves were compared by Caires et al. [2002] and it was found that in spite of day-to-day and monthly mean differences, the long-term behaviour of both winds and waves in various datasets was quite similar. In general, global wave variability during last 40 years was characterized by a slightly positive trend for significant wave heights at North Atlantic and negative trends in central Atlantic and equatorial Pacific. This corresponds with the WASA results and the results from Kushnir et al. [1997] and Wang and Swail [2001] for Atlantic region. There the changes in SWH fields were related to the changes in sea level pressure (SLP) fields. The revealed bipole SWH trend (increasing in Northeast Atlantic and decreasing south to 40°N) was supposed to be associated with enhanced positive phase

of the North Atlantic Oscillation (NAO) index, defined from the pressure difference between Island and Azores.

The next improved wind and wave hindcast for the sea areas around Europe was provided by HIPOCAS project described in section 2.1.2 with one of the goals to assess the changes in past winds, storm surge and wave climate. The obtained data is presently analyzed by our colleagues with respect to past changes in climatology for the entire North Sea. It is beyond the scope of this study to evaluate the wind and wave climate for the entire North Sea region. Instead, the tendencies and regularities relevant for the German Bight are explored more intently based on the HIPOCAS wind and wave data.

4.1.1 Analysis of the past regional wind and wave climate

Before coming to the analysis of local wave climate for Helgoland area, some attention has to be payed to the regional wind and wave conditions dominating in the area during last decades. The strong dependency of the local wave statistics on the regional one was shown in the previous chapter. Basically, it is assumed that the long-term changes in medium-scale wave statistics are reflected in local statistics as well. The wind statistics can be useful to understand better the regional wave climate. It has been shown in several studies (e.g. Kushnir et al. [1997], Wang and Swail [2001]) that the long-term changes in wave statistics are strongly linked to the changes in sea level pressure and wind climatology. That is why for the revealing of potential reasons of changes in local wave statistics the regional wind fields are considered. For this purpose the 10 meter height wind speeds and directions from the REMO simulation were extracted for the location near Helgoland. Instantaneous 3-hourly wind data for 1958-2001, annual percentiles of wind speeds and extreme wind statistics for this period were used for the analysis. As regional wave statistics, the 3-hourly SWH values from HIPOCAS hindcast have been extracted for the location near Helgoland.

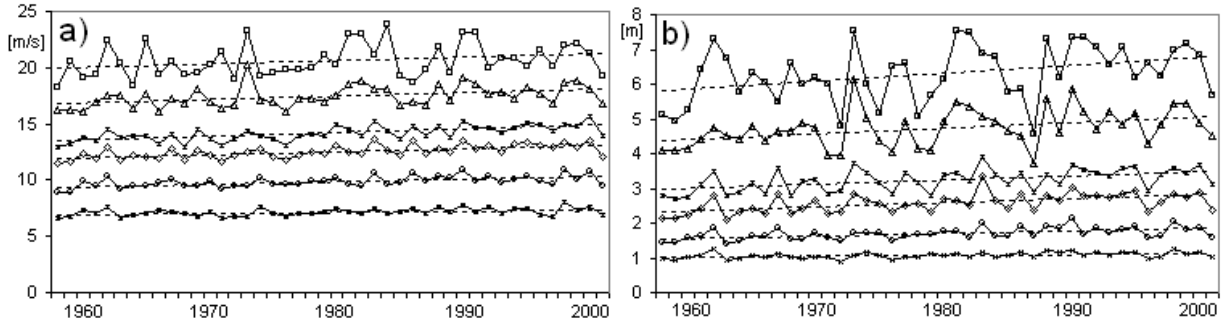

Figure 4.1: 50, 75, 90, 95, 99, 99.9 annual percentiles of the a) wind speed (solid) in m/s and linear trends (dashed) in m/s per annum b) SWH from HF in meters and linear trends.

First, annual percentiles of the reginal wind speeds and significant wave heights are considered independently of the wind directions. Figure 4.1 shows 50, 75, 90, 95, 99 and 99.9 annual percentiles for wind speeds (a) and SWH (b) together with fitted for each

Percentiles	50%	75%	90%	95%	99%	99.9%
Total	0.012	0.022	0.028	0.034	0.032	0.033
SW, W, NW	0.019	0.026	0.034	0.037	0.036	0.038 (sig. 95%)
N, NE, E, SE, S	N/S	N/S	0.015 (sig. 90%)	0.014 (sig. 90%)	N/S	N/S

Table 4.1: Magnitude of linear trends for wind speed annual percentiles in m/s per annum. The first line shows the trends for the percentiles obtained independently on wind direction. In second line only three westerly wind direction sectors are considered for percentile construction, the last line represents the trends for percentiles of the remaining five directional sectors. Significance level of the non-zero trend is 99% unless another is explicitly shown.

percentile linear trends. The increase of wind speeds during the analyzed period can be revealed for both extreme events (99, 99.9 percentiles) and medium wind speeds (50, 75 percentile). The linear trends were estimated and the hypothesis that they do not differ from zero was tested with the standard two-sided T-test. The low rate of auto-correlation for the annual wind speed percentiles allowed to use this method directly. The trends have been found to be significantly different from zero with 1% error level and their magnitudes vary from 0.012 to 0.034 m/s per annum (Table 4.1). The detected intensification of the winds during past 40 years is consistent with the conclusions of Alexandersson et al. [1998] for observational data from the North Sea region. In that study the U-shape behaviour of extreme winds during the past century (the magnitudes are similar for the begin and the end of the twentieth century with minimum magnitudes around 1960th) was revealed. This behaviour can not be tested with modeled data available at the moment for German Bight, longer wind hindcasts are required to be able to make the final statement about the nature of the detected increase in the wind speeds. For the present state, it should be taken into account that for the past decades the determined wind speed increase is probably part of natural variability. For the significant wave height percentiles in German Bight the situation is similar to the wind speeds, positive linear trends significantly different form zero were found for all considered percentiles. The considerations about the reasons for such behaviour are also similar to that for the winds.

Because the wave extreme events are of special interest for coastal applications, we investigate in more detail the wind conditions for such events and corresponding changes in wind and wave statistics. At first part of experiment, the SHW and wind speed annual maximums were obtained separately for eight wind direction sectors starting from [-22.5,22.5]. The mean values of 44 annual maximums associated with each direction sector are shown in Figures 4.2a,b for wave heights and wind speeds accordingly. For the wave heights the mean maximum magnitudes associated with three westerly wind sectors are significantly

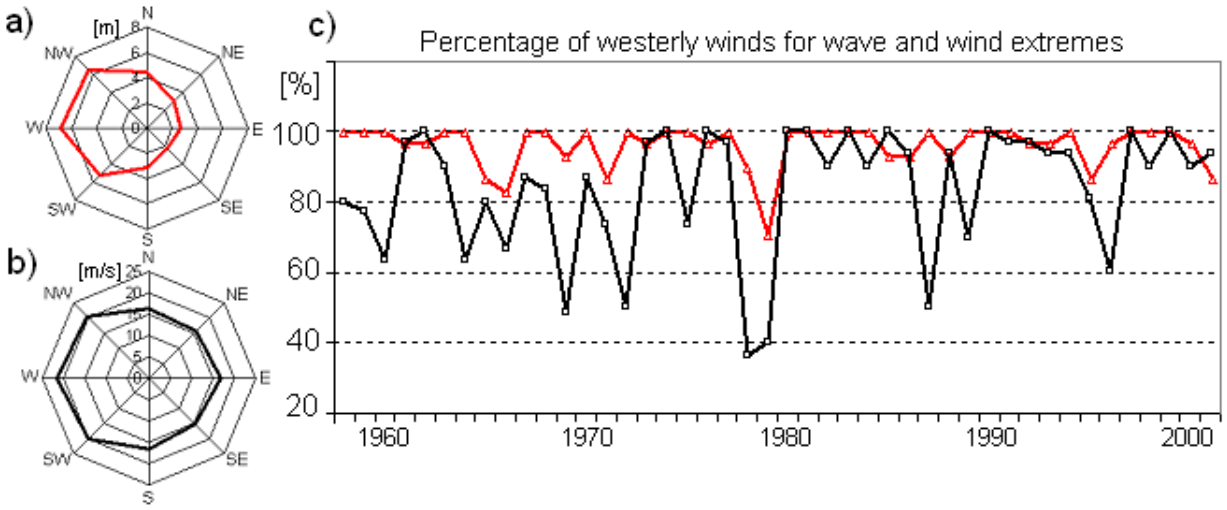

Figure 4.2: a) Mean of annual maximums of SWH for each direction sector for the period 1958-2001 b) Mean of annual maximums of wind speeds c) Frequencies of westerly winds associated with upper 1% of wind speeds (black) and upper 1% of the wave heights (red) in percentage.

larger than the values for other wind directions. Thus, for westerly winds the highest detected waves are about 7 m, while for easterly winds they reach only 3 m, which is twice less. For the wind speeds the discrepancy between westerly and easterly strongest winds is much smaller and amounts to about 25% of maximum (western) strongest winds.

Looking at the data from the other side, the annual 99-percentiles of SWH and wind speeds without directional separation were calculated, then the wind and wave events larger than 99-percentiles were selected and corresponding to this events wind directions were identified. For more convenience, the wind direction sectors were grouped in two parts, namely south-westerly (SW), westerly (W) and north-westerly (NW) directions referred to later as "westerly" winds and the remainder group as "easterly" winds. Finally, for each year the percentage of extreme wave and wind events associated with westerly winds was plotted (Fig. 4.2c). In average, about 83% of all wind extreme events are related to the westerly wind conditions with some exceptional years where this value goes down to 40% or rises up to 100%. For the waves the situation differs, here about 96% of annual strongest 1% of storm events occur under westerly winds. On the whole, the results presented in Figure 4.2 suggest the prevalence of the westerly wind conditions for the highest wave events, while the strongest winds can be more often associated with easterly wind directions. This means the storm events near Helgoland do not always occur simultaneously with the strongest winds and sometimes are rather associated with the slower but westerly, i.e. coming from the open sea, winds. This can be explained by the presence of the mainland about 70 km southward and eastward from the island, which prevents the full development of the waves coming from that directions even under strongest wind conditions. The westerly winds bring to the islands swell generated across the North Sea and wind waves developed over

long distances, resulting in higher waves in the German Bight and near Helgoland.

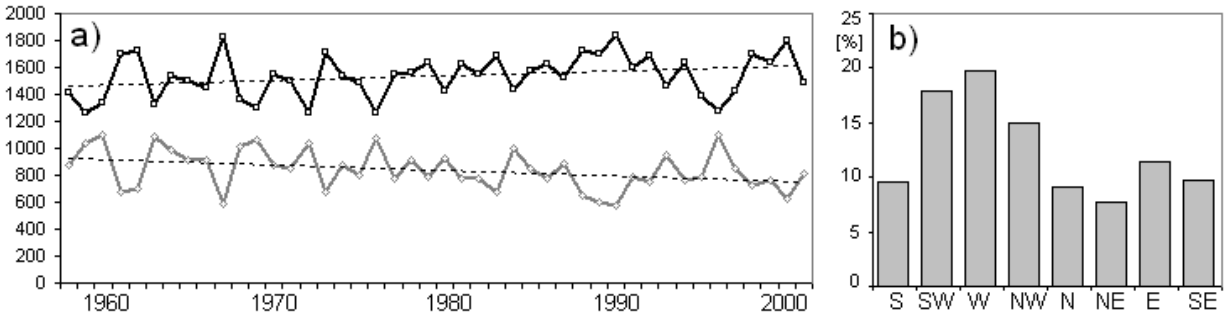

Figure 4.3: a) Number of cases per annum of NW, W, SW wind directions (black) and NE, E, SE wind directions (grey) and linear trends (dashed lines). b) Percentage of the winds from each direction sector for the period 1958-2001.

If the most of wave extreme events occur under westerly wind conditions, then first of all the changes in westerly wind frequency and magnitude can cause the changes in wave extreme statistics. Now the entire distribution of the wind speeds are considered again. The wind speed distribution percentiles were calculated for westerly (SW, W, NW) and all the other winds separately and the corresponding linear trends were estimated (Table 4.1). It appears that for westerly winds the increase in magnitude of all considered percentiles during past 40 years is more intensive than for the winds from all directions together. The winds from the easterly directions become only slightly more intensive for 90, 95 percentiles and for the extreme winds no significant increase in wind speeds have been found. Turning to the frequencies of the winds coming from different directions, at first the general distribution of the wind directions for the period 1958-2001 is presented (Fig. 4.3b). It appears, that more than 50% of all winds in the German Bight are coming from three western direction sectors, the most rare for the area are north-eastern, northern and southern winds. Annual number of cases for westerly and easterly (here NE, E, SE) winds is shown (Fig. 4.3a) to demonstrate the inter-annual changes in the wind direction distribution. One case here represents the 3-hourly wind. Despite rather high inter-annual variability, the clear long-term trends can be detected for both directional groups. The increase of the number of westerlies about 3.5 cases per annum with 95% level of significance was detected. At the same time the downward trend for the frequency of easterly winds is about 4 cases per annum. Together with the fact that the upper annual percentiles of wind speed also increased for westerly winds it can be concluded that the additional cases of westerly winds were, at least partially, corresponding to the wind extreme events.

Summarizing, significant positive inter-annual trends for the extreme and intermediate wind speeds and regional SWH were found for the past four decades. The increasing number of westerly winds was detected for this period. The magnitude of westerly extreme wind speeds was found to be increased as well. Consequently, the upward tendency for the frequency and intensity of the westerly wind extremes for the Helgoland area was revealed

for the past 44 years. This caused the increase of the extreme wave heights on regional scale detected for the German Bight. The impact of these changes on the local wave climate is investigated further.

4.1.2 Analysis of past local wave climate

In order to assess the past local wave climate, the 3-hourly significant wave height fields for the Helgoland area were simulated with the linear regression model (3.2.1) for the period 1958-2001. The annual 50, 75, 90, 95, 99 and 99.9 percentiles of the wave height distribution at each location were computed. To get an impression of the wave height spatial distribution dominating during past four decades, the means of these percentiles were derived and shown in Figure 4.4. In general, the SWH spatial distribution is characterized by the maximum wave heights in the western part of the model domain, gradual decrease of the wave heights further to the east and pronounced low wave area east to the islands. From the small-scale features the higher waves for the shoal north to the island and the higher waves directly to the south and south-east from the main island can be detected as well as constantly low wave region between the islands. This pattern is valid for all considered parts of SWH distribution and corresponds to the wave height spatial pattern associated with westerly wind conditions (Fig. 3.1). This is consistent with the findings about the prevailing wind directions for the region. Most of the storm situations occur under the westerly winds (Fig. 4.2), which explains the spatial patterns for the upper percentiles of wave height distribution. Considering the entire wave height distribution, the priority of NW, W and SW winds is not so pronounced but can still be detected (Fig. 4.3b). Here the proportion of westerly winds (here means only W and not NW or SW) is greater than the proportion of the winds from each of the other seven direction sectors. It is further supposed that the spatial patterns for the intermediate wave heights (50 or 75 percentiles) (Fig. 4.4a,b) demonstrate the wave distribution for this most frequent wind situation.

Together with the mean wave statistics, the changes in wave climatology occurring in the last decades are important. From the previous studies (e.g. WASA Group [1998]) and the conclusions about the wind climatology the existence of the inter-annual trend for the SWH percentiles is hypothesized for the North Sea area and German Bight in particular. On the regional scale, this hypothesis was tested within the HIPOCAS project using the SWH data from HF hindcast. Here the example from this analysis is shown, namely, the trends revealed for the annual 99-percentiles for the North Sea (Fig. 4.5). According to the HF hindcast the positive trends can be detected for the major part of the North Sea with the maximum in south-eastern part about 2.1 cm per annum. The area along northern part of the British coast is characterized by slightly decreasing wave extreme events. For the Helgoland surroundings a rather rough picture of the wave heights and, consequently, the changes in extremes is given by the HF simulation. Nevertheless, looking at the coastlines it can be seen that the increase of the magnitudes of high waves is more pronounced for the Helgoland and the main part of Netherland's coastal zone reaching 1.5 cm per annum, while the estimated increase for the most of German Bight coastlines is only about 0.3 cm per annum. To obtain more confident information about the tendencies of the extreme

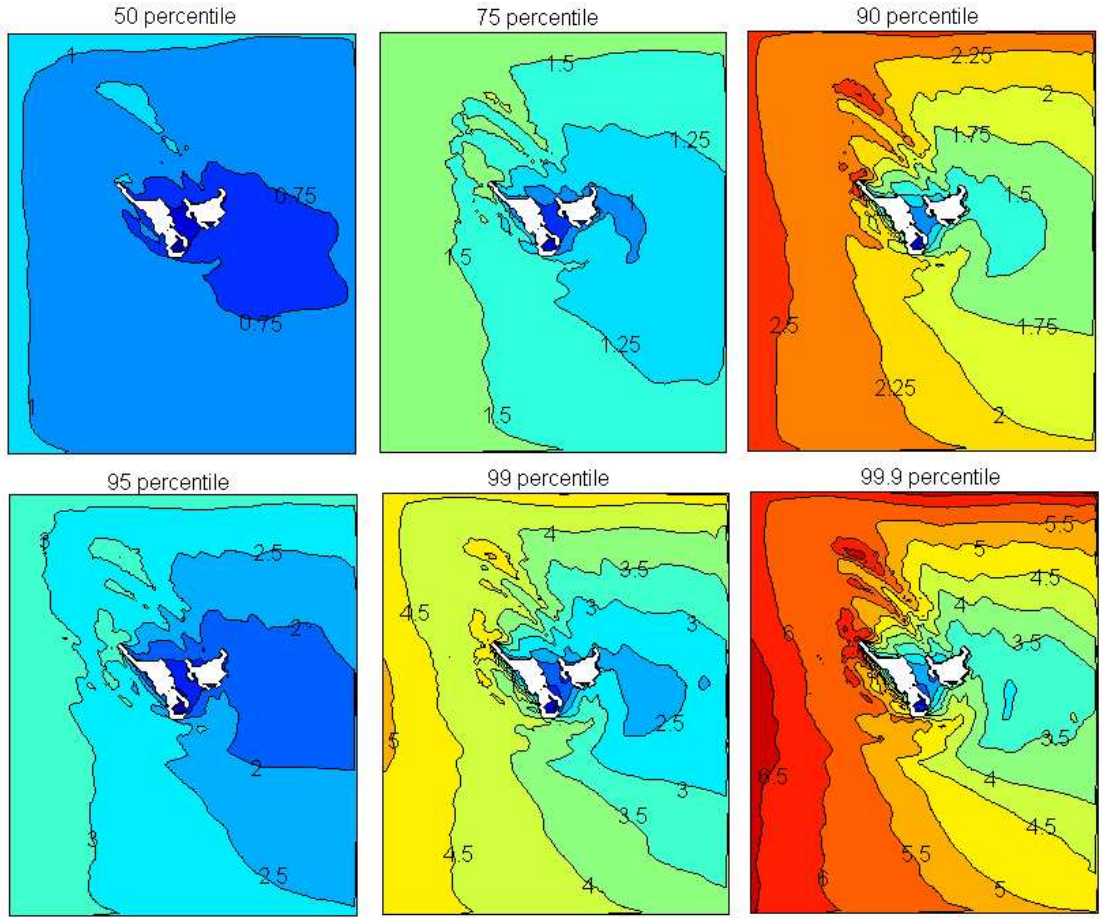

Figure 4.4: Mean of the SWH annual percentiles in meters for the period 1958-2001. Interval for contours is 0.25 m for top panels and 0.5 m for bottom panels.

wave heights in near-shore areas a more detailed wave representation is required.

For this purpose the LR hindcast was used. The linear trends for the selected six percentiles (similar to Fig. 4.4) of the wave height distribution at each location of the model domain were estimated and the results are presented in Figure 4.6. The significance of the obtained trends was tested with the two-sided T-test similar to the case of the wind speeds and it was found that the trends for 50-99 percentiles are significant with 1% error probability and for the 99.9 percentile with 5% error probability. The significance was detected for all locations of the model domain with the exception of the harbor area. Within the harbor the modeled wave heights do not show magnitudes higher than 1 m and are not affected by the intensification of the external wave extremes, which is the direct effect of the presence of the harbor with coastal protection constructions. On the other hand, the representation of the waves by the dynamical and statistical models within the harbor could not be completely adequate as the K-model and the linear regression method do not consider diffraction and were not designed for applications in such areas.

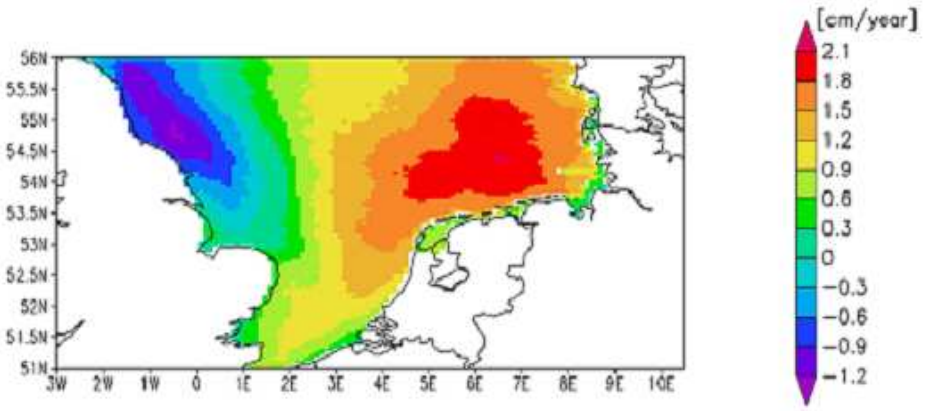

Figure 4.5: Linear trend in cm/yr for the SWH annual 99-percentiles obtained from the HF hindcast for the North Sea 1958-2001 period (from Ralf Weisse, perc. comm.

Comparing the trends estimated from two hindcasts, it can be seen that the magnitude of the LR trends along the western boundary of the small-scale model area is similar to the values of HF trends for the location west to the island and is about 1.6 cm yr^{-1}. There is also a good agreement between LR and HF for the area of lower trends east of the island, in both cases the trends are between 0.6 and 0.9 cm yr^{-1}. This is consistent with the nature of the LR hindcast obtained by downscaling of HF data. Any details and local tendencies, however, are available only from the high-resolution dataset. Coming to the discussion of the local changes in wave climatology, the first regularity to be mentioned is the pattern with the high values on the west and decreasing to the east with a minimum just east of the island, which is similar to the wave height spatial distribution for westerly winds. The percentiles of the wave heights are also distributed similarly and it can be seen from Figures 4.4, 4.6 that higher trends correspond to larger wave heights. The areas of the highest trends correspond to the areas for which the highest wave events were detected, such as along the western coast of the main island and the shoal north to the islands.

4.1.3 Wave directions for wave extreme events

In the Section 4.1.1 the statistics for wind and wave directions were assessed for one location on a coarse grid near Helgoland relevant for the description of the general situation in the region. The additional data analysis was carried out for the assessment of the local wave direction statistics and the prevailing wind directions for the local wave extremes in different locations of the high-resolution KMH model domain. For this experiment the dynamically obtained wave direction fields have been chosen as most accurate and having physical basis, which helps in the interpretation of the results. The time-slice experiments have been made for the comparison of dynamically estimated statistics at the beginning and at the end of the period considered. From the KMH experiment (2.1.3) the instantaneous

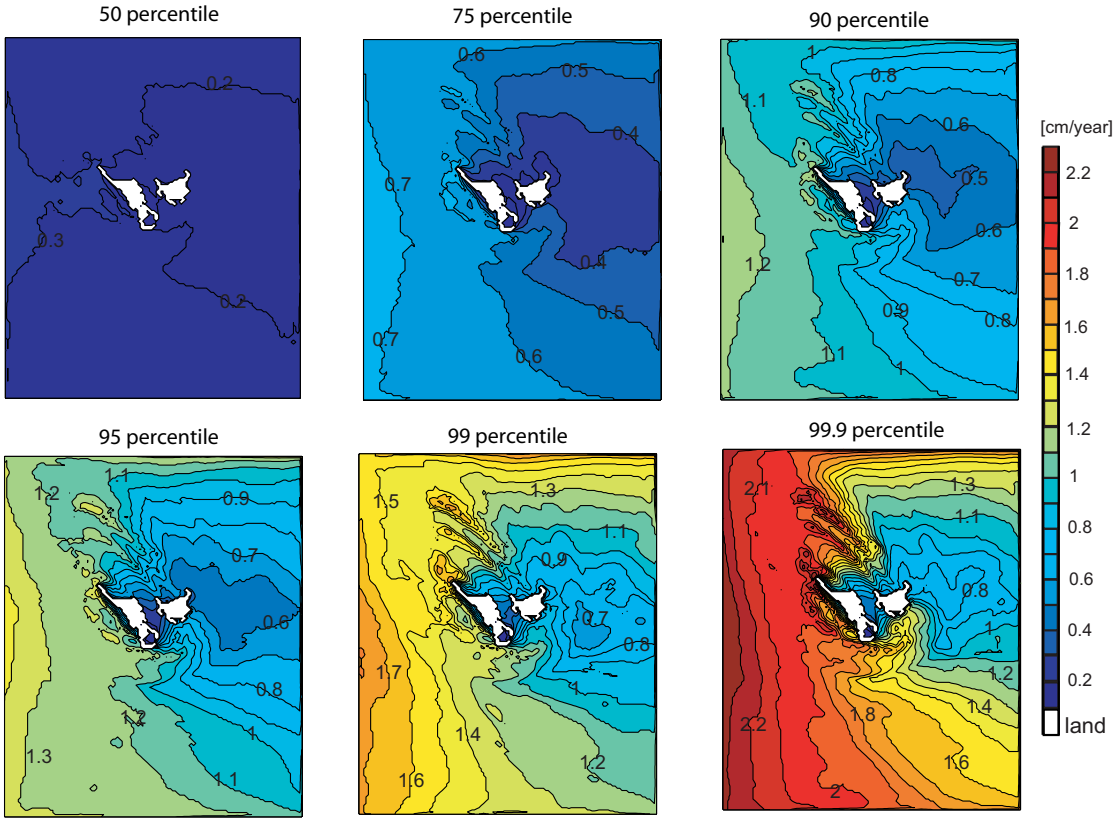

Figure 4.6: Trends for the annual percentiles of SWH estimated for 1958-2001 period in cm yr^{-1}. The contour interval is 0.1 cm yr^{-1}.

wave parameters were available for the period 1990-2001. In addition, wave parameters were simulated for the beginning of the 44-year period of the study, namely 1958-1965. From the 3-hourly modeled wave directions the records corresponding to the wave heights larger than annual SWH 99-percentiles were extracted for each location and each year for these two periods. In addition, for each location the wind directions corresponding to the upper 1% of the wave heights were derived from the dataset described in 4.1.1. From this data the mean wave and wind directions at each location were calculated for 1958-1965 and 1990-2001 periods. Standard deviations of the yearly samples of wind and wave direction were also calculated and the mean standard deviations for two periods were obtained. During the comparison of the mean and standard deviations for the beginning and the end of the considered 44-year period, no significant differences were detected for both wave and wind directions. Further on, the description of the directions for extreme events is limited to the 1990-2001 period.

As it could be expected based on the results of 4.1.1, most of the high wave events for the Helgoland surroundings occurred under westerly wind conditions (Fig. 4.7b) with the exception of the harbor. Here the waves penetrate the harbor directly only with easterly

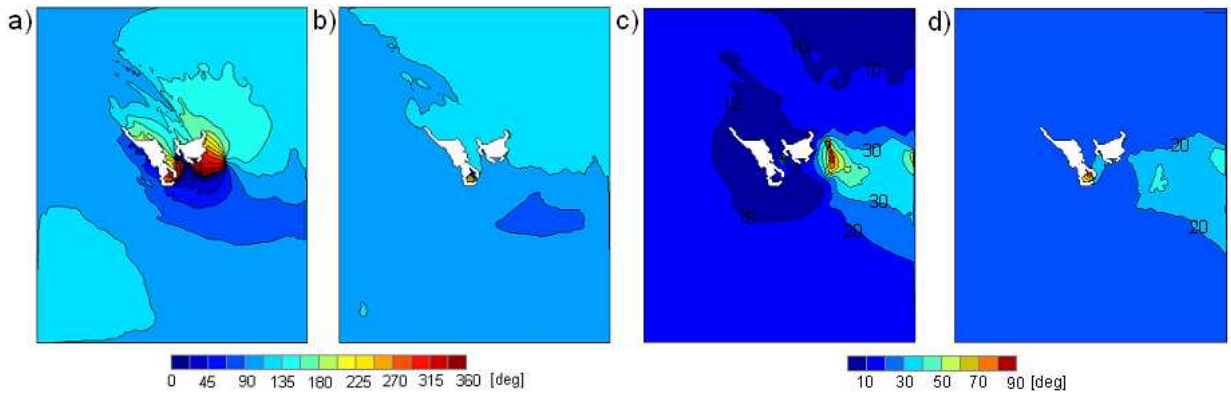

Figure 4.7: Mean wave (a) and wind (b) directions (going to) in degrees corresponding with the upper 1% of the wave heights for the 1990-2001 period. Mean of yearly standard deviations of the wave (c) and wind (d) directions for 1% of highest waves.

winds and in the other cases this is possible only for refracted waves which have already lost most of their energy and are not so high. So, the extreme wave events in the harbor are rather related to easterly winds and this is the direct consequence of the breakwater presence. The K-model considers this topographic feature and represent the consequences adequately. To asses the spread of the wind directions responsible for the high waves on the entire area, the standard deviations are shown in Figure 4.7d. For the major part of the model domain the deviation smaller than 30 degrees can be detected, which means all or almost all winds corresponding to high wave events are coming from the NW, W or SW directions. For the north-eastern part of the domain northerly wind conditions are also possible for the extreme wave occurrence. For the area of larger deviations located east of the island the opportunity of the high wave events under easterly winds can not be excluded. It appears that within this region the easterly winds caused the wave events with SWH larger than 99-percentile. For example, it was the case for the year 1996 (not shown) characterized by the largest number of easterly winds (Fig. 4.3a) and lowest upper percentiles for wave heights (Fig. 4.1b) for the entire 12-year period. The high waves under easterly winds do not occur often and do not influence the wind direction statistics significantly, but their existence should be taken into account.

Concerning the wave directions (Fig. 4.7a,c), for the deep water areas on the south, west and north of the model domain the wave directions for the high waves agree well to the wind directions and demonstrate the prevail of westerlies. For the shallow water locations around the island the wave directions are transformed due to refraction and high waves turn towards the island. Standard deviations here become smaller as soon as the wave directions are more influenced by the shallow water processes superimposed on the external wind/wave directions. The area eastward of the islands is most unsteady in terms of direction variability. In some locations the deviation is up to 80 degrees, which means that basically no prevailing direction can be detected. On the one hand, the high waves corre-

sponding to the westerly winds here become lower due to refraction and energy dissipation and their magnitudes can be comparable to the waves coming from the east. Some high wave events happened under easterly wind conditions and this is reflected by the increased wind direction variability (Fig. 4.7d). On the other hand, most of the high wave events can still be attributed to the westerly winds. In this case the wave spectra to the east of the island are developed by the influence of the two wave trains coming from the north and south of the island. These wave systems round the island enduring the strong changes by the shallow water processes, therefore, the specific shape of the resulting wave spectrum is dependent on the number of local processes and time-variable fields such as water depth and currents and to a minor extent on the external wind/wave directions. However, this highly uncertain area is small; for the locations directly east and south of the islands the wave direction patterns are defined quite clear with the prevailing westward and northward high waves. Further to the east from the uncertain area quite stable westerly high waves prevail again.

4.1.4 Extreme value analysis for significant wave heights

Normally, the information about the past wave climate is used as the basis for the estimation of the future wave extreme statistics required for the planning of the coastal and off-shore constructions. One of the methods of future climate assessment is the extension of the climate trends and dependencies detected for the past into the future. But for the successful application of this methodology, with reduced uncertainty, the existence of the data for very long period in the past (hundreds of the years in case of wave climate) is required. For shorter periods of time, for example several decades, the artificial trends in the data can be revealed, although, in reality they are attributed to the natural system variability on the timescales beyond those considered. In present study this is the case because it is not completely clear whether the increase of the extreme wave heights detected for the last four decades will take place in the near future or if it is just the property of the chosen time slice.

Another possibility to obtain the information about the most severe wave conditions expected during the lifetime of the coastal constructions is the use of the existing wave statistics for the estimation of wave height return values and return periods. Return value is by definition the value which is exceeded on average once during the considered period. Accordingly, this period is the return period for that value. In this study the SWH return value estimates were computed with the annual maxima method in which the Generalized Extreme Value Distribution (GEV) was fit to the sample of annual SWH maxima (for method description see e.g. Coles [2001]). The GEV family of distributions has the form:

$$G(z) = \exp\left\{-\left[1+\xi\frac{z-\mu}{\sigma}\right]^{-1/\xi}\right\}$$

defined for $\{z : 1+\xi(z-\mu)/\sigma > 0)\}$, with a location parameter μ, a scale parameter $\sigma > 0$ and a shape parameter ξ estimated by maximum likelihood method. The LR SWH dataset

for the period 1958-2001 was used for this analysis. For each location of the model domain and each year the SWH records were selected according to the corresponding wind directions and were grouped into eight SWH subsets according to the 45-degree wind direction sectors (similar as for LR model construction). The annual maxima at each group were then selected and the GEV distribution was fit for each location and each direction group based on the 44 SWH annual maxima. Finally, 20, 50 and 100-year return values were estimated from fitted distributions.

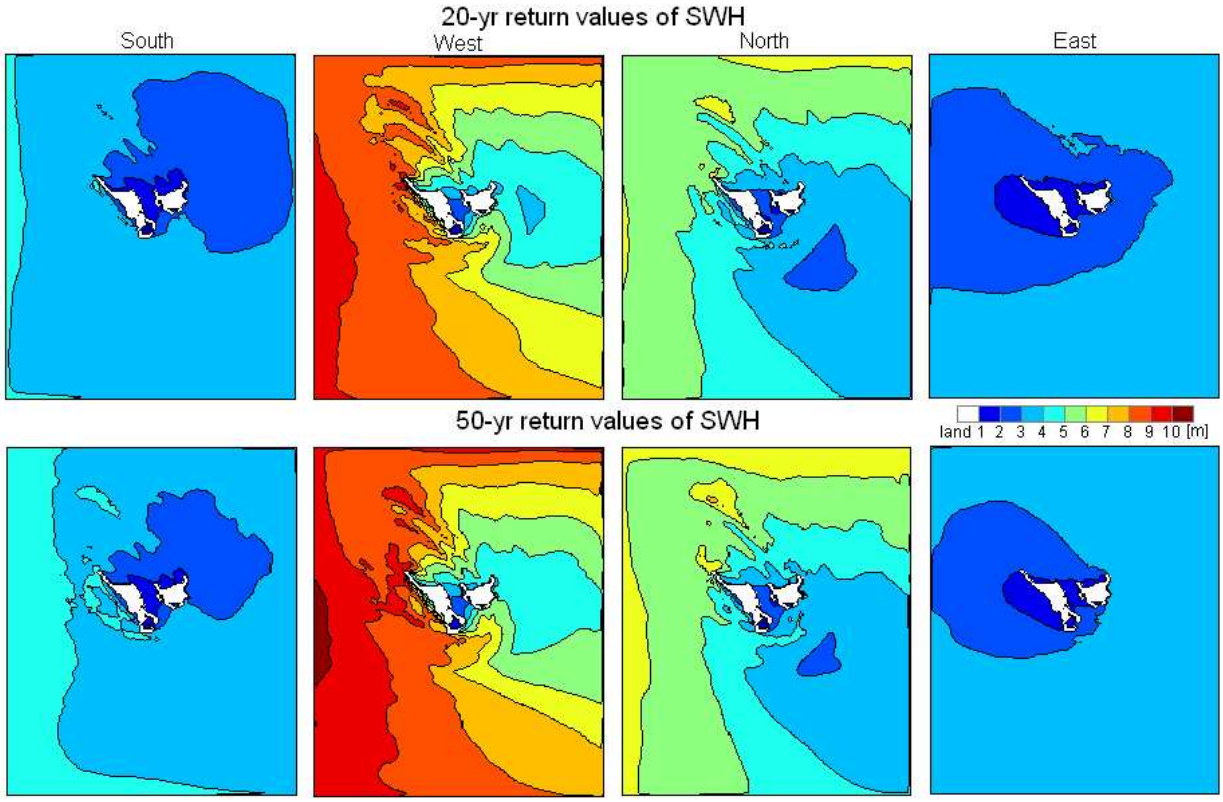

Figure 4.8: 20 and 50-year return values of SWH in meters estimated for the winds coming from southern, western, northern and eastern 45-degree sectors.

In Figure 4.8 the examples of the SWH 20 and 50 year return values for four wind direction sectors are shown. Here the spatial structure of the 20-year and 50-year return value fields is similar for the same wind directions and, as expected, the magnitudes of the estimated 50-year return values are slightly higher than 20-year values. Significant differences between the return values associated with different wind directions were revealed. While for easterly and southerly winds the 50-year return values appears to be not larger than 5 meters, for westerly winds the estimated return values amount to 10 meter magnitude. The presence of the largest return values for westerly winds corresponds with the findings of the previous section concerning the prevailing westerly storms and the occurrence of the highest waves under westerly wind conditions. The spatial pattern of return values for

westerly winds is close to that for the SWH 99.9-percentiles (Fig. 4.4) with both 20 and 50 year return values demonstrating larger magnitudes than the SWH 99.9-percentiles. This is consistent with the definition of the return value as an event happening once within a certain period (here 20 or 50 years) and the definition of the percentiles from which follows that for the LR wave data the events with wave heights equal or larger than annual 99.9 percentiles occur 3-4 times a year.

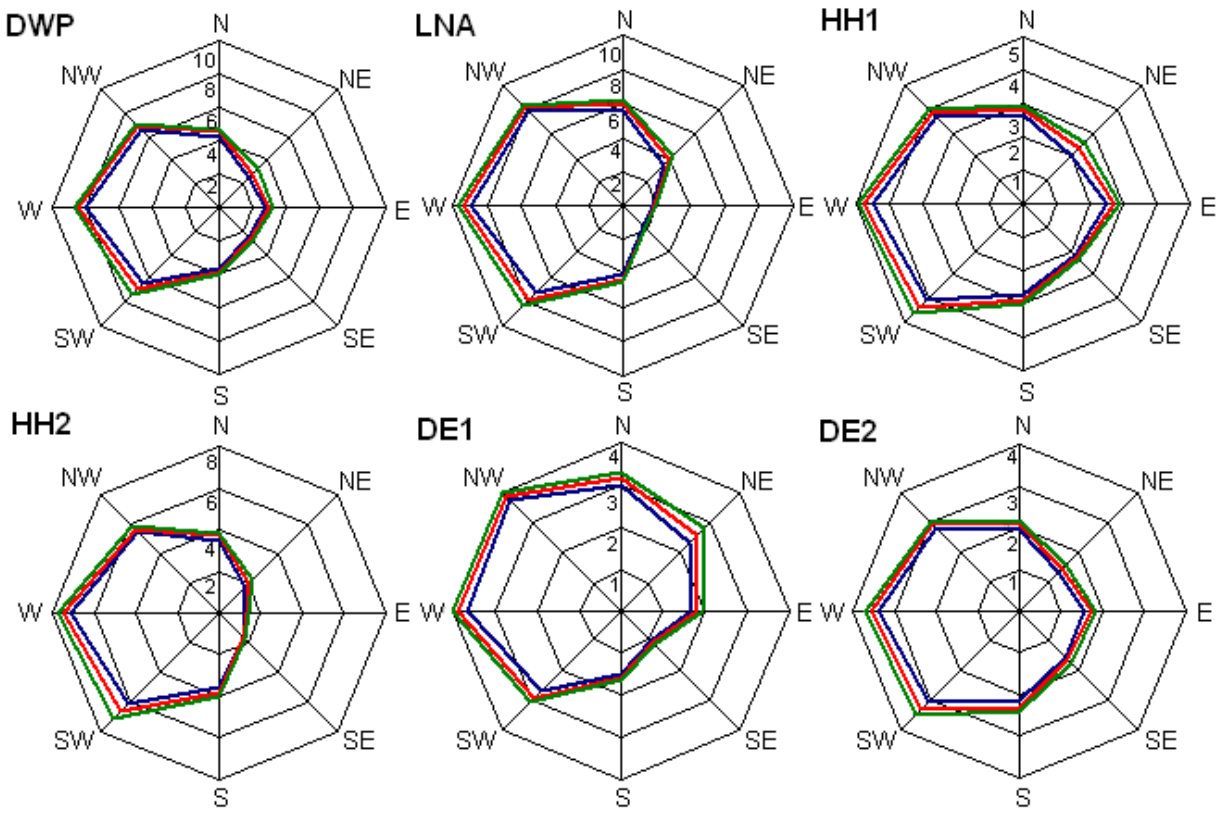

Figure 4.9: 20 (blue), 50 (red) and 100 (green) year return values for SWH in meters for selected locations and 8 wind direction sectors (winds are coming from). For the exact locations see Fig.2.1

The estimation of return values for different wind directions can be useful for engineering applications because it defines the magnitude of the waves developed under certain wind conditions and the direction of its approach. As an example of the directional return value distribution, the 20, 50 and 100 year return values for the selected locations near Helgoland are shown in Figure 4.9. Some peculiarities related to the situation of the locations (see Fig. 2.1) and revealed earlier in this work for the extreme wave directions (3.3.1, 4.1.3) and wave height extremes (4.1.2) can be detected for the return values as well. For LNA and DE1 the southeasterly winds produce minimum waves because of the island and breakwater presence; for the locations situated behind the island with respect to westerly winds, such as HH1, DE1, DE2, the return values are smaller than for the other locations. For each

location the conditions and the approaching directions of the extreme events are detected. Similar information for any place of interest can be obtained with GEV models.

The attempts to estimate wave extremes for the Helgoland surroundings were undertaken in earlier works dedicated to the Helgoland wave climatology (e.g. Vierfuss [2002]). But for several reasons previous results can hardly be compared quantitatively with the results obtained within this study. At first, the wind forcing used in Vierfuss [2002] originated from the pressure fields of the weather analysis produced by Norwegian Meteorological Institute (DNMI), some deficiencies of this wind data with respect to REMO winds used in present study were investigated and discussed in Weisse and Plüss [2005]. Further differences between present and earlier small-scale extreme wave estimations comprise the use of different wave models for medium-scale wave simulations serving as the basis for the local wave estimations (WAM (WAMDI Group [1988])for present and HYPAS (Günther and Rosenthal [1985]) for earlier work), and the use of different methodology for obtaining the local wave statistics. For this study the small-scale instantaneous wave data were obtained with the statistical-dynamical approach and then the extreme wave statistics were estimated from the datasets. For the previous study only selected high-wave situations were dynamically simulated with the SWAN model and then the wave statistics obtained from the medium-scale hindcast were extended to the local wave statistics. As a result of the described differences, it is difficult to attribute the discrepancies in two works. This study seems to be the qualitatively new update of the extreme wave analysis presented in Vierfuss [2002] due to the use of the improved forcing fields and wave models as well as the ability to produce long-term local wave simulations used for the final statistical analysis.

4.2 Future wave climate and scenario study

Currently, the quality of long-term wave hindcasts make them an appropriate tool for obtaining past wave statistics if the adequate atmospheric data are available. But for the evaluation of future wave climate the knowledge of the previous statistics may be not enough if climate undergoes changes unexplained by the internal system variability. From the past wave climate analysis for Helgoland it was not completely clear if the changes in wave statistics were caused by natural variability or were the results of the anthropogenic influences. It was shown that storminess and wave characteristics are strongly dependent on the atmospheric situation and that, additionally, in the face of global climate change the response of the wave climate has to be studied. Anthropogenic emission of green house gases and aerosols is named as one of the main sources of global climate change and the problem of anthropogenic influence on different natural systems in the past and future has been intensively investigated during last couple of decades. The overview of the main problems and areas of investigation as well as achieved results can be found, for example, in the IPCC Reports (e.g. McCarthy et al. [2001]). From the whole range of the climate change impacts on the coastal zones, attention was mainly payed to the sea level change. This can be attributed to strong sensitivity of low-lying coastal areas to even small changes of sea level and to the fact that during past 100yr the average sea level rose by 1-2 mm/yr and

further acceleration of this rate is anticipated (IPCC TAR 2001). In addition, the response of the sea level on climate change is one of the most definitive results of investigated climate change impacts, unlike other parameters, whose responses are often not so clear either for the past observations or for the future projections, and vary for different parts of the globe.

Recently, more attention was paid to changes of regional wave and surge climate and several scenario studies were carried out. They adhered to the generally accepted structure where a global climate model first simulates the response of the climate system to a certain future scenario and then the obtained data are fed into the regional atmospheric, wave or surge models. Finally, the obtained projections are compared with the results of the same regional model for control or present day conditions to evaluate the rate of differences which could occur for the altered climate. Within WASA project (WASA Group [1998]) two 5-year time-slice experiments for present climate and double CO_2 conditions were carried out for winds and waves in North Atlantic based on the results of atmospheric GCM experiments. The extended study was made within STOWASUS-2100 (regional STOrm, WAve and SUrge Scenarios for the 2100 century) project (Kaas and STOWASUS-Group [2001]), here two 30-year time-slice experiments were made for North Atlantic with the dynamical wave and surge models. The control run for the period of 1970-1999 and a double carbon dioxide run for the period of 2060-2089 were carried out. The results for wind conditions showed increase up to 10% for the extreme wind speeds in the North Sea and the Norwegian Sea under enhanced carbon dioxide conditions. The changes in wave climate followed from the difference between two experiments were characterized by the increasing of average significant wave heights by 5% at the North sea and 10% at Norwegian sea, and for extreme waves by the increase of about 10% for the Norwegian Sea and decreasing in southwest North Atlantic. In the study carried out by Wang et al. [2004] the scenario assessment experiments were made with a statistical model which connected seasonal wave height fields with sea level pressure fields for the North Atlantic. The sea level pressure fields were obtained for three different anthropogenic emission scenarios. For all three, the projected wave heights showed increase for northeast and decrease for southwest Atlantic for winter and fall seasons, which corresponds to the WASA and STOWASUS findings, disregarding differences in time-slices, projected scenarios and models. In these studies the strong dependency of the wave statistics on the atmospheric forcing has been detected. It was also pointed out that the uncertainties in the realizations of atmospheric fields obtained with different GCM or RCM may cause significant quantitative differences in the projected wave statistics.

4.2.1 PRUDENCE project as the basis for the small-scale future wave climate assessment.

Recent study of the assessment of the changes in regional atmospheric and ocean fields due to anthropogenic climate change was carried out within the PRUDENCE (Prediction of Regional scenarios and Uncertainties for Defining EuropeaN Climate change risks and Effects) project (Christensen et al. [2002]). The main goal of the project was the evaluation of uncertainties for the projected atmospheric climate that occurred due to the use of

different global (GCM) and regional (RCM) climate models. Further, the influence of the differences in atmospheric data representation on the uncertainties for the projected regional ocean climatology obtained with these atmospheric data was also partly investigated. A number of experiments were performed for the project. Here the part of them related to the atmosphere/ocean climate of the North Sea region is briefly described following the work of Woth et al. [2005]. The set of ensemble simulations were performed with the different RCM forced by the same General Circulation Model (HadAM3H) for "control" (1961-1990) and "climate change" (2071-2100) time slices. The climate change scenario was the IPCC A2 SRES scenario (Houghton et al. [2001]). It was revealed that 10-meter height wind fields simulated with different RCM for the North Sea showed the general underestimation of the upper wind speed percentiles for the control run with respect to the hindcast for the same period. The differences between the upper percentiles of the wind speeds from A2 SRES scenario and control run were found to be similar for different RCM simulation. They were characterized by a slight increase of the wind speeds with respect to control run. The maximum increase was detected for the westerly winds, for 99-th percentiles of 6-hourly wind speeds the differences vary from 1.4 to 2 m/s depending on the RCM.

The use of the regional atmospheric fields from different RCM models as the driving forcing for the regional ocean and wave models allows for the investigation of the differences in the response of the ocean fields to climate change in the interpretation of different models. The study concerning the storm surges for the North Sea was carried out and the main results can be found in Woth et al. [2005], Woth [2005]. Similar investigation of uncertainties and changes of the wave climatology for the altered climate using different driving atmospheric forcings is being carried out at the present time for the North Sea region. The study is not completed yet, but some available data is used in present study to provide the example of a local scenario study. Here, the obtained medium-scale wave data is used for further downscaling and assessment of the changes in local near-shore wave climate around Helgoland for the future development scenarios. The instantaneous wave fields in 5x5 km resolution (similar to the HIPOCAS fine grid data (2.1.2)) are available for the control run (1961-1990) with present day green house gas concentrations and for A2 and B2 SRES emission scenarios for the end of the century (2071-2100) Ralf Weisse, pers. comm.). The scenarios are described in the *IPCC Special Report on Emission Scenarios* (SRES; http://www.grida.no/climate/ipcc/emission). The A2 scenario is focussed on self-reliance and preservation of local identities, while the B2 is oriented toward more environmental protection and social equity. The medium-scale wave datasets were obtained with the WAM wave model driven by the results from regional atmospheric model RCAO from Swedish Meteorological and Hydrological Institute (Döscher et al. [2002]). For the convenience these datasets are referred later as HFC, HFA and HFB or just HF. For the assessment of potential wave climate change for the Helgoland area this data is used together with the linear regression downscaling technique described in 3.2.1. Three 30-year time slices of the 6-hourly high-resolution significant wave heights were simulated with the spatial characteristics similar to that described in 2.1.3 and referred later as LRC, LRA and LRB datasets (linear regression control, A2 and B2). As soon as the changes in wave extremes

are of the most importance for the coastal planning, the investigation of the wave climate scenarios is limited to the assessment of changes for extreme wave statistics. For that the annual 99-percentiles of SWH were extracted from the small-scale datasets and used for further analysis.

4.2.2 Downscaling of the wave extremes vs. instantaneous wave height downscaling.

In many studies dedicated to the investigation of regional climatology that use the concept of statistical downscaling for obtaining the regional/local data, the seasonal or annual statistics of the field in question is downscaled instead of the instantaneous fields (e.g. Kushnir et al. [1997], WASA Group [1998], Wang et al. [2004] etc.). In this study the instantaneous downscaling approach has been applied and explored following the needs of the coastal applications and the fact that the time-series of instantaneous small-scale and medium-scale SWH are highly correlated. In the case of the construction of long-term scenario projections and subsequent assessment of the climate change, only statistical characteristics are normally considered for the analysis. It is proposed, therefore, to apply the downscaling procedure to the percentiles of SWH fields directly. In this section the results of this experiment are compared to the results of instantaneous downscaling procedure.

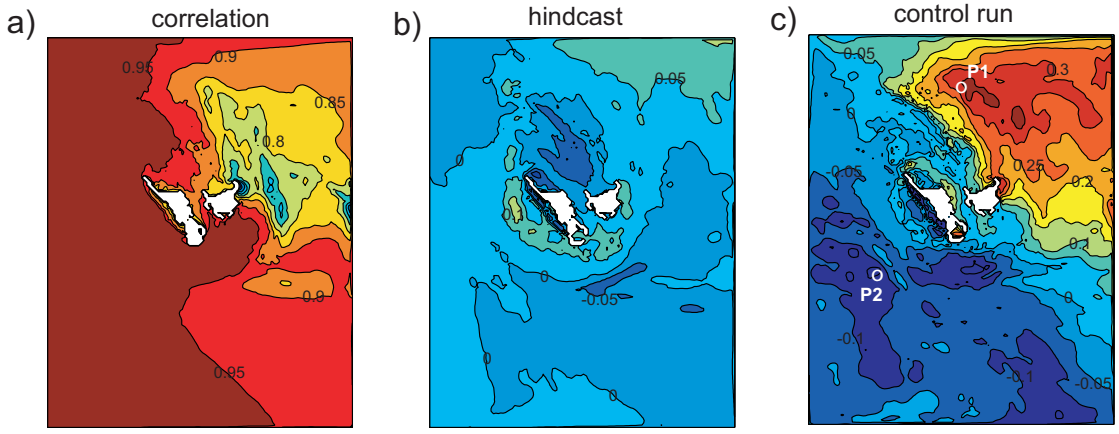

Figure 4.10: a) Correlation between annual 99%-tiles of SWH obtained from KMH and LP (for details see 4.2.2). Differences in meters between mean annual 99%-tiles from b) LPH and LR for hindcast 1958-2001, c) LPC and LRC for control run 1961-1990.

The linear regression model which connects the annual 99-percentiles of medium-scale SWH at the location near Helgoland (the same as for simple linear regression) and the high-resolution SWH annual 99-percentiles was constructed. The SWH fields simulated with HF and KMH for 1958-1965 and 1990-2001 periods were used to train the model. Due to the limited amount of data there is no possibility to separate the dataset into independent parts for training and validation of the regression model and the cross-validation

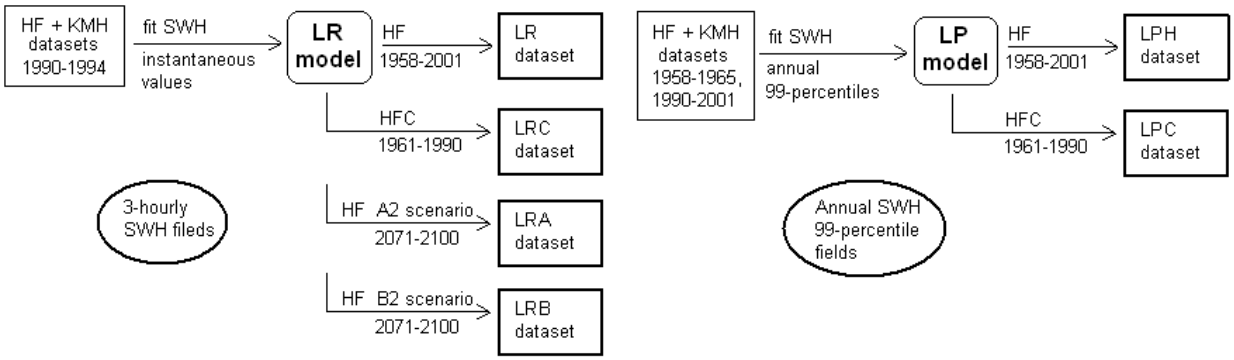

Figure 4.11: Statistical models and local wave datasets obtained by downscaling of different medium-scale wave data with these models.

procedure is used instead (e.g. von Storch and Zwiers [1999]). To do so, each year was successively excluded from the sample, for the remaining pairs of the SWH 99-percentiles the model coefficients were fit for each location with the least squares method. Using these coefficients high-resolution 99-percentiles of SWH for the excluded year were reconstructed at each location. To test the skill of the fitted models, a sequence of 22 SWH 99-percentile fields reconstructed with 22 different statistical models was obtained and correlation between reconstructed and KMH-modeled SWH percentiles at each location was calculated (Fig. 4.10a). The coefficients of the statistical models, constructed using different subsets of the sample, are close to each other, with the variance of the sequence of coefficients for each location less than 0.5% of the coefficient magnitude, which means that each subset captures the properties of the empirical distribution function of the whole sample. Finally, the model based on the whole sample (22 years) and referred later as LP (linear regression of percentiles) is fit and used for further SWH percentiles reconstruction. The correlation skill score demonstrates the ability of the models built for different subsets, and to some extent the ability of the LP model to reconstruct the inter-annual SWH percentile behaviour. For the major part of the model domain a correlation higher than 0.9 was detected. For the area north-east of the islands the correlation between KMH and downscaled SWH annual percentiles is higher than 0.7. This area is characterized by a weaker dependency between used medium-scale wave parameters from HF at the location west to Helgoland and local wave parameters. This was revealed for the peak period instantaneous values (3.3.2) and was not so pronounced for SWH instantaneous values, for which the correlations between HF (west location with respect to island) and KMH local values as well as between HF west location and HF east location are higher than 0.92 (not shown). The annual SWH 99-percentiles appear to be less dependent and correlation between HF west and east locations is about 0.79.

The LP regression model was applied to the HF hindcast SWH data (1958-2001) and HFC data for scenario control run (1961-1990), and obtained high-resolution 99-percentiles are referred later as LPH (Linear regression Percentile Hindcast) and LPC (Linear regres-

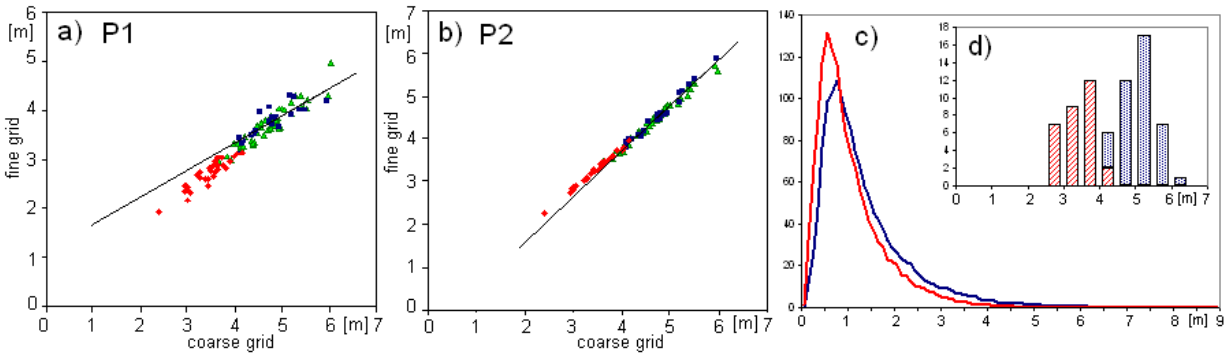

Figure 4.12: Scatter plots for annual 99%-tiles for locations P1 (a) and P2 (b): HF hindcast vs. KMH (blue) and corresponding fit, HF hindcast vs. LR (green) and HFC control run vs. LRC (red). c) Empirical probability density for HF instantaneous SWH from hindcast (blue) and control run (red). d) Histograms for HF annual SWH 99%-tiles from hindcast (blue) and control run (red).

sion Percentile Control run). In Figure 4.11 the main datasets used in this experiment are presented. To asses the differences in representation of extreme wave statistics by instantaneous and direct percentile downscaling, the mean annual 99-percentiles from LPH and LPC were compared with the mean 99-percentile values obtained from the LR and LRC instantaneous SWH datasets for two periods (hindcast and control run). The results of the comparison are shown in Figure 4.10b,c. For the hindcast the models demonstrate rather similar results with differences less than 0.05 m for the most of the area. No systematic bias between LR and LPH percentile representation attributed to the methods and independent on the location were detected. For the control run, the differences become more pronounced and the distinct areas of positive and negative relations can be detected. For the north-eastern part of the model domain the direct downscaled percentiles are higher than the percentiles obtained from instantaneous SWH fields, with maximum difference about 0.4 m, and for the south-eastern part the direct percentiles are underestimated with maximum differences less than 0.2 m. The spatial patterns of the differences for the hindcast and control run are different.

The changes in percentile distribution for the control run climate with respect to the hindcast are considered as one of the reasons for the increased discrepancy between LR and LP model results. To investigate this problem closer the normalized empirical distribution densities of the instantaneous HF SWH were built for the hindcast (1958-2001) and the control run (1961-1990) (Fig. 4.12c). The shape of the SWH probability density is similar for both periods, with the tendency towards the smaller wave heights for the control run. This corresponds with the findings of Woth et al. [2005] concerning the underestimated representation of the wind speeds over the North Sea region, which causes the underestimation of the wave heights. Nevertheless, the significant wave heights for two periods vary approximately within the same interval and the downscaling LR model fitted with one

dataset (here hindcast) can be successfully applied to the downscaling of the other (control run). For the same two periods the histograms of the annual 99-percentiles of HF SWH were constructed (Fig. 4.12d). The distributions of percentiles demonstrate significant difference and the control run extreme waves appears to be much lower than the hindcast data. This is consistent with the differences found for the instantaneous SWH distributions, but in contrast to the instantaneous SWH statistics, the annual percentile values have only a slight overlap for two considered periods. The LP model was fit to the hindcast dataset and showed good skills in representation of the SWH percentiles from the same distribution. However, it has limited, if any, skill in the representation of the SWH percentiles from the control run distribution.

To illustrate the uncertainty of the downscaling results obtained with the model which was fit and applied to differently distributed data, the annual SWH 99-percentiles from two periods were compared for the example locations P1 and P2 (for locations see Fig. 4.10c). For these locations the largest positive and negative differences between LRC and LPC 99-percentiles were detected. In Figures 4.12a,b the scatter plots of the medium-scale HF and high-resolution KMH hindcast (1958-1965,1990-2001) are shown, this is the data used for the LP model construction. Thus, all 99-percentiles obtained with LP model for any period and these location have to lie close to the shown linear curves. For comparison the scatter between HF and LR hindcast (1958-2001) are shown, the LR percentile representation only slightly differs from KMH. The last group of data is the HFC control run annual percentiles versus LRC 99-percentiles. The "control run" pair follow the linear pattern of the "hindcast LR" as soon as the same model is used for their reconstruction. The differences presented in Figure 4.10b,c are basically explained by the discrepancy between the linear fit of HF-KMH percentiles and the HF-LR instantaneous fit, which appears to be lower for the hindcast and larger for the control run. The absence of the high-resolution 99-percentile data correspondent to the HF wave heights of the 3-4 m magnitude gives no opportunity to fit the LP model properly for all the range of the driving (HF) SWH data, as well as no ability to check if the modeled with existed LP model percentiles are adequate for the control run period.

4.2.3 Future climate projections

Due to the uncertainties detected for the LP downscaling model in the representation of the wave statistics, projections for the future climate change scenarios are built using the linear regression for instantaneous SWH and the analysis is based on this data only. The mean of annual 99-percentiles of SWH obtained for the A2 and B2 scenarios with linear regression model (LRA, LRB) are compared with the mean of 99-percentiles for control run (LRC). The estimated differences between extreme wave SWH for the altered climate with respect to present one are shown in Figure 4.13a,b. For comparison the analogous differences for the medium-scale SWH were obtained for the German Bight (Fig. 4.13c,d). Here the annual 99-percentiles were calculated from the HF data. The projected mean SWH percentiles are higher for both scenarios with respect to control run for the most part of the bight. The maximum positive differences of about 20 cm can be detected in

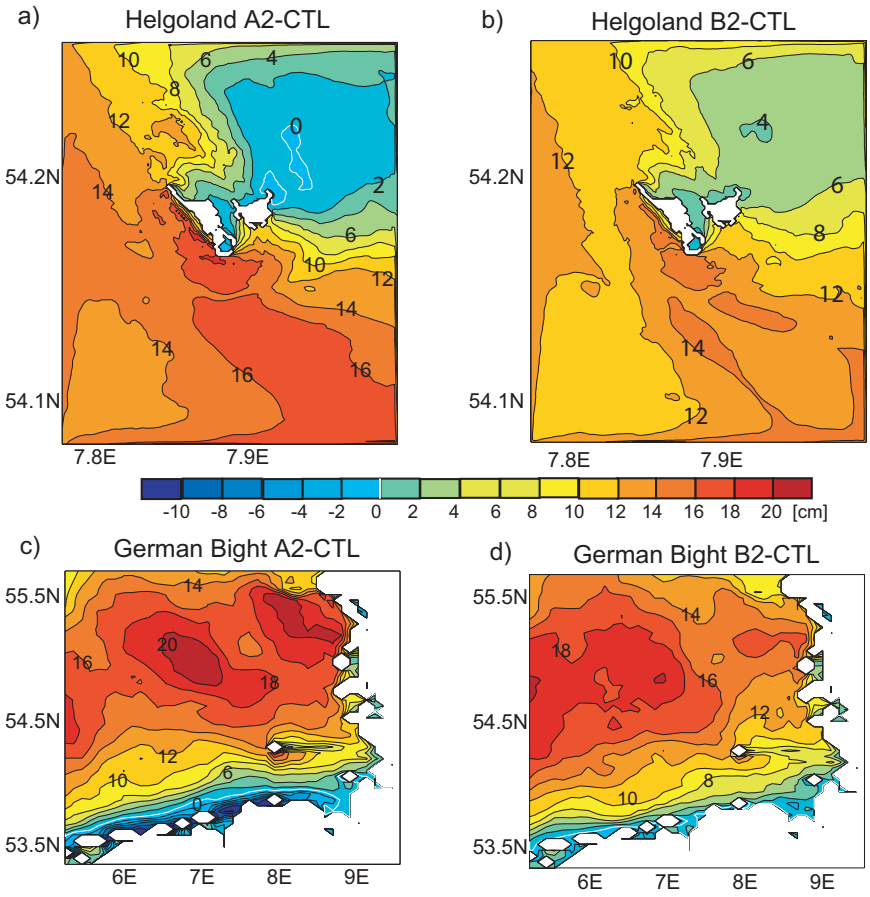

Figure 4.13: Differences in centimeters between the mean annual 99%-tiles of SWH obtained for scenarios and control runs a) with the LR model for the A2 SRES scenario, b) with the LR model for the B2 SRES scenario, c) with the HF model for A2 d) with the HF model for B2.

the northern part of the bight. That is about 5% of the control run mean 99-percentiles. At the same time the differences are negative along the southern coastline, where the projected SWH extremes are lower than the extremes from the control run. The maximum negative difference is about 15 cm. For the area around Helgoland the extreme wave heights for both scenarios appear to be higher than the control run results. The differences for the area to west from the island reach 13-15 cm and for the eastern part they are about 5-8 cm (Fig. 4.13c,d). For the high-resolution wave representation (Fig. 4.13a,b) the spatial distribution of the differences between the scenarios and the control run has similar structure, but they are more detailed and variable with respect to the regional case. Thus, the area of very low increase or even decrease of the SWH 99-percentiles for the scenario A2 can be distinguished to the north-east from the island. For the B2 scenario this area is also characterized by smaller differences between the scenario and the control run. The maximum local differences can be found for the A2 scenario in south-eastern part of the

area. They reach 16 cm, that is about 6% of the mean SWH 99-percentiles from the control run. This corresponds to the regional picture of the wave extremes (Fig. 4.13c), where the area to the south-east from the island is also characterized by the larger scenario/control run differences with respect to nearby locations.

The differences between two scenarios can be seen for the regional and the local wave representations. The significance of these differences was tested for the local and regional data separately. The next hypothesis was tested for each location: the means of the annual SWH 99-percentiles from the A2 and B2 scenarios can not be distinguished. The standard T-test was applied and it appeared that the hypothesis can not be rejected for all locations of the regional as well as of the local wave height projections. This means, no clear statistical distinction between the A2 and B2 SRES scenarios for the SWH extremes is possible. This corresponds to the findings of Woth [2005] for surge residuals, where no significant difference was found between two scenarios based on HadAM3H GCM.

The next considered question is how the projected changes in local wave climate caused by the anthropogenic climate change correspond to the actual changes detected for the last decades. It is not completely valid to compare the inter-annual trends obtained for the hindcast with the absolute differences between the time-slice data for the scenarios, but the spatial distribution of the changes and a rough approximation of the trends for the annual 99-percentiles can be justified. The projected changes are lower and have slightly different spatial pattern in comparison with the changes for the past wave climate (Fig. 4.6). Thus, for the hindcast the magnitude of SWH changes decreases from the west to the east, while for both scenarios the decrease in the north-east direction was detected. The largest changes for the proposed scenarios are about 16 cm. Looking at the largest annual changes for the hindcast, that are about 1.8 cm yr^{-1}, it can be estimated that the changes of magnitude 16 cm can be expected after approximately 9 years, if the similar tendency would be held. At the same time the scenarios are constructed for the end of the century. Different nature of the changes of SWH extremes for the scenarios and the hindcast could cause the shown discrepancy. The anthropogenic influence is the crucial reason for the changes projected by the scenarios. For the hindcast the reasons are not so clear. Here the high increasing trends can be partially explained by the choice of the period considered for the analysis (see 4.1.1).

The estimated differences between the scenario and the control run for the SWH extremes appear to be lower than the differences obtained and shown in other works dedicated to the scenario studies, for example in the STOWASUS-2100 project. There the estimated differences for the 99-percentiles of SWH between the scenario and the control run were about 25-50 cm for the North Sea region. One reason for the differences can be the formulation of the used in STOWASUS-2100 scenario, which differed from the scenario used in this study (double CO_2 vs. A2 SRES). Other reasons include the use of different GCMs, RCMs and coarser resolution used for the wave simulations in the STOWASUS-2100 project with respect to HF and LR models (75 km vs. 5 km and 100 m).

Finally, it should be pointed out that in this study only one realization for each of two scenarios was shown. It is important to produce the assessments of local wave cli-

mate changes for the entire range of obtained with different RCM/GCM regional atmosphere/ocean data for different scenarios. This provides the opportunity of evaluating the uncertainty level of the projected local wave climate response to different realizations of global climate change scenarios and on different scenarios themselves. However, the task is beyond the scope of this study, it is proposed as further step towards the evaluation of the local near-shore wave climate for the future and assessment of potential local changes due to different rates of anthropogenic activities.

4.3 Summary

Summarizing results for the wind and wave hindcast for the last four decades, significant increase of the wind speeds and the increase of the number of westerly winds for the medium as well as for extreme wind events was found for the Helgoland region. Significant upward trends were detected for annual medium and upper percentiles of the regional and local SWH fields. The magnitude of the trends is dependent on the location and wave height with a general tendency for higher waves and larger trends for the area west from Helgoland and lower waves and trends east of the island. The maximum trend for the 99-percentile revealed from local LR data is about 1.7 cm yr^{-1}, which corresponds with the trends obtained from the medium-scale HF wave data for the Helgoland. The wave direction statistics for the high waves remains unchanged during last decades. The spatial pattern of the prevailing wave directions for the deep water part of the area is mainly influenced by westerly wind conditions, for the near-shore zone the shallow water processes are dominating the wave direction development.

The trends for the extreme wave and wind events were found to be significantly positive for the examined period, however, their nature was not clearly identified. The analysis of regional wind and wave statistics for longer periods, carried out in earlier studies (e.g. Alexandersson et al. [1998], Bärring and von Storch [2004]) for the North Sea region, has shown no significant changes for the last decades with respect to the beginning of the century. In this way, the trends for the wave extremes found in this study can be rather attributed to the inter-decade variability than considered as climate change signal. If for the assessment of future wave climate the wave data from the only last 40 years is used, it can cause artificial increase in intensity and frequency of estimated wave extremes.

The future local wave climate was evaluated based on two approaches. The first one is the extreme value analysis, which allows the assessment of the return values and periods for the wave heights and considers only past wave statistics but not the trends for the extreme events. Here no assumptions about the directions of future global or local development were made. The second approach was the scenario study. The past wave climate was not considered here, instead, the scenarios for the future climate which undergone different degrees of anthropogenic influence were elaborated. The results of the first type of the future climate analysis can be used directly for the engineering purposes as soon as they summarize to great extent the knowledge about the realistic local wave climate. The second approach gives rather the assessment of the potential and often extreme changes in wave

climate. This helps to evaluate the range of possible responses of the system on the external perturbations.

In this work the examples of the local and regional wave responses were examined. One of the goals of this experiment was to test whether there is a need for the local wave climate scenario studies or if local changes simply replicate the regional ones. This seems not to be the case and Figure 4.13 demonstrates, in particular, the impact of the local structure on changes of wave extremes. The other aim of the experiment was to demonstrate the applicability of the statistical-dynamical methodology to such problems. It appears that, although, in general, the local changes associated with the scenarios follow the regional rate of changes, the more detailed representation of the local wave climate changes can be obtained with the proposed downscaling method. The consideration of further scenarios and different realizations of each scenario is needed to provide the comprehensive picture of the potential changes in local wave statistics. The reasonable computational resources required for the multi-decade simulations with the proposed method allow for the consideration of as much scenarios or scenario realizations with different RCM as necessary.

Chapter 5

Conclusions and Discussion

In this study the problem of long-term near-shore wave data localization was investigated with the main goal to provide the tools for the simulation or extraction of high-resolution wave statistics and to analyze the obtained wave climatology for the example Helgoland island area. The idea of downscaling of medium-scale wave hindcast for obtaining local wave statistics was elaborated. The application of the dynamical wave model to the task was successful, but due to computational constraints an alternative approach was developed. The combination of the statistical downscaling model and dynamical wave model was proposed for obtaining instantaneous local wave fields from medium-scale data. Using the statistical-dynamical method, the high-resolution wave statistics for Helgoland surroundings were obtained for the last four decades, thus providing the source of data for various coastal applications. The results concerning each part of the study were summarized after the corresponding chapters. Here the outline of the work as well as the possible directions of further investigation and development are discussed.

- The dynamical K-model was set up for the Helgoland area using the medium-scale wave data as the boundary conditions. The test runs showed the practical difficulty of the multi-decade simulations of high-resolution wave data because of the large computational resources required by the model. After producing a series of model modifications, the local wave hindcast was obtained with the K-model for 22 years. It was concluded that the multi-decade high-resolution wave simulations are hardly feasible at the present state of affairs. Further improvements of the model effectiveness and significant increase of the available computational resources are needed for successful application of the spectral wave model for the long-term high-resolution wave hindcasts and especially for scenario studies, where the multiple multi-decade simulations are often required.

- The results of the K-model local wave simulations were compared with measurements at two locations. The model demonstrated good skills in representation of such instantaneous wave parameters as significant wave height, peak period and wave direction with the tendency to overestimate SWH for high waves. For the wave statistics for longer periods a good agreement with observations was also found, although,

an overestimation of high waves was detected. This was mainly attributed to the overestimated high waves provided by boundary conditions. Thus, it was pointed out that the quality of the local wave statistics obtained with dynamical wave model was strongly dependent on the quality of the regional wave data used as corresponding boundary conditions. The lack of observational data in different parts of the modeled area and especially near the shore makes difficult any categorical conclusion about the quality of the model results at each location. At the same time, most of the spatial and temporal features of the simulated local wave fields can be reasonably explained by local physical processes like shoaling, bottom dissipation and current influence. Finally, the agreement with available measurements, successful K-model performance for another near-shore area and adequate behaviour of the modeled wave parameters suggests that the K-model wave simulation is realistic and appropriate for the use as the substitute for reality further in the study.

- The added value obtained by the local wave modeling with respect to the original medium-scale data has been assessed. It was demonstrated that the HIPOCAS medium-scale wave data is adequate for the general representation of the near-shore wave statistics. The spatial features in wave statistics attributed to the high-resolution bathymetry, coastline shape and local processes are not reproduced and can not be directly extracted from the medium-scale dataset. It was concluded that additional elaboration of the medium-scale wave data was required for obtaining adequate local wave statistics and one of successful methods for such localization procedure is the dynamical wave modeling.

- The combination of dynamical and statistical approaches to the downscaling of medium-scale wave data was proposed as a faster alternative to the purely dynamical method. Three statistical models were built approximating the relation between instantaneous medium-scale and dynamically obtained local significant wave heights. All three methods showed good skills in the representation of the wave height statistics, their results were comparable with the dynamically obtained results for long-term wave statistics and significantly improved the medium-scale data. That means most information about the local wave statistics was contained in the regional data and time-independent local features such as bathymetry, whereas the variable in time local fields such as currents or water level change played only a minor role in the formation of local wave statistics. Several issues concerning the methods have been addressed in the study and linear regression was chosen as the optimal statistical model for further experiments. Although suffering from some uncertainties and limitations, the statistical-dynamical model has an irrefutable advantage of short computational time since the model is built for a certain area. The question of the applicability of the described method for other coastal areas has been discussed and no principal objections were found, except that the considered area should have the connection to the open sea and, at least partially, be dependent on the regional wave climate. Of course, in each case the peculiarities of the area should be additionally considered.

- Linear regression method, in combination with the dynamical wave model, allowed the production of a 44-year high-resolution wave hindcast for the Helgoland area, providing the wave statistics with the quality required by numerous coastal applications. The analysis of the past wind and wave statistics showed that, in general, regional and local wave extreme events occurred under the westerly wind conditions. During the last decades there has been a slight, but statistically significant, increase in the intensity and frequency of westerly winds. Positive linear trends were revealed for annual extreme and mean wave heights on both regional and local scale, which corresponds with the results from earlier studies for the south-eastern North Sea (i.e. WASA Group [1998]). Although the general behaviour of annual wave extreme statistics was similar for the medium-scale and local data, the magnitude of the local wave extreme events as well as the rate of the inter-annual trends for high-resolution wave data differed significantly within the model domain, demonstrating the significance of local effects for the wave statistics. The reasons for the intensification of the storm events in German Bight for the last four decades are not completely clear. The assessment of the return values for the local wave heights was made based on the past wave statistics using the extreme value analysis. This method does not consider any inter-annual trends for the wave extreme events and, thereby, the nature and the direction of the trends are not important for this type of the analysis.

- The problem of the local system response to anthropogenic climate change was partially considered in the study by the localization of two global change scenarios. The proposed statistical-dynamical methodology was tested for this application and it was found that the downscaling of the instantaneous wave parameters is more robust in the altered climate environment than the downscaling of the annual extreme wave statistics. The analysis of the projected local and regional instantaneous wave data showed the increase of the magnitude of wave extreme events for the most part of the German Bight, with the maximum difference between the altered and the present date climate of about 20 cm for the SWH 99-percentiles. At the same time, the areas of the wave height decrease were detected for the southern coastline of the German Bight. The differences between two SRES scenarios were found to be insignificant. It was pointed out that for the adequate evaluation of the possible future responses of the local wave climate it is important to consider the full range of regional scenarios obtained with different RCM, which gives the estimation of the uncertainty level for the wave climate projections.

Further development of the proposed statistical-dynamical methods or the consideration of the other methods within the presented concept, depending on the particular application, may be the next step towards obtaining of the more accurate and comprehensive local wave data. The longer local wave hindcast and the consideration of various climate change scenarios are supposed to improve the description of the long-term variations of the local wave statistics. This helps to understand the mechanisms governing these perturbations and to reveal the role of the anthropogenic influence on the local waves and wave extreme events.

Consequently, the more confident evaluation of the future wave climate is possible, which allows the better adaptation of the coastal areas to the estimated future wave conditions and the better grounded policy making for the present day global and regional development.

Acknowledgements

First of all I am very grateful to Hans von Storch for giving me the opportunity to work, learn and make the thesis at GKSS Institute for Coastal Research, for the scientific guidance and great support. I want to express my sincere thanks to Ralf Weisse for the day-to-day supervision, for the numerous advises and useful discussions and for the improving of my writing skills.

I would like to thank Gerhard Gayer and Heinz Günther for the numerous valuable discussions and help with the K-model and spectral wave modeling. I also want to thank Eduardo Zorita who helped me with statistical methods, provided subroutines for the Analog and CCA methods and gave useful advices. I am grateful to Dieter Schrader from the BSH, Olaf Outzen from Oceanwaves GmbH and Saskia Esselborn from GFZ-Potsdam for providing the observational data and useful comments.

I am thankful to Jörg Winterfeld and Sebastian Wagner for the valuable comments to this thesis. My gratitude goes to Dennis Bray and Julie Jones for the patient and careful help with my English. I am grateful to Andrey Pleskaschevsky for the everyday support and the mood.

I would like to express my hearty thanks to my family, who helped me, believed in me and whose love I feel all the time.

Bibliography

H Alexandersson, T Schmith, K Iden, and H Tuomenvirta. Long-term variation of the storm climate over nw europe. *Global Atmos. Ocean Sys.*, 6:97–120, 1998.

S Bacon and DJT Carter. Wave climate changes in the north atlantic and the north sea. *Int. J. Climatol.*, 11:545–558, 1991.

L Bärring and H von Storch. Scandinavian storminess since about 1800. *Geophys. Res. Lett.*, 31:L20202, doi:10.1029/2004GL020441, 2004.

RG Barry and AH Perry. *Synoptic climatology: methods and applications*. Methuen&Co, Ltd, London, 1973.

F Baur, P Hess, and H Nagel. Kalender der Grosswetterlagen europas 1881-1939. *Bad Homburg*, page 35 pp, 1944.

D Bonicel, V Thouvenin, and H Haji. CLIOSAT: Calibration and validation of satellite data. In *Proceedings of 3-rd ERS Symposium*, Italy, Florence, March 17-22, 1997.

E Brauer and R Weisse. Determination of high-frequency wind variability from observations and application to North Atlantic wave modeling. *J. Geophys. Res.*, 105(C11):26179–26190, 2000.

S Caires, A Sterl, J-R Bidlot, N Graham, and V Swail. Climatological assessment of reanalysis ocean data. In *Proceedings of 7th international workshop on wave hindcasting and forecasting*, pages 1–12, Banff, Alberta, Canada, 2002.

VJ Cardone and DT Resio. An assessment of wave modeling technology. In *Proceedings of 5th international workshop on wave hindcasting and forecasting*, pages 468–495, Melbourne, Florida, 1998.

L Cavaleri and PM Rizzoli. Wind wave prediction in shallow water - theory and application. *J. Geophys. Res.*, 86:10961–10973, 1981.

JH Christensen, T Carter, and F Giorgi. PRUDENCE employs new method to assess European climate change. *EOS*, 83:147, 2002.

S Coles. *An introduction to statistical modeling of extreme values*. Springer-Verlag, London, 2001.

AT Cox and VR Swail. A global wave hindcast over the period 1958-1997: Validation and climate assessment. *J. Geophys. Res.*, 106(C2):2313–2329, 2001.

RG Crane and BC Hewitson. Doubled co_2 climate change scenarios for the Susquehanna Basin: Precipitation. *Int. J. Climatol.*, 18:65–76, 1998.

M Cui and E Zorita. Analysis of the sea-level variability along the chinese coast and estimation of the impact of a co_2-perturbed atmospheric circulation. *Tellus*, 50A:333–347, 1998.

B Denis, R Laprise, D Caya, and J Cote. Downscaling ability of one-way nested regional climate models: the Big-Brother Experiment. *Clim. Dynamics*, 18:627–646, 2002.

R Döscher, U Willén, C Jones, A Rutgersson, HEM Meier, U Hansson, and LP Graham. The development of the coupled regional ocean-atmosphere model RCAO. *Boreal Env. Res.*, 7:183–192, 2002.

F Feser, R Weisse, and H von Storch. Multi-decadal atmospheric modeling for europe yields multipurpose data. *EOS Transactions*, 82(28):305–310, 2001.

F Giorgi, B Hewitson, J Christensen, M Hulme, H von Storch, Whetton P, R Jones, L Mearns, and C Fu. Regional climate information evaluation and projections. *in Climate Change 2001: Scientific Basis*, pages 583–638, 2001.

H Günther and W Rosenthal. The hybrid parametrical (HYPAS) wave model. In *Ocean wave modelling, Swamp group*, pages 211–214. Plenum Press, New York, 1985.

H Günther and W Rosenthal. A wave model with a non-linear dissipation function. pages 138–147, 1997.

H Günther, S Hasselmann, and PAEM Janssen. The WAM Model cycle 4.0. User Manual. Deutsches Klimarechenzentrum Hamburg, technical report no. 4, 1992.

H Günther, W Rosenthal, M Stawarz, JC Carretero, M Gomez, I Lozano, O Serrano, and M Reistad. The wave climate of the Northeast Atlantic over the period 1955-1994: the WASA wave hindcast. *Glob. Atmos. Ocean Sys.*, 6:121–163, 1998.

K Hasselmann, TP Barnett, E Bouws, H Carlson, DE Cartwright, K Enke, JA Ewing, H Gienapp, DE Hasselmann, P Kruseman, A Meerburg, P Müller, DJ Olbers, K Richter, W Sell, and H Walden. Measurements of wind-wave growth and swell decay during the JOint North Sea WAve Project (JONSWAP). *D. Hydrogr. Z.*, A8(12):1–95, 1973.

K Hessner, K Reichert, J Dittmer, JC Nieto Borge, and H Günther. Evaluation of WaMoS wave data. pages 221–231, San Francisco, 2001.

BC Hewitson and RG Crane. Climate downscaling: Techniques and application. *Climate Research*, 7:85–95, 1996.

H Heyen and JW Dippner. Salinity in the southern German Bight estimated from large-scale climate data. *Tellus*, 50A:545–556, 1998.

N Hogben. Increase in wave heights over the North Atlantic: A review of evidence and some implications for the naval architect. *Trans. Roy. Inst. Naval Arch.*, W5:93–101, 1994.

LH Holthuijsen, N Booji, and L Bertotti. The propagation of wind errors through ocean wave hindcasts. *Journal of Offshore Mechanics and Arctic Engineering*, 117:184–189, 1996.

JT Houghton, Y Ding, DJ Griggs, M Noguer, PJ van der Linden, X Dai, K maskell, and CA Johnson, editors. *Climate Change 2001: The Scientific Basis*. Cambridge University Press, UK., 2001.

E Kaas and STOWASUS-Group. Regional strom, wave and surge scenarios for the 2100 century. Final report., DMI, [Available online at http://www.dmi.dk/pub/STOWASUS-2100/.], 2001.

E Kalnay, M Kanamitsu, R Kistler, W Collins, D Deaven, L Gandin, M Iredell, S Saha, G White, J Woollen, Y Zhu, M Chelliah, W Ebisuzaki, W Higgins, J Janowiak, KC Mo, C Ropelewski, J Wang, A Leetmaa, R Reynolds, R Jenne, and D Joseph. The NCEP/NCAR reanalysis project. *Bull. Am. Meteorol. Soc.*, 77:437–471, 1996.

RW Katz and MB Parlange. Mixtures of stochastic processes: applications to statistical downscaling. *Clim. Res.*, 7:185–193, 1996.

GJ Komen, L Cavaleri, M Donelan, K Hasselmann, S Hasselmann, and PAEM Janssen. *Dynamics and modelling of ocean waves*. Cambridge University Press, UK., 1994.

Y Kushnir, VJ Cardone, JG Greenwood, and MA Cane. The recent increase in North Atlantic wave heights. *J. Climate*, 10(8):2107–2113, 1997.

H Langenberg, A Pfizenmayer, H von Storch, and J Sündermann. Storm related sea level variations along the North Sea coast: natural variability and anthropogenic change. *Cont. Shelf Res.*, 19:821–842, 1999.

MS Longuett-Higgins, DE Cartwright, and ND Smith. *Ocean Wave Spectra*, chapter Observation of the directional spectrum of sea waves using the motions of a floating buoy. Prentice Hill, 1963.

JJ McCarthy, OF Canziani, NA Leary, DJ Dokken, and KS White, editors. *Climate Change 2001: Impacts, Adaptation & Vulnerability*. Cambridge University Press, UK., 2001.

S Moghimi, G Gayer, H Günther, and M Shafieefar. Application of 3-rd generation shallow water wave models in a tidal environment. *Ocean Dynamics*, 55(1):10–27, 2005.

J Monbaliu, R Padilla-Hernandez, JC Hargreaves, JCC Albiach, W Luo, M Sclavo, and H Günther. The spectral wave model, wam, adapted for applications with high spatial resolution. *Coastal engineering*, 41:41–62, 2000.

J Murphy. An evaluation of statistical and dynamical technniques for downscaling local climate. *J. Climate*, 12:2256–2284, 1999.

W. Collins S. Saha G. White J. Wollen M. Chelliah W. Ebisuzaki M. Kanamitsu V. Kousky H. van den Dool R. Jenne R. Kistler, E. Kalnay and M. Fioriono. The NCEP/NCAR 50-year reanalysis: Monthly means CD-ROM and documentation. *Bull. Am. Meteorol. Soc.*, 82:247–267, 2001.

RC Ris. *Spectral wave modelling of wind waves in coastal zones*. PhD thesis, Delft University of Technology, 1997.

RC Ris, LH Holthuijsen, and N Booij. The third-generation wave model for coastal regions: 2.verification. *J. Geophys. Res.*, 104(C4):7667–7681, 1999.

C Schneggenburger. *Spectral wave modelling with nonlinear dissipation*. PhD thesis, Univ. of Hamburg, 1998.

C Schneggenburger, H Günther, and W Rosenthal. Shallow water wave modelling with nonlinear dissipation. *Deutsche Hydrographische Zeitschrift*, 49:431–444, 1997.

T Schöne, A Braun, M Rentsch, CK Shum, and Ch Reigber. Concept for using GPS-buoys for radar altimetry drift monitoring. In *ESA ERS/ENVISAT Symposium, Oct. 16-20*, Gothenburg, Sweden. Also available at http://www.gfz-potsdam.de/pb1/op/seal, 2000.

AJ Simmons and JK Gibson. The ERA-40 project plan, ERA-40 project report series No.1 WCMWF. Technical report, Shinfield Park, Reading, UK, 2000.

CG Soares, R Weisse, JC Carretero, and E Alvarez. A 40 years hindcast of wind, sea level and waves in european waters. In *Proceedings of 21st International Conference on Offshore Mechanics and Arctic Engineering*, 2002.

A Sterl, GJ Komen, and PD Cotton. Fifteen years of global wave hindcasts using winds from the European Centre for Medium-Range Weather Forecasts reanalysis: Validating the reanalyzed winds and assessing wave climate. *J. Geophys Res*, 103:5477–5492, 1998.

VR Swail and AT Cox. In the use of NCEP-NCAR reanalysis surface marine wind fields for a long-term North Atlantic wave hindcast. *J. Atmospheric Oceanic Technology*, 17: 532–545, 2000.

U Vierfuss. Ermittlung der Seegangsbelastung fur Helgoländer Molenbauwerke. *Hansa*, 139:68–73, 2002.

H von Storch and FW Zwiers. *Statistical analysis in climate research*. Cambridge University Press, 1999.

H von Storch, E Zorita, and U Cubasch. Downscaling of global climate change to regional scales: an application to Iberia rainfall in wintertime. *J. Climate*, 6:1161–1171, 1993.

H von Storch, B Hewitson, and L Mearns. Review of empirical downscaling techniques. In T Iversen and BAK Hoiskar, editors, *Regional climate development under global warming. General Technical Report No. 4. Conf. Proceedings RegClim Spring Meeting, Jevnaker, Torbjørnrud, Norway*, pages 29–46, 2000.

WAMDI Group. The WAM model - a third generation ocean wave prediction model. *J. Phys. Oceanogr.*, 18:1775–1810, 1988.

XL Wang and VR Swail. Changes of extreme wave heights in Nothern Hemisphere oceans and related atmospheric circulation regimes. *J. Climate*, 14:2204–2221, 2001.

XL Wang, FW Zwiers, and VR Swail. North Atlantic ocean wave climate change scenarios for the twenty-first century. *J. Climate*, 17:2368–2383, 2004.

WASA Group. Changing waves and storms in the Northeast Atlantic? *Bull. Am. Meteorol. Soc.*, 79(5):741–760, 1998.

A Weichert and G Bürger. Linear versus nonlinear techniques in downscaling. *Clim. Res.*, 10:83–93, 1998.

R Weisse and A Plüss. Storm-related sea level variations along th North sea coast as simulated by a high-resolution model 1958-2002. *Ocean Dynamics*, 2005.

R Weisse, F Feser, and H Günther. A 40-year high-resolution wind and wave hindcast for the Southern North Sea. In *7th International workshop on wave hindcasting and forecasting, Banff, Alberta, Canada*, pages 97–104, 2002.

RL Wilby and TML Wigley. Downscaling general circulation model output: a review of methods and limitations. *Progress in Physical Geography*, 21:530–548, 1997.

DS Wilks and RL Wilby. The weather generation game:A review of stochastic weather models. *Progress in Physical Geography*, 23:125–136, 1999.

K Woth. North Sea storm surge statistics based on projections in a warmer climate: How important are the driving gcm and the chosen emission scenario? *Ocean Dynamics*, 2005. in press.

K Woth, R Weisse, and H von Storch. Climate change and North Sea storm surge extremes: An ensemble study of storm surge extremes expected in a changed climate projected by four different Regional Climate Models. *Ocean Dynamics*, (DOI 10.1007/s10236-005-0024-3), 2005. in press.

E Zorita and H von Storch. The analog method as a simple statistical downscaling technique:comparison with more complicated methods. *J. Climate*, 12:2474–2489, 1999.

E Zorita, J Hughes, D Lettenmaier, and H von Storch. Stochastic characterisation of regional circulation patterns of climate model diagnosis and estimation of local precipitation. *J. Climate*, 8:1023–1042, 1995.

Appendix A

Techniques for variability analysis

A.1 Empirical Orthogonal Functions

The Empirical Orthogonal Function (EOF) analysis allows determination of main patterns of variability of statistical fields. Usually, a m-dimensional vector $\vec{x_t} = \{x_1(t), \ldots, x_m(t)\}$ is considered and one needs to identify simultaneous variations of the components of the vector. The anomaly vector

$$\vec{x_t'} = \vec{x_t} - \vec{\mu} \tag{A.1}$$

is formed to describe the these variations. Here $\vec{\mu}$ is estimate of the mean. Then anomalies are expanded into a finite series

$$\vec{x_t'} = \sum_{i=1}^{k} \alpha_{i,t} \vec{e^i}. \tag{A.2}$$

The patterns $\vec{e^i}$ are called Empirical Orthogonal Functions, they are chosen to be orthogonal and to minimize the error

$$\sum_t (\vec{x_t'} - \sum_{i=1}^{k} \alpha_{i,t} \vec{e^i})^2. \tag{A.3}$$

The time coefficients $\alpha_{i,t}$ are called EOF coefficients or principal components. They are obtained by projecting the anomalies $\vec{X_t'}$ onto the patterns $\vec{e^i}$. In addition, optimal coefficients satisfy:

$$\sum_t \alpha_{i,t}\alpha_{j,t} = 0, \qquad i \neq j. \tag{A.4}$$

The procedure for determination of EOFs for an arbitrary field is summarized in the next theorem.

Theorem. *Let $\vec{X}$ be m-dimensional vector with mean $\vec{\mu}$ and covariance matrix Σ. Let $\lambda_1 \geq \lambda_2 \geq \cdots \geq \lambda_m$ be the eigenvalues of Σ and let $\vec{e^1}, \ldots, \vec{e^m}$ be the corresponding eigenvectors of unit length. Since Σ is Hermitian, the eigenvalues are non-negative and the eigenvectors are orthogonal. Then The k eigenvectors that correspond to $\lambda_1, \ldots, \lambda_k$*

minimize

$$\epsilon_k = E(\|(\vec{X} - \vec{\mu}) - \sum_{i=1}^{k} \langle \vec{X} - \vec{\mu}, \vec{e^i} \rangle \vec{e^i}\|^2) \tag{A.5}$$

and the next relations are valid:

$$\epsilon_k = Var(\vec{X}) - \sum_{i=1}^{k} \lambda_i \tag{A.6}$$

$$Var(\vec{X}) = \sum_{i=1}^{m} \lambda_i. \tag{A.7}$$

The eigenvectors of the covariance matrix are taken as empirical orthogonal functions. The variance of $\vec{X}$ is split into m components associated with the EOFs $\vec{e^i}$. The variance explained by the kth component with respect to the total variance is $\lambda_k / \sum_{i=1}^{m} \lambda_i$. Usually, the components are ordered by the size of eigenvalues. In this case the first component represents the major part of variance among all the others, the second one represents the second significant variance and so on. The main part of the variance of the field can often be explained by k EOFs, where $k \ll m$. This allows the approximation of the field by truncated sum of only k EOFs with an error not less than ϵ_k.

A.2 Canonical Correlation Analysis

The Canonical Correlation Analysis (CCA) is used for the study of the simultaneous variability of two dependent statistical fields. Let $\vec{X}$ be an m-dimensional vector and $\vec{Y}$ be an n-dimensional vector. For the CCA one seeks such vectors $\vec{f_X}$ and $\vec{f_Y}$ that for $\beta^X = \langle \vec{X}, \vec{f_X} \rangle$ and $\beta^Y = \langle \vec{Y}, \vec{f_Y} \rangle$ the correlation

$$\rho = \frac{Cov(\beta^X, \beta^Y)}{\sqrt{Var(\beta^X) Var(\beta^Y)}} = \frac{\vec{f_X^T} Cov(\vec{X}, \vec{Y}) \vec{f_Y}}{\sqrt{Var(\langle \vec{X}, \vec{f_X} \rangle) Var(\langle \vec{Y}, \vec{f_Y} \rangle)}} \tag{A.8}$$

is maximized. In addition, the normalization of $\vec{f_X}$ and $\vec{f_Y}$ is chosen:

$$Var(\langle \vec{X}, \vec{f_X} \rangle) = 1 \tag{A.9}$$

$$Var(\langle \vec{Y}, \vec{f_Y} \rangle) = 1. \tag{A.10}$$

Then the correlation has a form:

$$\rho = \vec{f_X^T} \Sigma_{XY} \vec{f_Y} \tag{A.11}$$

where Σ_{XY} is the cross-covariance matrix of the vectors $\vec{X}$ and $\vec{Y}$. After solving the maximization problem for A.11 the vectors $\vec{f_X}$ and $\vec{f_Y}$ can be found as eigenvectors of the matrices $\Sigma_{XX}^{-1} \Sigma_{XY} \Sigma_{YY}^{-1} \Sigma_{XY}^T$ and $\Sigma_{YY}^{-1} \Sigma_{XY}^T \Sigma_{XX} \Sigma_{XY}$ accordingly. Together with them

the first pair of canonical correlation coordinates β^X and β^Y and correlation $\rho = \sqrt{\lambda}$ are found. Here λ is the largest eigenvalue of both matrices.

Similar method allows the derivation of the next $k = min(m, n)$ patterns $(\vec{f_X^i}, \vec{f_Y^i})$, canonical coordinates and corresponding correlations ρ_i in such a way, that the canonical coordinates are uncorrelated, i.e. $Cov(\beta_i^X, \beta_j^X) = Cov(\beta_i^Y, \beta_j^Y) = 0$ for $i \neq j$. They are ordered according to the value of the correlation. Finally, the canonical correlation patterns $\vec{F_X^i}$ and $\vec{F_Y^i}$ are defined as the columns of the matrices $\Sigma_{XX}\mathbf{f}_X$ and $\Sigma_{YY}\mathbf{f}_Y$. Here $\mathbf{f}_X$, $\mathbf{f}_Y$ are matrices containing vectors $\vec{f_X^i}$ and $\vec{f_Y^i}$ as columns. The original fields can be represented as

$$\vec{X} = \sum_i \beta_i^X \vec{F_X^i}, \qquad \vec{Y} = \sum_i \beta_i^Y \vec{F_Y^i}. \tag{A.12}$$

If the fields were first transformed with EOF analysis and thus can be approximated by k_X, k_Y EOF patterns and EOF coefficients, then for the CCA the vectors $\vec{X'} = (\alpha_i^X, \ldots, \alpha_{k_X}^X)$ and $\vec{Y'} = (\alpha_i^Y, \ldots, \alpha_{k_Y}^Y)$ are used instead of original fields. This simplifies the CCA procedure significantly if $k_X \ll m$ and $k_Y \ll n$.

Appendix B

List of acronyms

BAW	Bundesanstalt für Wasserbau (Coastal Division of the Federal Engineering and Research Institute)
BSH	Bundesamt für Seeschiffahrt und Hydrographie Federal Maritime and Hydrographic Agency
CFL	Courant-Friedrich-Levy criterion
DE1, DE2	Düne island position (Fig. 2.1)
DKRZ	Deutsches Klimarechenzentrum Hamburg
DWP	deep water buoy position (Fig. 2.1)
EOF	empirical orthogonal function
ERS2	European Remote Sensing satellite (Bonicel et al. [1997])
GCM	General Circulation Model
GFZ-Potsdam	GeoForschungsZentrum Potsdam
HH1, HH2	Helgoland harbor position (Fig. 2.1)
HIPOCAS	Hindcast of Dynamic Processes of the Ocean and Coastal Areas of Europe (Soares et al. [2002])
HYPAS	shallow-water version of HYbrid PArametrical wave model (Günther and Rosenthal [1985]
IPCC	Intergovernmental Panel on Climate Change (www.ipcc.ch)
LNA	Lange-Anna position (Fig. 2.1)
NCEP	National Center for Environmental Prediction
PRUDENCE	Prediction of Regional scenarios and Uncertainties for Defining EuropeaN Climate change risks and Effects project (Christensen et al. [2002])
RCAO	Rossby Centre regional Atmosphere-Ocean model (Döscher et al. [2002])
RCM	Regional Climate Model
rms	root mean square error
SRES	Special Report on Emissions Scenarios

STOWASUS-2100	Regional STOrm, WAve and SUrge Scenarios for the 2100 century (Kaas and STOWASUS-Group [2001])
SWH	significant wave height
TOPEX	satellite altimeter data from the TOPography EXperiment for Ocean Circulation mission Schöne et al. [2000]
WAM	third generation WAve Model (WAMDI Group 1998)
WaMoS	Wave and Surface Current Monitoring System radar (Hessner et al. [2001])
WASA	Waves and Storms in the North Atlantic (WASA Group [1998])

Wetzel, P. (2005): **Interannual and Decadal Variability in the Air-Sea Exchange of CO_2.**
Reports on Earth System Science, Max Planck Institute for Meteorology, No. 7/2004, pp. 77

Stier, P. (2005): **Towards the Assessment of the Aerosol Radiative Effects - A Global Modelling Approach.** Reports on Earth System Science, Max Planck Institute for Meteorology, No. 9/2004, pp. 111

Zuo, X. (2005): **Annual Hard Frosts and Economic Growth.**
Department of Economics, University of Hamburg, Hamburg, pp. 112

Jung, M. (2005): **Carbon sequestration options in the international climate regime.**
Department of Economics, University of Hamburg, Hamburg, pp. 119

Zhou, Y. (2005): **Economic Analysis of Selected Environmental Issues in China**
Department of Economics, University of Hamburg, Hamburg, pp. 101

Devasthale, A. (2005): **Aerosol Indirect Effect in the Thermal Spectral Range as Seen from Satellites**
Reports on Earth System Science, Max Planck Institute for Meteorology, No. 16/2005, pp. 70

Zandersen, M. (2005): **Aerosol Valuing Forest Recreation in Europe: Time and Spatial Considerations**
Department of Economics, University of Hamburg, Hamburg, pp. 125

Xuefeng Cui (2005***):*** **Interactions between Climate and Land Cover Changes on the Tibetan Plateau**
Reports on Earth System Science, Max Planck Institute for Meteorology, No. 17/2005, pp. 125

Stehfest, Elke (2005***):*** **Modelling of global crop production and resulting N_2O emissions**
Zentrum für Umweltsystemforschung Universität Kassel pp. 125

Kloster, Silvia (2006***):*** **DMS cycle in the ocean-atmosphere system and its response to anthropogenic perturbations.** Reports on Earth System Science, Max Planck Institute for Meteorology, No. 19/2006, pp. 82

Criscuolo, Luca (2006***):*** **Assessing the Agricultural System and the Carbon Cycle under Climate Change in Europe using a Dynamic Global Vegetation Model**
Reports on Earth System Science, Max Planck Institute for Meteorology, No. 21/2006, pp. 140

Tiwari, Yogesh Kumar (2006***):*** **Constraints of Satellite Derived CO_2 on Carbon Sources and Sinks**
Technical Reports, Max-Planck-Institut für Biogeochemie, No.7/2006, pp.125

Schurgers, Guillaume (2006***):*** **Constraints Long-term interactions between vegetation and climate - Model simulations for past and future -** Reports on Earth System Science, Max Planck Institute for Meteorology, No. 27/2006, pp. 135

Ronneberger, Kerstin Ellen (2006***):*** **The global agricultural land-use model KLUM - A coupling tool for integrated assessment -** Reports on Earth System Science, Max Planck Institute for Meteorology, No. 26/2006, pp. 123

Woth, Katja (2006***):*** **Regionalization of global climate change scenarios: An ensemble study of possible changes in the North Sea storm surge statistics**
Department for Earth Sciences, University of Hamburg, Hamburg, pp. 97

Hoelzemann, Judith Johanna (2006***):*** **Global Wildland Fire Emission Modeling for Atmospheric Chemistry Studies**
Reports on Earth System Science, Max Planck Institute for Meteorology, No. 28/2006, pp. 206